Modelling and assessment of the dispersion of particles in the ESS instrument hall

Ettore Carini

Department of Risk and Safety Management

Aalborg University – Esbjerg

Denmark

Division of Fire Safety Engineering

Lund University – LTH

Sweden

Report XXXX, Lund 2017

Master's degree Thesis at the Risk and Safety Management program of Aalborg University – Exchange thesis project at the International Master in Fire Safety Engineering of LTH

AALBORG UNIVERSITY
DENMARK

EUROPEAN SPALLATION SOURCE

LUNDS UNIVERSITET
Lunds Tekniska Högskola

This report has been financed by the European Spallation Source ERIC

Modelling and assessment of the dispersion of particles in the ESS instrument hall

Ettore Carini

Lund, 2017

Foreword

This project, in collaboration with the European Spallation Source (ESS), aims at the modelling and assessment of a worst-case scenario in which a dispersion of potentially radioactive particles from the target area of the ESS reaches one of the instrument halls in the aftermath of a fire in the target itself.

Making use of CFD (Computational Fluid Dynamics) software the scenario is simulated and assessed. The choice of the software tools, of the dispersion model and its accuracy are discussed. Results of the simulation will allow for a qualitative assessment of the risk for the instrument hall and the surrounding environment and for the possible modes of intervention.

Where not specified, illustrations are made by the author.

The author is responsible for the content of the report.

ESS supervisors: Fredrik Jörud, Per Nilsson

LTH supervisor: Bjarne Husted

Aalborg University supervisor: Anders Schmidt Kristensen

Acknowledgements

This project was an effort that could have never been completed without the help and support of the people I would like to thank here:

- **Fredrik Jörud** (main supervisor, European Spallation Source ERIC), for his constant support and advice, for giving me the opportunity to participate in workshops and visits.
- **Per Nilsson**, (CFD simulation specialist, technical supervisor at the European Spallation Source ERIC), for the meetings, the technical advice and the shared knowledge
- **Bjarne Husted** (CFD specialist, supervisor at LTH), for supporting and advising me, for the hardware and software support, for all the time and effort put in this project
- **Michael Plagge** and **Oriol Rios Rubiras** (CERN) for the advice and the feedback
- The participants at the - Workshop on fire protection for physics research facilities - for the positive feedback and the encouragement on the project

Title

Modelling and assessment of the dispersion of particles in the ESS instrument hall

Author

Ettore Carini

Report

ISRN

Number of pages: 92

Keywords

European Spallation Source, ESS, CFD, particle dispersion, tungsten, bunker fire, instrument hall, LES

Abstract

This project, in collaboration with the European Spallation Source (ESS), aims at the modelling and assessment of a worst-case scenario in which a dispersion of tungsten particles from the target area of the ESS reaches one of the instrument halls in the aftermath of a fire in the target itself, concurrently with a fire developed in the bunker area connecting the hall and the target.

Making use of the ANSYS Fluent CFD (Computational Fluid Dynamics) software the scenario is simulated and evaluated. Simulations undertaken on a scaled down geometry indicate that larger fires lead to larger numbers of particles escaping the hall in shorter times; a further calculation with the full-scale geometry of the instrument hall shows that particle escape does not occur from ground level openings.

Tungsten particles tend to be spread to all heights inside the hall, while less than 11% of their mass escape to the environment. The smallest particles, of diameters of the order of 0,1 µm, are those most likely to escape.

The risk picture arising from this scenario indicates that the personnel inside the instrument hall would be likely exposed to tungsten toxicity, while the environmental hazard would be lesser in magnitude but still relevant.

Summary

The European Spallation Source (ESS) is an ongoing research project pursued by 17 European countries to build a neutron source, of unprecedented size and scope, through linear acceleration of protons colliding a tungsten-made target.

Such kind of installations present a challenge in safety, since there is little experience and documented history on their operational hazards. This implies that there is a need for studying possible worst-case scenarios that could jeopardize the functionality of the installation as well as the safety of the workers and the nearby populations.

The high level of ionizing radiation produced in the spallation reaction process makes the integrity of containment of radioactive material in the target an issue of high priority. Hence, the study of a hypothetical scenario of a dispersion of potentially radioactive particles from the target area is considered relevant.

This report focuses on the modelling and assessment of a worst-case scenario in which, in the aftermath of a liquid hydrogen fire originating in the target area, a dispersion of radioactive tungsten trioxide particles reaches one of the two main instrument halls, while a fire has developed inside the bunker situated in the hall.

Such scenario is simulated through a CFD (Computational Fluid Dynamics) simulation, made with the ANSYS® Fluent software tool, which was chosen over other tools (FDS and OpenFOAM) due to its versatility and easy learning curve. A transient solution using the Large Eddy Simulation (LES) turbulence model is employed because of the unsteady nature of the flow, while the particle phase is modeled as a set of tungsten particles whose diameters are sorted by the Rosin-Rammler distribution in a range between 0,1 and 2,3 µm.

The fire in the bunker is simulated via a simplified model that saves computational power and focuses on the mass-flow of hot air it generates to influence the dispersion of particles. This model is also benchmarked to a validated pool-fire simulation to obtain a partial validation.

The scenario is first simulated in a scaled down geometry, where the focus is placed on the effect of the heat release rate of the fire on the particle dispersion. Repeating the simulation for different magnitudes (330 kW - 1 MW) of the fire shows how for larger fires the particles escape more quickly and in larger numbers.

The simulation with the larger 1 MW fire is taken then for the complete geometry of the instrument hall, showing how after 20 minutes only 11% of the particle mass has escaped the building, and that no particles escaped through the ground level door but only from the ceiling level outlet, although the spread of tungsten particles is on all heights inside the hall. The calculation also indicates that smaller particles of diameters around 0,1 µm constitute the almost totality of the escaping particles.

A brief qualitative risk assessment based on the simulation results concludes that the hazard for the personnel inside the instrument hall, due to possible tungsten inhalation, is the one deserving highest priority, while the environmental damage arising from the particles escaping the building is smaller in magnitude, but still deserving further attention. The lack of escaping particles from ground level opening may influence future rescue and evacuation plans.

Table of Contents

1 INTRODUCTION

The European Spallation Source is since 2015 a European Research Infrastructure Consortium (ERIC), evolving from a joint venture between the Swedish and Danish governments. The scope of the ESS is to become the world's most powerful neutron source, since its capacity will be 30 times larger than the best currently achievable. Such a facility will create new research opportunities for a wide variety of science fields, where neutrons can be used to study properties of materials to an atomic level that could not be seen otherwise.

1.1 BACKGROUND

ESS consists of a linear particle accelerator which accelerates protons towards a target wheel made of tungsten; the spallation of the heavy nuclei caused by the high velocity impact generates a flux of neutrons that can be directed towards instruments used to study properties of materials.

The target wheel is placed in a monolith structure sided by the instrument halls. To control the spallation process, a liquid hydrogen moderator is placed around the tungsten wheel, providing neutron moderation that is necessary to slow down and direct the flux of neutrons.

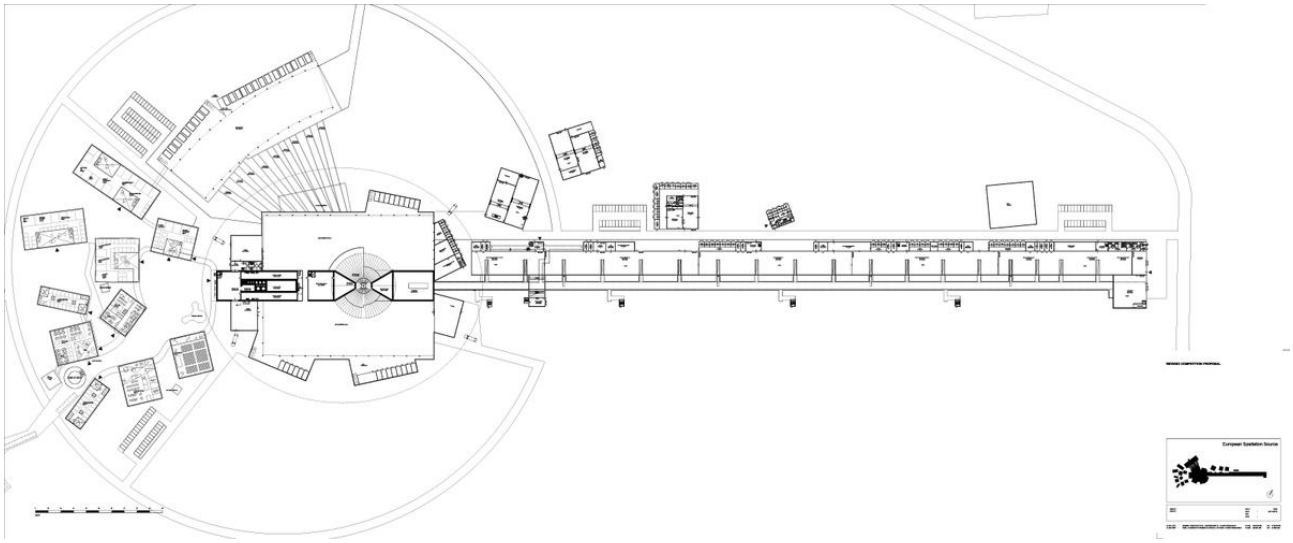

Figure 1 A map showing the layout of the ESS structure: the linear accelerator can be seen on the right while on the left side are the target monolith and the instrument halls besides it. (European Spallation Source, 2016)

1.2 THE SCENARIO

The scenario which will be assessed is considered a highly improbable event, physically possible from a chain succession of unlikely occurrences whose probability is not easily quantifiable. This comes from the fact that there are very few structures comparable to ESS and there are no recorded cases of accidents as of the time of writing of this project.

This scenario is triggered inside the central monolith area, where the tungsten rotating wheel target is placed and irradiated by the high-speed protons inbound from the linear particle accelerator as seen in Figure 2.

As previously mentioned, liquid hydrogen is used for neutron moderation from the target wheel in which the spallation process takes place; the moderator has a "butterfly" design placed around the wheel sector where spallation will take place. Each liquid hydrogen moderator has a volume of approximately one liter and it is surrounded by water pre-moderators and a beryllium reflector, to slow down and direct neutrons from approximately 10% of the speed of light to velocities comparable to the speed of sound.

The target area is a tightly confined space; in such an enclosed volume, a leakage of hydrogen, known for being prone to autoignition and for the rapidity of its combustion processes, could likely result in an explosion, leading to direct damage on the target wheel and a release of particles from it.

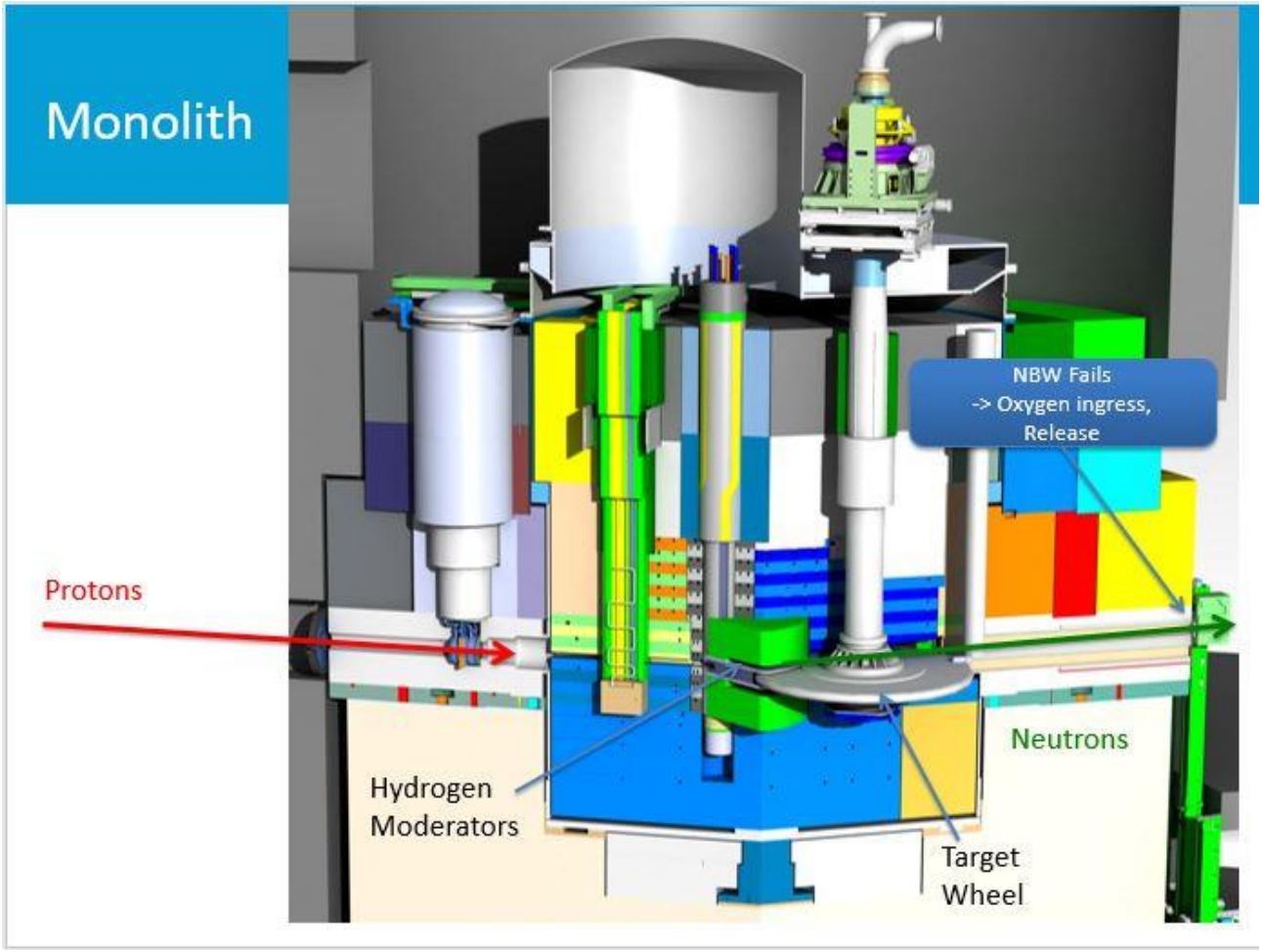

Figure 2 Section of the target monolith; the green moderators are clearly visible (European Spallation Source, 2016)

This kind of event might be triggered by a failure in one of the Neutron Beam Windows (NBW), beam tubes placed radially around the target to extract the neutrons from the target wheel. This may cause oxygen to ingress and reach the target wheel, oxidizing it and causing a release of superficial particles.

Concurrently, a failure of the neutron moderators may cause a leak of liquid hydrogen inside the monolith, which paired to the target wheel failure could trigger an ignition: given the relative quantities of hydrogen in such an enclosed space and the speed of the combustion process, it could result in a strong explosion in the monolith (see image below).

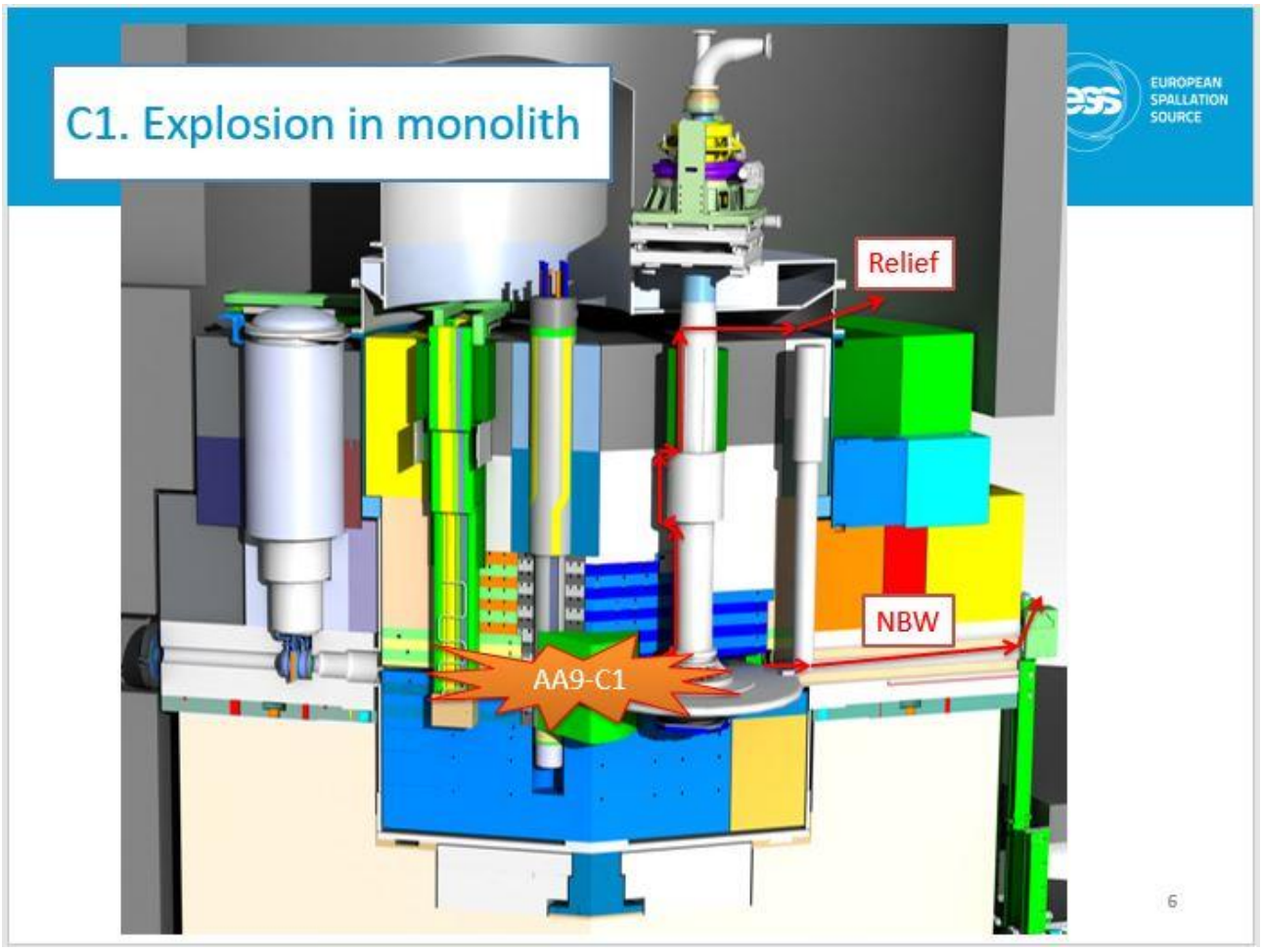

Figure 3 The liquid hydrogen-triggered explosion inside the monolith (ESS, 2016)

The overpressure and the expelled material could both be expelled from relief openings in the monolith and through the NBW spread to the bunker placed between the monolith and the instrument halls; the ejected cloud could trigger another explosion inside the bunker, as seen in the image below, causing severe damage to its roofing and interstice walls separating it from the instrument halls.

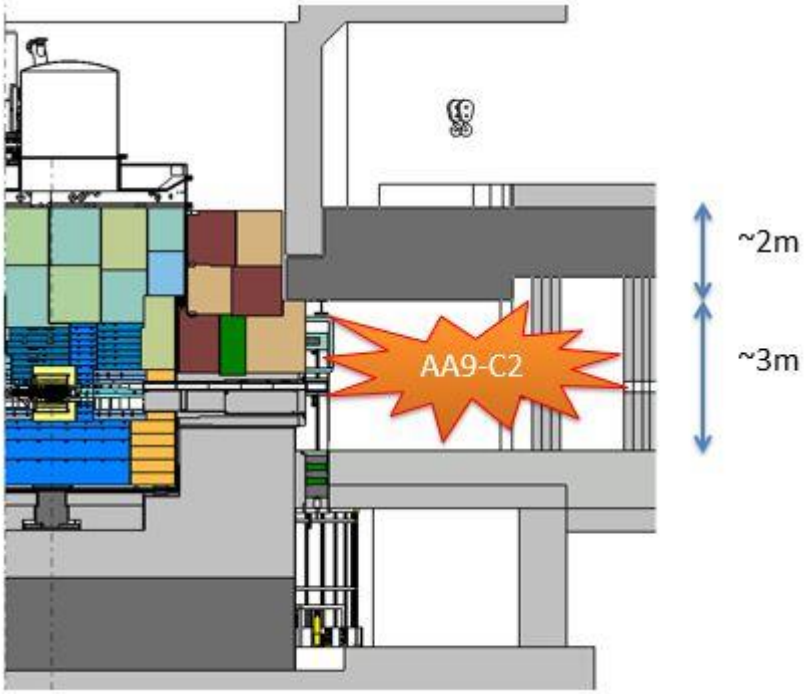

Figure 4 Explosion in the bunker. The monolith is still visible on the left (ESS, 2016)

The bunker would then be exposed to the instrument halls (both, or only one of them), allowing the spread of particles from the target area. A fire would likely develop inside the bunker, directly affecting, together with the radioactive particle dispersion, the instrument hall(s).

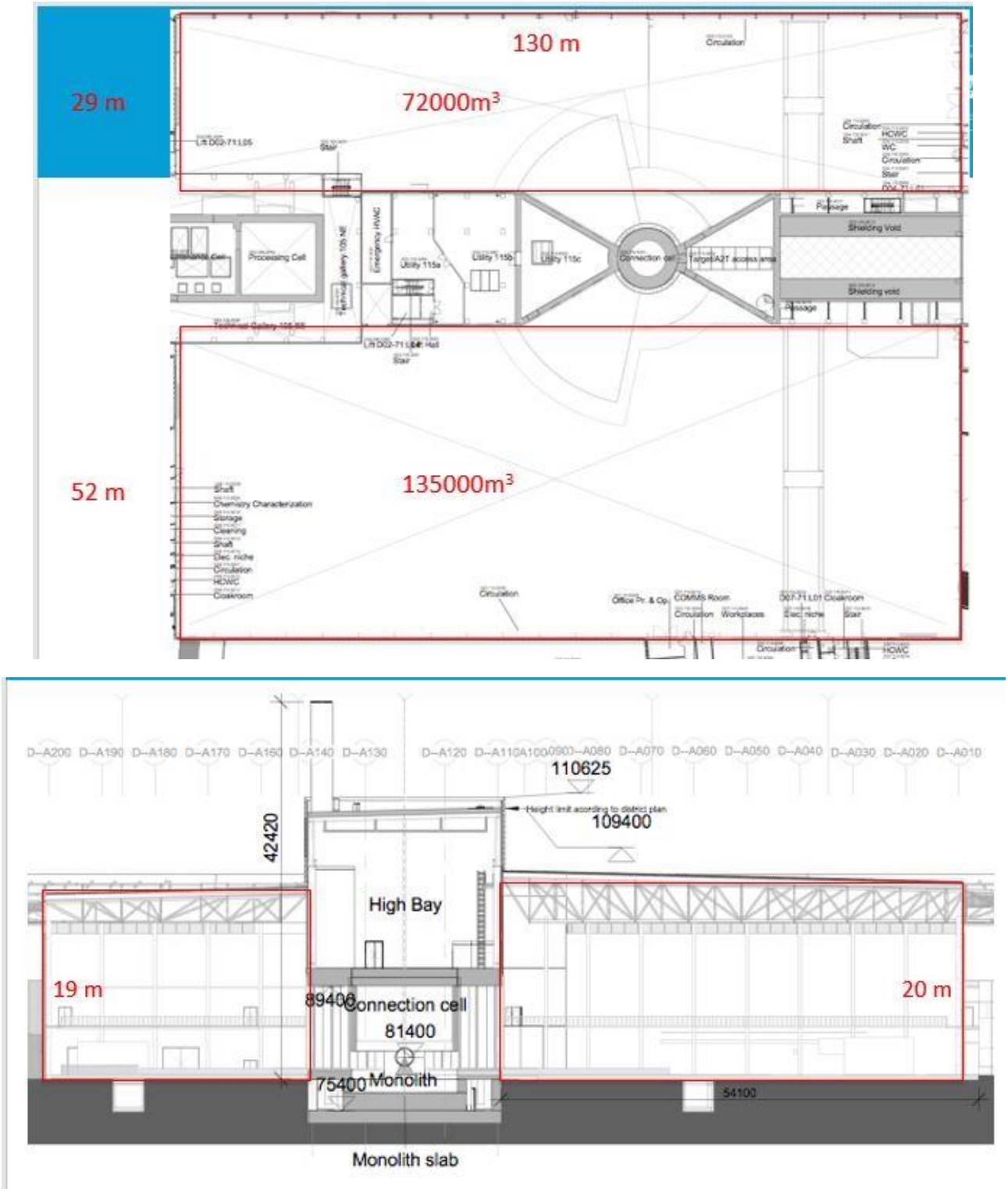

Figure 5 Top and side view of the monolith with the instrument halls, highlighted in red. (ESS, 2016)

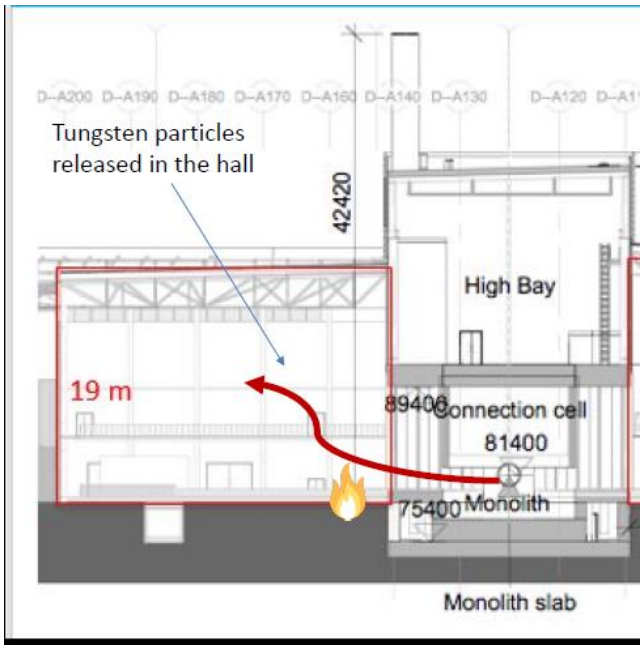

Figure 6 Stylized side view of the fire spreading from the bunker to one of the instrument halls (ESS,2016)

The scenario would thus be a fire developing in the bunker, left exposed by the hydrogen-driven explosion, concurrent with a dispersion of tungsten oxide particles from the monolith to the bunker and the instrument halls.

1.3 PROBLEM DEFINITION

This project aims at assessing a hypothetic scenario as unlikely as it might result in challenging consequences for the still unfinished design. The project consists in a computer-generated modelling of one of the instrument halls of ESS, that associates its geometry to a domain discretized in finite volumetric elements, in which the flow of air and particles can be calculated.

The purpose of this project consists in building a model for the dispersion of particles in this closed environment, justifying any simplification or setup choice and using it to provide an assessment of the risk posed by the scenario based on quantitative data.

The challenge is to build a working model that can provide an accurate enough representation of the case, so to answer to some questions about the development of this accident scenario:

Does the fire in the bunker have a remarkable influence on the particle dispersion?

How do particles behave? Do they escape the instrument hall?

What are the main safety issues about the accident scenario that can be deduced from the model?

1.4 PROBLEM DELIMITATION

Due to the inherent complexity of the whole scenario, several restrictions have been decided on the final project. The simulation only concerns one of the instrument halls and the bunker, to save on geometrical complexity and computational expense. The particles that are going to be simulated and evaluated are only the tungsten particles. Phenomena such as radiation from heat and the impact from smoke are not evaluated.

The simulation only concerns calculation on the air flow and the particle behavior, without accounting for the internal layout of the building, the number and position of people inside the hall or their behavior. The air flow is calculated and considered only inside the hall and the bunker.

While the project describes the theoretical basis and justification for the choices of physical and mathematical models, it does not delve in full detail on their description, leaving it to the bibliography references.

1.5 METHODOLOGY

The method used in the report follows this order:

- Initial meetings with ESS – Initial definition of the scenario
- Literature and technical review – evaluation and choice of the software tools
- Definition of the boundaries and restrictions of the scenario
- Development of the dispersion model – meetings with ESS and LTH supervisors
- Calculation of the modeled scenario – meetings with LTH supervisor
- Post-processing and analysis of results
- Discussion and conclusions

In the preliminary meetings in ESS, the full case scenario was discussed, to delimitate the problem to its most relevant and feasible components. In the meantime, a research on literature of similar cases and studies was carried out, while CFD software tools were tested and evaluated, leading to Fluent as the software of choice for the project.

Literature search was first undergone to review cases and descriptions of particle dispersion in enclosed environments, with an emphasis on tungsten particles. Afterwards, literature review was focused on the mathematical description of fluid and discrete phases in a CFD simulation, especially regarding the forces affecting solid particles dispersed in an air flow.

To choose the CFD software to be employed in the dispersion model, literature review was paired to their empirical testing, including a research for benchmarking and validation of CFD modeling and on ensuring and assessing quality for CFD simulations. Finally, the literature on health effects of tungsten on humans and environment was researched.

The dispersion model was then developed, followed by the ESS and LTH supervisors, first in its geometry, boundaries and grid meshing, then defining the characteristics of the bunker fire and of the particles'. The case was then run and modified to adjust it and make it reach convergence thus yielding satisfying and reliable results. The definitive calculations were finally carried out at LTH with hardware support from the supervisor.

2 DEFINITION OF FLUID AND DISCRETE PHASES

2.1 COMPUTATIONAL FLUID DYNAMICS: WHAT IS CFD

Computational Fluid Dynamics (CFD) is the branch of fluid dynamics that uses numerical calculation methods (most commonly with finite volume methods) to solve problems involving fluid flows. A CFD software can simulate a case in which a fluid flow occurs interacting with an environment. This requires a number of steps:

Pre-processing: the geometry of the scenario is built through a CAD software or an embedded application, to define the contours of the domain and its characteristics. Then, as CFD implements a finite volume method, a mesh is generated to discretize the computational domain in said finite volume elements where the equations that govern the fluid flow can be solved. The quality of the mesh grid structure must be taken into high consideration, since the overall quality and convergence of the solution will depend greatly on it.

Solving: To define the case, the boundary conditions of the flow domain must be set, including the initial conditions of the case. Then the solver is set (if possible) to establish the physical models that will be implemented to solve the governing equations, including, most notably, the turbulence modelling and the particle tracking. The solution calculation can be initiated; for each assigned time step of the simulation a likewise assigned number of iterations is set to calculate the governing equations in the grid cells of the domain. Once the calculation is completed and the results obtained, the residuals and the convergence of the solution can be assessed.

Post-processing: the desired data obtained from the calculation is collected and visualized, often through a specific software tool.

The case scenario involved in this project shows two different phases for the fluid flow that must be solved; the proper fluid phase of the air flow and the discrete phase representing the dispersing particles. Before describing the software and scenario choices and settings, it is appropriate to include the mathematical description of the fluid and discrete phases

2.2 THE FLUID PHASE

The Computational Fluid Dynamics simulation must calculate the governing equations of the fluid phase of the chosen domain; to do so, it also must employ a certain degree of modelling of said equations and of the phenomena, such as turbulence, that they describe and imply.

Therefore, this chapter describes the governing equations of the fluid flow and outlines the turbulent models employed in the CFD simulation.

The main equations governing fluid dynamics are the continuity equation, the momentum (Navier-Stokes) equations and the energy equation (Davidson, 2016):

2.2.1 Continuity equation

The continuity equation for a continuous domain expresses the mass balance in the domain. If ρ is the density of the fluid and v is the velocity, for each *i* component:

$$\frac{d\rho}{dt} + \rho \frac{\partial v_i}{\partial x_i} = 0$$

For an incompressible flow, where ρ = constant, the continuity equation becomes:

$$\boldsymbol{\frac{\partial v_i}{\partial x_i} = 0}$$

2.2.2 The momentum equation

Starting from the momentum balance equation for a continuum:

$$\rho \frac{dv_i}{dt} = \frac{\partial \sigma_{ji}}{\partial x_j} + \rho f_i$$

Where the terms on the right side are respectively the net force due to the surface forces' stress tensor (σ_{ji}) and due to volume forces *f*.

Using the definition of stress tensor σ_{ji} and viscous stress tensor τ_{ij} for a Newtonian viscous fluid:

$$\sigma_{ji} = -P\delta_{ij} + \tau_{ij} = -P\delta_{ij} + 2\mu S_{ij} - \frac{2}{3}\mu S_{kk}\delta_{ij}$$

Where P represents the pressure, S is the symmetric strain-rate tensor and μ indicates the dynamic viscosity. Substituting in the momentum equation yields the "proper" *Navier-Stokes equations*:

$$\rho \frac{dv_i}{dt} = -\frac{\partial P}{\partial x_i} + \frac{\partial}{\partial x_j}\left(2\mu S_{ij} - \frac{2}{3}\mu \frac{\partial v_k}{\partial x_k}\delta_{ij}\right) + \rho f_i$$

In most studies, including this report, the flow is considered incompressible, while the dynamic viscosity can be regarded as constant. Taking from the continuity equation above, the second term inside the parenthesis becomes zero, while the first one can be rewritten, using the definition of S_{ij}:

$$S_{ij} = \frac{1}{2}\left(\frac{\partial v_i}{\partial x_j} + \frac{\partial v_j}{\partial x_i}\right)$$

Thus:

$$\boldsymbol{\rho \frac{dv_i}{dt} = -\frac{\partial P}{\partial x_i} + \mu \frac{\partial^2 v_i}{\partial x_j \partial x_j} + \rho f_i}$$

2.2.3 The energy equation

The energy equation for a volume of continuous and incompressible fluid phase can be written as:

$$\boldsymbol{\rho c_p \frac{\partial T}{\partial t} = \Phi + \frac{\partial}{\partial x_i}\left(k \frac{\partial T}{\partial x_i}\right)}$$

Where c_p is the heat capacity at constant pressure (assumed to be constant) while $\Phi = 2\mu S_{ij} S_{ij} - \frac{2}{3}\mu S_{kk} S_{ii}$ represents the viscous terms, whose components are above described; $-k\frac{\partial T}{\partial x_i}$ is the expression of the conductive heat flux according to the Fourier law. (Davidson, 2016)

2.3 DEFINITION OF TURBULENCE

Fluid motion can be described as turbulent or laminar; almost all the situations involving fluid flows in real-life are turbulent. The characteristics of turbulent fluid flows are:

Irregularity: as the term itself suggests, turbulent flow is irregular and apparently disorganized, despite being still governed by the Navier-Stokes equations. The chaotic flow is still deterministic in nature, even though it cannot be yet described in such sense.

Diffusivity: Turbulent flow increases diffusivity, in the exchange of momentum, mass, energy and heat. This implies effects such as increasing attrition and heat transfer in enclosed flows, or delays in flow separation around bodies. The increased diffusivity is a defining feature of turbulent flows, as the apparent randomness of some flows (e.g. wing contrails) is not sufficient to call them turbulent.

Large Re: Turbulence always occurs at high Reynolds numbers, meaning that a growing ratio between inertial and viscous forces has an important role in destabilizing flows

3D: turbulent flow is always three-dimensional, the vorticity fluctuations and stretching being an essential component

Dissipation: Turbulent flow is always dissipative, meaning that kinetic energy is dissipated by viscous stresses into thermal energy. Dissipation also implies that turbulent flows, unless supplied by energy, are bound to rapidly decay.

Continuum: Turbulence is not a property of the fluid medium but of the flow, and knowing that the smallest turbulent structures are still orders of magnitude larger than molecular scales, turbulent flow can safely be regarded as a continuous domain. (Davidson, 2016)

2.3.1 Turbulent scales

The turbulent flow can be visualized as building up in eddies of different sizes, or turbulent scales, defined by their length scale and velocity. The larger scale eddies usually have dimensions of the order of magnitude of the domain (l_0).

A turbulent flow thus presents different dimensional scales, or eddies, where kinetic energy is transferred from larger scale eddies to smaller ones, until reaching the smallest scales at which viscous effects become predominant, dissipating the kinetic energy into thermal energy. This phenomenon is called the *cascade process.*

The transferred kinetic energy per time interval remains the same for each scale size; although the viscous friction forces are present at all turbulent scales, the vast majority of the kinetic energy in the larger eddies is dissipated at the smallest scales, therefore also called dissipative scales (l_η).

The smallest dissipative scales are called Kolmogorov scales; they are defined by the kinetic viscosity, since the viscous forces determine the dissipation of the kinetic energy, so the larger the viscosity, the larger the dissipative scales.

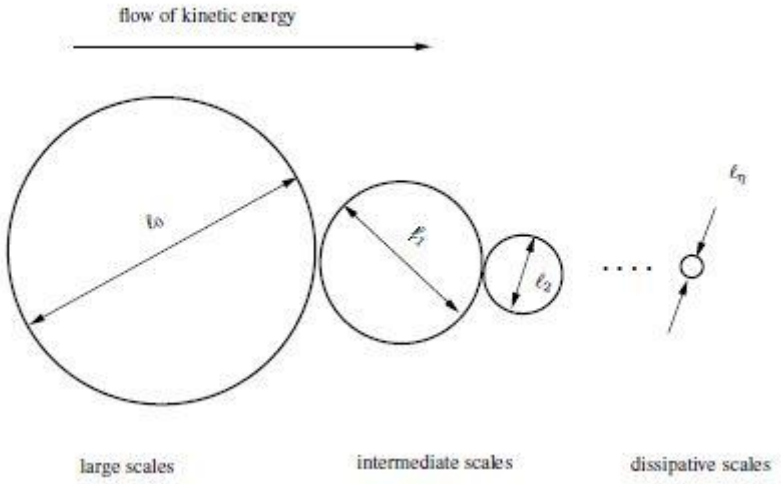

Figure 7 A graphical representation of the cascade process (Davidson, 2016)

2.3.2 Estimate of turbulent length scales

A precise estimation of turbulent scales depends on many factors, including dimensions and characteristics of the domain and the magnitude of the Reynolds number in the flow. One way to have a basic estimate of the dissipative scales relates directly to the length of the largest energy scales and their Reynolds number:

$$\eta = \frac{l}{Re^{0.75}}$$

Where *l* is the length of the largest scales, η is the length of the dissipative scales and Re the Reynolds number proper of the larger scale *l* in the flow. (McMurtry, 2000)

For our case, a rough and conservative estimate of η can be made considering *l* ≈ 20 m and a Reynolds number between 2000 and 3000, typical of lower intensity turbulent flows and suitable for a large room without large velocity magnitudes (5-10 m/s). This yields a range for the dissipative scales between 0.05 and 0.067 m.

2.4 DISCRETE PHASE

This section will describe the definition of the particles and the methods used for their tracking and their interaction with the fluid flow phase. There will be a description of the assumptions made regarding the particle definition and boundary conditions, the coupling between fluid and discrete phase and the forces involved.

2.4.1 Particle definition

Particles can be defined in several ways, for example as massless particles or droplets. As for this case, since they are composed of heavy oxidized metal and assumed not to breakup or combust, it is assumed that they are inert particles, also considering that the primary interest rests in their dispersion behavior.

Inert particles obey force balance equations and inert cooling/heating equations.

2.4.2 Particle material

All the particles in the simulation are set to be made of tungsten (tri) oxide (WO_3), the material expected to be expelled from the tungsten target wheel and to be the main source of ionizing radiation. The material properties used are listed in Table 1 (Samokhin et al., 2015) (Wikipedia.org, 2017). It is assumed that these properties will remain constant throughout the whole simulation since the temperatures will not be close to the melting temperature of tungsten.

Table 1 Particle material properties of tungsten trioxide

Density (Kg/m^3)	**12110**
C_p – Specific heat (J/Kg-K)	130
Melting point (K)	1746

2.4.3 Particle sizes

As seen in other studies, the dispersed particles of WO_3 are designed to have a variety of sizes approximated to a range between 10^{-7} and 10^{-5} m. (Samokhin et al., 2015)

The distribution of the particle dimensions in the simulation follows the Rosin-Rammler probabilistic distribution, which is an adaptation of the widely-used Weibull distribution function first adapted to particles by P. Rosin and E. Rammler in 1933.

Basing on the assumption that there is an exponential relation between the particle diameter (d) and the mass fraction of particles whose diameter is larger than d (Y_d), the equation for this distribution can be written as:

$$Y_d = 1 - e^{-(\frac{d}{\bar{d}})^n}$$

Where n is the spread (size distribution) parameter and $\bar{d}$ is the size constant, in this case the mean diameter (Ansys, 2016).

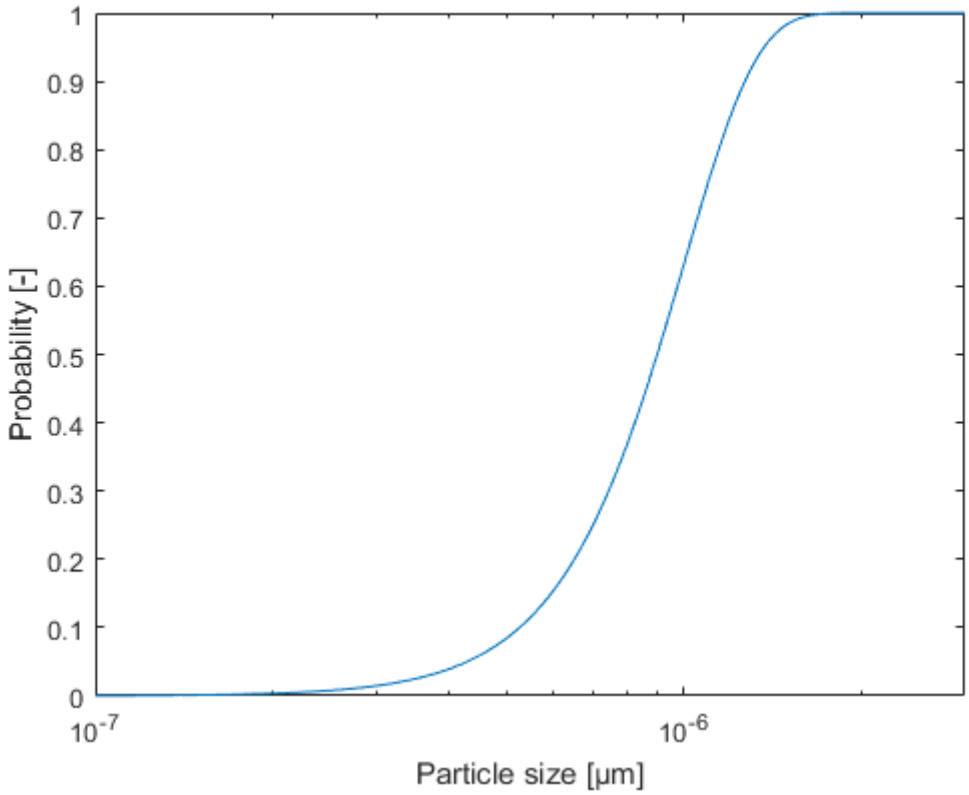

Figure 8 The Rosin Rammler probabilistic distribution

Considering the size range of particles and their number, which can be expected as very high, and the graph above showing the correlation between particle size and probability of occurrence, that takes into account the mass fraction of the particle size, a majority of the particles is expected to belong to the smaller sizes (therefore, around 10^{-7} m diameter), since all the particles have the same density.

2.4.4 Particle tracking method definition

Particles are tracked following a Eulerian-Lagrangian frame method. This method integrates the equations of motion of the particle to yield its properties.

Thus, the trajectory of the particle is calculated integrating the force balance equation from Newton's second law of motion:

$$\rho_P \frac{du_i^P}{dt} = \rho_P F_{drag}\left(u_i - u_i^P\right) + g_i(\rho_P - \rho) + F_i$$

Where F_{drag} is the drag force dependent on relative velocity, the $g_i(\rho_p - \rho)$ is the gravity force component, while F_i represents all the other forces involved in the particle motion (Bakker, 2006b).

The Basset-Boussinesq-Oseen law, written in 1983 to describe the forces acting on a rigid, non-rotating sphere, and they sum up all the forces acting on a solid particle:

$$F_{tot} = F_{drag} + F_{lift} + F_{hist} + F_{admass} + F_{thermop} + F_{buoy} + F_g$$

These forces are now quickly listed and evaluated: deciding which forces have the most influence in the particle motion is of capital importance, since adding more forces to the simulation will increase its accuracy but inevitably will result in heavier computational cost. Therefore, where possible and justified, some of these forces may be excluded from the calculation.

Drag force (F_{drag})

The drag force is one of the primary forces affecting bodies moving in a fluid, and the inert particles we are considering make no exception. Drag force is directed opposite the direction of the particle motion; it manifests due to differences in velocity between the body and the fluid flow around it and it's caused by the friction between the boundary layer on the surface of the particle and the fluid.

The term appearing in the above expressions is defined as:

$$F_{drag} = \frac{18\,\mu\,C_d\,Re}{24\,d_p^2}$$

Where μ is the molecular viscosity of the fluid, C_d is the drag coefficient and Re is the (relative) Reynolds' number.

$$Re = \frac{\rho\,d_p|u_p - u|}{\mu}$$

Saffman's lift force (F_{lift})

This term includes the lift force due to shear, i.e. the force caused by the passage of the particle through shear layers. It depends on the variation of speed in the fluid flow, akin to the drag force. This velocity difference causes a pressure difference that creates a net force directed towards the lower pressure region.

The expression for Saffman's lift force is:

$$F_{lift} = \frac{2\,K\sqrt{v}\,\rho_f\,d_{ij}}{\rho_p d_p (d_{ij}d_{ji})^{1/4}}\,(u - u_p)$$

Where d_{ij} is the deformation tensor and K is a fixed value.

Basset's history force (F_{hist})

This force is dependent on the history of accelerations in the fluid flow, and the time delay that they cause in the development of the boundary layer. It is defined as:

$$F_{hist} = \frac{3}{2}d_p^2\sqrt{\pi\rho_f\mu_f}\int \frac{\frac{du}{dt} - \frac{du_p}{dt}}{\sqrt{t - t'}}\,dt'$$

Virtual added mass force (F_{admass})

This force is caused by the acceleration of the particle, that also accelerates the fluid in its close vicinity, thus making it behave as if it belonged to the particle itself. It can be written as:

$$F_{admass} = \frac{\pi}{12}d_p^3\rho_f\left(\frac{du}{dt} - \frac{du_p}{dt}\right)$$

Thermophoretic force $(F_{thermop})$

The thermophoretic force acts as an effect of the large temperature gradients in the fluid flow around the particle: the difference in kinetic energy between the cool and the hot molecules colliding the particle cause it to experience a net force directed towards the lower temperature region. Given $D_{t,p}$ as the thermophoretic coefficient for the particle, this force is defined as:

$$F_{thermop,x} = -D_{t,p}\frac{1}{m_p T}\frac{\partial T}{\partial x}$$

Photophoresis force is another thermodynamic effect on the solid particle, and it's a force occurring similarly to the thermophoretic force above descripted, caused by the net difference in radiation heat transfer and the momentum transfer through photons colliding with the particle

Buoyancy force (F_{buoy})

An easily noticeable macroscopic force, buoyancy is the well-known force that is produced by the hydrostatic pressure gradients in the fluid flow surrounding the solid particle. The buoyancy effects in fires are a well-known phenomenon, and in this case, they are expected to play a major role:

$$F_{buoy} = \frac{\pi}{6}d_p^3\rho_f\frac{du}{dt}$$

Gravity (F_g)

As already defined above, the effect of gravity on the particle is also accounted for.

The Brownian motion force was left aside as it is relevant only for very small particles in a laminar flow, which is not certainly the case here in this report.

2.4.5 Assessment of forces not to consider

Since the difference in density between the fluid (air) and the particles (tungsten tri-oxide) is of several orders of magnitude, forces such as the Basset's history force, Saffman's lift force and virtual mass force can be neglected. As already said, the regime of the flow is not laminar, so the Brownian motion can be safely cast aside. Since there will be no modelling of radiation, the photophoresis force is also neglected, as well as the thermophoretic force, since in most of the fluid flow significant temperature gradients are not expected, and the particles are not small enough to be affected in a remarkable way (Ansys, 2016).

The equations describing the force balance of the particles can therefore be rewritten:

$$F_{tot} = F_{drag} + F_{buoy} + F_g$$

$$\rho_P\frac{du_i^P}{dt} = \rho_P F_{drag}\left(u_i - u_i^P\right) + g_i(\rho_P - \rho) + F_{buoy}$$

The drag, gravity and buoyancy forces, those that are going to be considered in the particle tracking, are indeed those that the software Ansys Fluent considers by default, as can also be seen in the user interface.

In particular, the buoyancy force, while still included, gives a very small contribution; this can be evaluated with a quick hand calculation, which shows that for a 1 µm particle the value of the buoyancy force is of the order of 10^{-18} N.

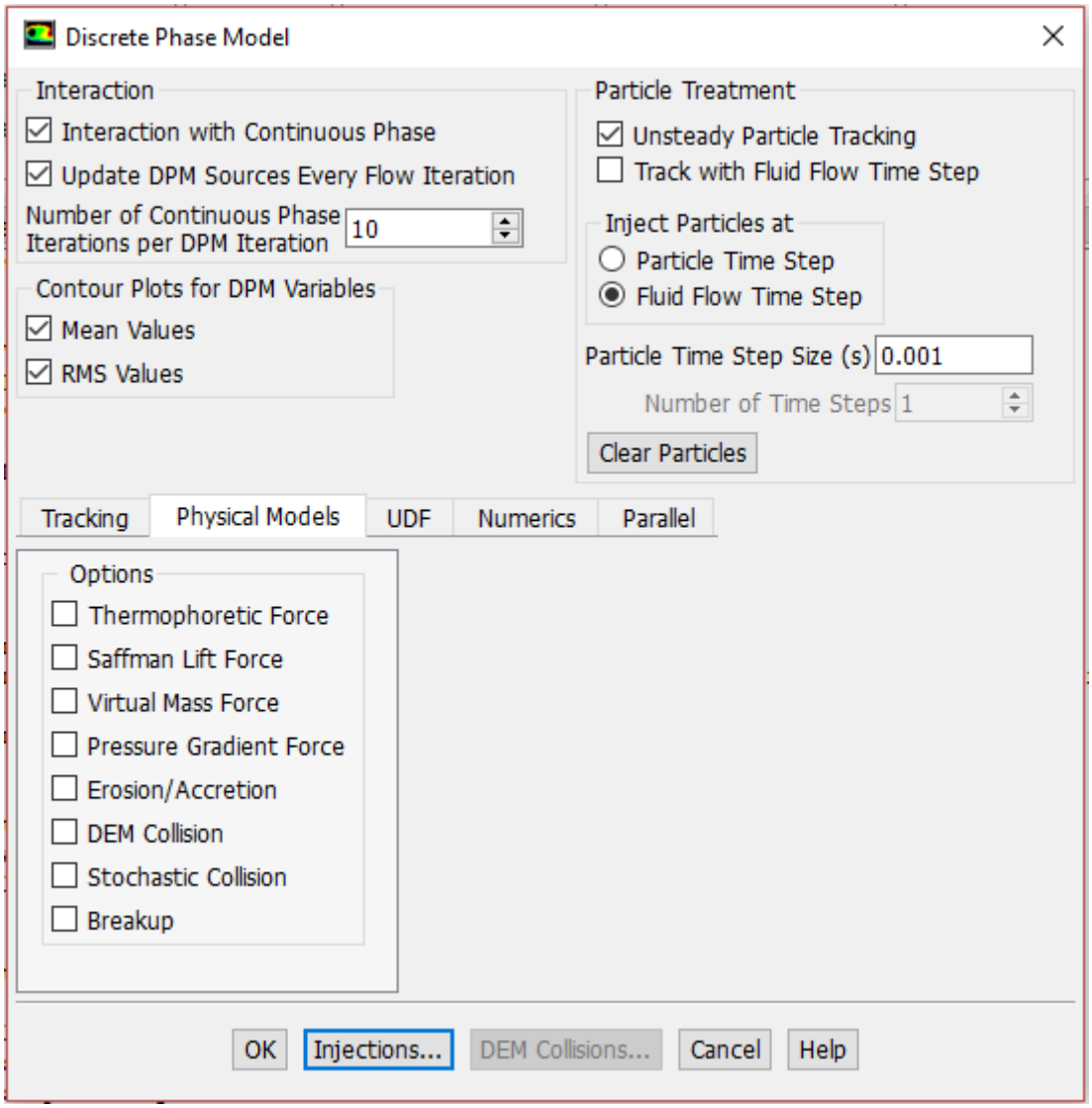

Figure 9 The setup interface in ANSYS Fluent for the discrete phase. It is shown how the previously mentioned forces to be neglected can be easily switched off from the model

.

2.4.6 Coupling between phases

The fluid and discrete phase interact with each other in terms of exchange of heat, momentum and energy; the nature of the interaction between the particles and the fluid is very important in determining the setup of the flow field.

The coupling between phases is usually divided into three categories; one-way, two-way or four-way coupling. They are defined as follows (Bakker, 2006b):

- One way coupling: or 'uncoupled' approach, the fluid phase influences the discrete phase through transfer of pressure and velocity values, especially from drag forces and turbulence. The particles have no influence whatsoever on the fluid phase; therefore, this approach is the least computationally expensive.

- Two-way coupling: the fluid influences the discrete phase as in the one-way approach, while also the particles influence the fluid phase through source terms of heat, momentum and energy

- Four-way coupling: adding to the interactions already described, the four way coupling also has the particles colliding, thus influencing each other in terms of heat, momentum and energy exchange, so that added to the two-way interaction with the fluid there is a two-way interaction between the components of the discrete phase itself.

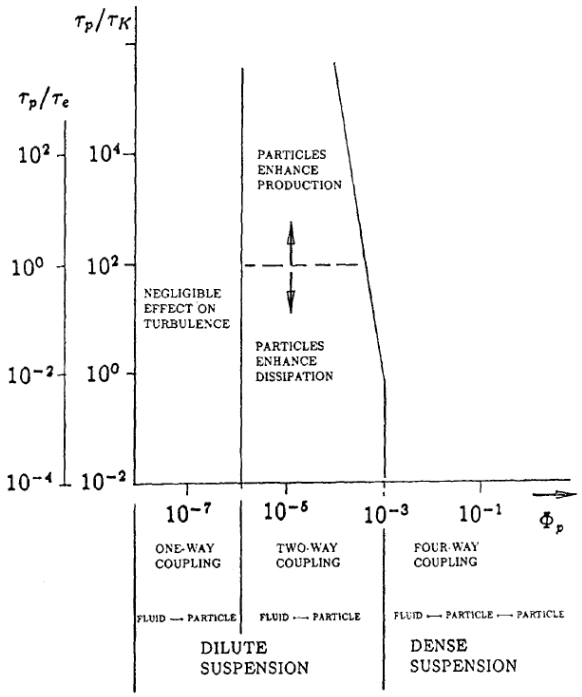

Figure 10 Table comparing volume fraction of particles to the effect on the fluid turbulence (Jadidi et al., 2015)

As can be seen from the above figure (Jadidi, Moghtadernejad, & Dolatabadi, 2015), there are two main regimes that can be defined regarding a flow with two distinct phases; dilute suspension and dense suspension state. The regime nature is used to assess what type of coupling is worth implementing.

A dilute suspension state occurs when the spacing between particles is large enough to consider an interaction between two particles as statistically rare, so that the forces governing the fluid phase take full control on the particle trajectories.

To assess this, the volume fraction of the particles in relation to the domain must be assessed; it is defined as:

$$\varphi_p = \frac{NV_p}{V}$$

Considering a maximum quantity of particles as around 1 kg and the volume of the bunker only, we have NV_p= 1/12110 and V = 300 m^3 thus we obtain $\varphi_p \approx 2.75 \cdot 10^{-7}$ which is well within the one-way coupling side for the dilute regime of the above graph (which is set as $\varphi_p \leq 10^{-6}$) also bearing in mind that the full volume of the domain was not even considered.

It can be safely said that a one way coupling between the fluid and the discrete phase is suitable and justified in this simulation.

Summary

The CFD software's central task is to solve the governing equations of the fluid flow, which is considered as a continuous domain. These equations consist in the continuity equation, the momentum Navier-Stokes equations and the energy equation. Additionally, the fluid flow is considered incompressible and with a constant value of dynamic viscosity (Davidson, 2016).

The tungsten-trioxide particles that are dispersed in the domain are modelled as a separate discrete phase that interacts with the fluid flow. The CFD software's task is to calculate the trajectories of the particles and track them inside the domain. To do so, a Eulerian-Lagrangian tracking frame method is used, solving the force balance equation of the particles (Ansys, 2016).

To simplify the calculations, only the forces that are relevant to the particle motion are taken into account: the gravity force, the buoyancy force and the drag forces caused by the velocity and pressure gradients around the particles.

3 SOFTWARE CHOICE AND MODELLING SETTINGS

3.1 COMPARISON AND CHOICE OF CFD SOFTWARE

The choice of the specific CFD software tool to be used in the simulation is not a trivial task; software limits and capacity can vary substantially and have a remarkable role in the final quality of the simulation.

For this project, three software tools were considered; following is a list of their general characteristics and the reasons that led to the final choice.

3.1.1 Fire Dynamic Simulator (FDS) 6

Developed by the U.S. governmental agency NIST (National Institute of Standards and Technology) as a completely freeware CFD tool, FDS 6 was naturally the first software to be considered. It is of course the most used CFD program used for fire engineering purposes, and its freeware status makes it easy to obtain.

FDS is a very straightforward program; although based on text files written in Fortran-based language, the code it uses to setup parameters is rather simple and unambiguous. The main applications of FDS are in the modelling of low speed flows, putting particular emphasis on heat transfer and smoke, as the primary reason for its development is the study of evolution and dynamics of fire.

FDS uses a Large Eddy Simulator solver, which implements the Deardoff sub-grid scale model as of the 6th version (while previous ones used the Smagorinsky-Lilly model). There is no possibility of switching to other turbulence models and there is only one solver available.

FDS allows only for hexahedral mesh cells to be used, and geometric features are pretty limited to simplified shapes that have to be written in the code, with little to no possibility for an import of more complex geometries from CAD software. Moreover, FDS requires the mesh structure to adapt to the geometry of the domain, not allowing to do vice versa.

Nevertheless, FDS has Smokeview, a well-built companion software for viewing and post processing output results, versatile and with a simple menu interface, which FDS itself does not have. FDS also gathers data easily collectible in Excel spreadsheets (McGrattan et al., 2014).

FDS is very stable and provides results in little time, provided it is used within the range of its intended use, for which it has been extensively validated (U.S.N.R.C., 2007). Other applications, such as the tracking of particles which is the focus of this report, have not been developed as well as the fire dynamics in such software, while the difficulty in adapting geometries and grid structure does not allow for much versatility in the meshing.

3.1.2 OpenFOAM

OpenFOAM is an emerging freeware and open source CFD software which, quite opposite to FDS, is not being developed by a single organization but rather from a foundation where users contribute to the development of the code (Jasak, 2009). Therefore, OpenFOAM proves to be extremely versatile and adaptable to many applications. Several types of solvers have been developed, including RANS and LES turbulence models or solvers specialized in fire dynamics (such as FireFOAM) or particle tracking. It is possible to implement different types of mesh and export of grid structures or geometries built in third-party software is allowed. The input files, code-based as in FDS, use a highly customizable code. Post-processing software, such as ParaView, is also open-source and versatile (OpenFOAM, 2016).

On the other hand, OpenFOAM has a fragmented user community, and little to no unified documentation; the learning curve is steep and implementation of customized applications may prove rather arduous. As in FDS, there is no graphical user interface. Additionally, OpenFOAM cannot rely on the level of validation enjoyed by FDS.

Despite its versatility, the difficulty in using such software did not make it the best choice for this project.

3.1.3 ANSYS Fluent

A well-known proprietary software developed by ANSYS, Fluent is a reliable and user-friendly software, which includes an in-built CAD tool as well as a meshing tool, which allow for several different applications. Fluent has a good array of choices for turbulence modelling (including LES and several RANS based models) and for meshing. It has a graphical user interface which makes its learning curve significantly easier than with the other two software tools (Ansys, 2016).

The lower side of Fluent is its post processing tools, from which is not easy, or sometimes even possible, without using additional software, to obtain the desired data.

Fluent was chosen as the CFD software tool as it is one of the most used programs, with a sizeable documentation and support from both community and the developers; together with its relatively easy learning curve, it made the best choice for particle tracking modelling, since it has been extensively used for such purpose.

3.2 TURBULENCE MODELLING: GENERAL STRATEGIES

To be able to model and calculate the turbulent effects in a viable way, several strategies have been devised to be implemented in CFD simulations.

The main issue in describing turbulence is managing to consider the contribution from all dimensional scales. A turbulence model consists in devising a method to effectively solve the Navier-Stokes equations. A brief description of the most prominent turbulence model strategies will now follow.

3.2.1 DNS (Direct Numerical Simulation)

Conceptually it is the simplest strategy: it consists of a numerical calculation of the Navier-Stokes equations on all possible scales, with no "compromises": the equations are numerically solved as they are without any turbulence modelling. Given the inherent complex nature of the governing equations of the fluid flow, this translates in an exceedingly high computational expense, making DNS calculations suitable for simple flows only. Given today's available computational capacity, DNS is not viable for complex turbulent flows, let alone those involving combustions or particle tracking (Versteeg & Malalasekera, 2007).

In a not-too distant future, if the Moore's law on computational power holds true (Moore, 2006), DNS calculations will probably become more commonplace to industrial and research applications (Wols, 2011).

3.2.2 RANS (Reynolds-Averaged Navier-Stokes equations)

It's the most used family of turbulence modelling; RANS models aim at solving an averaged mean flow, decomposing the variables of the fluid flow in a component averaged in time and a fluctuation component, this process called Reynolds decomposition; for example:

$$u = \bar{u} + u'$$

Where u is the velocity, decomposed into the time-averaged mean term $\bar{u}$ and the fluctuating term u'. The same decomposition is applied for pressure, stresses and so on.

RANS methods calculate the mean flow, while modelling the fluctuating parts to define how much the turbulence affects the fluid flow. This method is very computationally efficient; it is independent from the mesh grid, while the time averaging allows for steady-state solutions. On the other hand, by time-averaging the variables of the flow, most instantaneous effects are lost or underestimated (Versteeg & Malalasekera, 2007).

3.2.3 Choice of turbulence model: Large eddy simulations (LES)

This turbulence modelling strategy derives from the intuition of Russian mathematician Andrej Kolmogorov that turbulent structures with high Reynolds numbers are dependent on the domain geometry at larger scales, while they are more universal at smaller scales.

Developing from this idea, the LES turbulence model consists in explicitly resolving the larger eddies of the flow while implicitly modelling the smaller ones through a sub-grid-scale (SGS) mathematical model. So, instead of being averaged in time, the flow is filtered in space (averaged in volume). This also implies that LES simulations are time-dependent (transient).

The disadvantage of the LES model is that its accuracy is dependent on the quality of the grid mesh and on the time steps; this also implies that LES is a computationally expensive model, especially when compared to RANS (Davidson, 2016).

Nevertheless, given a fine enough mesh and an adequate time step interval, LES solutions are remarkably accurate. LES was chosen over RANS because of its ability to grasp stray and unsteady variations in the flow, that would be lost in the averaged solutions provided by the RANS model. Furthermore, the benchmarking with the validated Steckler room case is to be made with a software, FDS, that uses LES by default. (Bakker, 2006a).

Furthermore, most of the forces and effects affecting the discrete phase are expressed in the larger eddies' scales: solving them in the most accurate way is therefore essential to obtain significant results. It is then assumed that small-scale viscosity dissipation does not indeed play a large role in the particles' behavior.

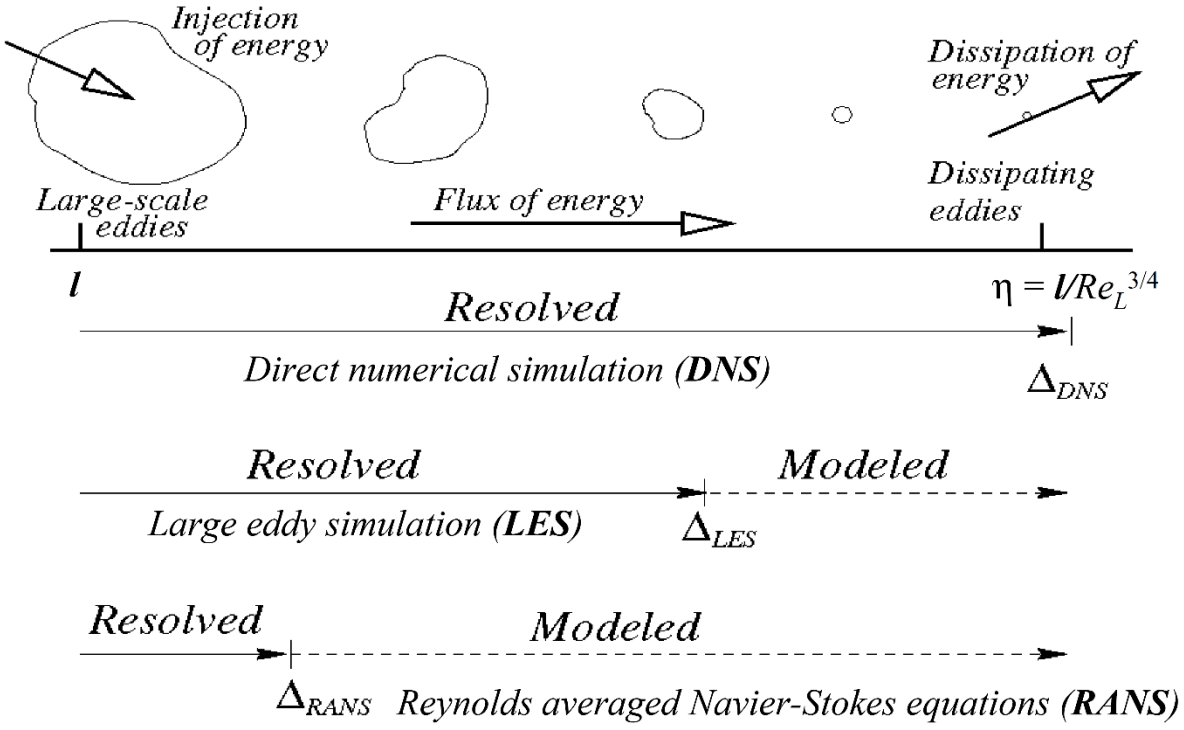

Figure 11 A comparison between the main turbulence modelling strategies (Bakker, 2006a)

ANSYS Fluent allows to model turbulence with LES; subsequently, the Smagorinsky-Lilly sub-grid-scale model was chosen to deal with the smaller scale turbulent structures.

The Smagorinsky-Lilly model is one of the simplest and most proven SGS model (Ansys, 2016); it was chosen to save computational time, given how the smaller scales have relatively little importance in the large scales involved in this project.

3.3 SOLVER SETTINGS AND METHODS

ANSYS Fluent allows to choose the main settings of the solver software; the setting of choice consists in a pressure-based transient solver, since the case is decidedly time-dependent and would not be properly described by a steady-state solution. This type of solver is implicit, and it uses momentum and pressure as its main variables. The solver algorithm can be segregated (where momentum and pressure are solved in sequence) or coupled (where they are solved simultaneously); the second option is chosen since it is more computationally efficient, employing the SIMPLE (Semi-Implicit Method for Pressure-Linked Equations) scheme, that is based on a pressure-velocity coupling and is the default coupling algorithm for ANSYS Fluent, as well as the most robust (Ansys, 2016) (Ansys, 2006).

The turbulence model, as already described, is the Large Eddy Simulation (LES), associated with the Smagorinsky-Lilly sub-grid scale model.

The buoyancy in the flow is modelled through the Boussinsesq approximation model, which treats density as constant throughout all solved equations, except for the buoyancy term (included in the f_i volume forces' term) in the momentum equation. This model is suitable as long as small changes in density and temperature are expected in the domain.

Discretization

Spatial discretization consists of the interpolation scheme that is used for the main variables (pressure and momentum) as well as for the gradients and the energy equation. The schemes employed are as follows:

Table 2 Discretization settings

Pressure	**Second Order discretization, slower convergence but more accurate results**
Momentum	Bounded Central Differencing, since it is the best suited for LES turbulence models
Gradient	Least Squared Cell Based, accurate scheme recommended for polyhedral meshes
Energy	Second Order Upwind

The schemes used have all second order precision, to make the best of the available grid refinement; likewise, the transient formulation (the time discretization) follows the Bounded Second Order Implicit scheme.

3.4 MESHING

As this model is based on a finite volume discretization method, it is naturally implied that the mesh cells which make up the computational domain assume great importance.

There are several ways to create and implement a mesh in a CFD simulation; for this project, the embedded mesh builder included in the ANSYS Workbench was the tool of choice, given its obvious accessibility and versatility.

The meshing tool in ANSYS allows to choose the shape of the grid cells, which is not the case, for example, of FDS. Since the shape of the cells can have a remarkable influence on the overall solution, choosing the right one is rather relevant.

ANSYS Meshing automatically generates meshes composed of tetrahedral cells; this because this shape is the most adaptable to different and complex geometries while also having a high degree of grid generation automation. The downside of this cell shape is that it usually builds up irregular and randomized structures that negatively influence the calculation time and efficiency (Ansys, 2014).

For this reason, a hexahedral cell configuration was chosen: the limit of this kind of grid is the relative difficulty to adapt to complex geometries; such is not the case of this project, where the domain is a combination of parallelepipedal bodies.

On the other hand, the hexahedral cells give the best computational efficiency, in terms of both time and resources; ideally, cells should be cubic or almost cubic, as this geometry is proven as the best to capture the flow vorticity. Conveniently, the ANSYS meshing tool allows to adapt a hexahedral grid to the geometry (Ansys, 2014).

It has already been mentioned that the LES turbulence model is based on the direct resolution of the larger scale eddies while on the sub-grid scales the flow would be modeled. This implies that the quality and accuracy of the solution of LES simulations relies heavily on the mesh refinement.

As previously mentioned, the turbulence model relies on the subdivision of the turbulence structures into dimensional scales; ideally, the grid size is based on the scales of turbulence that occur into the domain. There is no reliable general or formal definition for the turbulent scales, which depend on each case and geometry.

Since the LES models the dissipative – viscous smaller scales, and solves the larger energy scales, the size of the grid cells should be in the intermediate inertial scales range, to ensure that the “cut-off” between the solved scales and the Sub-Grid modeled scales occurs within the order of magnitude of the cells. Ideally, the best grid refinement has the cells of the order of magnitude of the dissipative scales, but this is generally too costly for most cases (Zhiyin, 2015).

There are several empirically proven ways to improve and ensure the quality of a mesh grid; first and foremost, the mesh cells should be as geometrically homogeneous as possible, avoiding excessive stretching or distortion of the single cells as well as ensuring smooth and gradual transition between cells, i.e. not letting cell density change abruptly (Ansys, 2014).

There are verifiable parameters that can quantify these features:

- Skewness (generally recommended to be kept < 0,95): this parameter indicates how close the cell is to an ideal shape, be it equilateral or equiangular, where 0 corresponds to the ideal and 1 to a completely degenerate shape. In the case of hexahedral cells, the closest the cell is to a cube, the lower (and better) the skewness parameter.

- Aspect ratio: the ratio of the sizes in a cell, namely between the longest and shortest side; it should ideally be close to 1. This parameter tells how much the cells are stretched.

- Orthogonal quality (recommended to be at least > 0,1): it indicates, on a scale from 0 to 1 (1 being the best value) how well connected the cells are to the adjacent ones, through the calculation of the face normal vectors.

These parameters can be easily verified on ANSYS Fluent or on the meshing tool (Ansys, 2016).

3.5 CONVERGENCE

Convergence is defined by the software as the achievement of a small enough difference between the solutions obtained in consecutive iterations of the calculation. It is then a very important part of the evaluation of the simulation results. (Ansys, 2016)

It is often stated that, in any CFD simulation, the convergence at each time step and the number of iterations needed to achieve it is an immediate sign of the quality of the simulation. For example, the default convergence criterion for ANSYS Fluent is for the continuity equation residuals, scaled using a factor representative of the flow rate, to drop to 10^{-3} and for the energy residuals to drop to 10^{-6} (Ansys, 2006).

But that is not always the case, especially when dealing with large domains and meshes; a converged solution can still yield unrealistic results.

A way to check the qualitative convergence of the solution is to control the history of residuals during the iterations. Residuals of the calculated variables are counted and stored at each iteration.

A common approach is to check that, during the calculation, the unscaled residuals drop by (at least) three orders of magnitude. This is particularly suitable for this project, in which a pressure-based solver is used.

Even so, this requirement could not be entirely valid; if the initial conditions of the simulation are a good enough guess, the unscaled residuals might drop by less than three orders of magnitude.

Residuals will be addressed in the evaluation of simulation results.

Another parameter that influences convergence is the *under-relaxation factor* (URF) of the governing equations. The under-relaxation of equations controls how variables are updated through each iteration, for all equations that are calculated by the solver software, and it can be set by the user at their discretion. (Ansys, 2016).

3.5.1 Errors and their mitigation

As easily predictable, there are several sources and causes of error in a CFD simulation, as for any other engineering application (Ansys, 2014). the type and description of these errors are now listed, together with their possible reduction or mitigation.

- Model errors

They include the errors caused by incorrect or overly imprecise models for the simulation, such as unrealistic boundary conditions, geometry issues, or inadequate mathematical models. Provided that the case is well posed and its settings well understood, this kind of error is the most easily avoided. Examples of model errors may come from inadequate solver settings (steady-state instead of transient), turbulence models (RANS vs LES), combustion or particle coupling models.

Systematic errors caused by excessive approximation of geometry or boundary conditions may hinder the solution even though the best possible models are employed.

Validation of the model, if possible, can help detect and solve this type of errors, otherwise an empirical justification of the employed models must suffice.

- Solution (discretization) errors

Consisting of the difference between the properly converged solution and the exact “actual” solution of the governing equations. Ideally, an infinitely refined grid would yield the exact solutions. This is of course an error source that cannot be eliminated, but which depends on the level of mesh refinement. When possible, the solution error can be quantified if there is documentation on the exact solutions for the case, therefore, if verification of the model is achievable.

It is also possible to decrease the discretization error by choosing a higher order discretization scheme; for example, Fluent allows to choose between 1^{st} or 2^{nd} order upwind discretization. 2^{nd} order generally yields better solutions for less refined meshes and its use is advised by the developers for LES turbulence models.

- Iteration errors

It’s the error between the converged solution and the result at a certain iteration. Convergence criteria, such as those discussed above, are what determine the extent of these errors.

- Round-off errors

They are determined by the numerical precision at which the computing machine works; the truncation errors caused by approximating infinite sums as finite are an example. Choosing to run the case at double precision, as ANSYS Fluent allows, minimizes round-off errors.

Summary

Since it can be hard to correctly determine the accuracy yielded by the grid refinement, what can be done to ensure maximal reduction of errors is ensuring the quality of the mesh is the best achievable, by checking its geometrical properties and the parameters above mentioned, in addition to the best possible grid refinement. Second order space and time discretization, although making the calculation slower and more computationally heavy, yield better precision, as well as the implementation of double precision of the computing machine. (Ansys, 2014)

4 VERIFICATION AND VALIDATION

When using CFD, the issue of how it sticks to the models it is based from, as well as how it is a reasonable representation of reality, is of course very important.

In the common terminology, *verification* consists in the process to determine whether the implementation of a mathematical model by the CFD software complies with the expected solution of the governing equations of such model, i.e. to ensure the equations are solved properly (Oberkampf & Trucano, 2002).

Validation is instead the process to confirm that the model employed and the solution provided by the software is an accurate enough representation of reality and therefore that the right model and governing equations are employed and solved. It is good practice to have it always preceded by verification (Oberkampf & Trucano, 2002).

Validation is obtained by comparing results with relevant experimental data, which means that it could be problematic or impossible to achieve for cases where there are no previous measurements available, or there is no possibility to run experiments to compare the results.

In the case of this project, it has already been stated that recreating the conditions that it is meant to simulate would be extremely expensive and dangerous, the main reason being the large size of the enclosed environment.

Consequently, a direct validation appears to be beyond the possibilities of this project; but the use of benchmark cases, which have been themselves validated, could yield at least an indirect validation of the model or of parts of it.

4.1 THE MODELLING OF THE FIRE

In the situation to be simulated in this project, the presence of a fire in the bunker is of particular concern, for two main reasons:

- The fire is, expectedly, the main driving force for the particle motion in the domain, since it provides strong buoyancy effect

- The fire can also be computationally demanding to model, affecting the overall calculation timespans

The bunker fire, apart from the estimations carried out by ESS on its heat release rate (Jörud, 2013), is also rather loosely defined, making it necessary to generalize its characteristics, since it is not known at this point what materials and equipment will be present on site.

Therefore, some attempts have been made to offer a simplified yet accurate enough model for the fire in the bunker. They are quickly listed here:

4.1.1 Simple heat source

ANSYS Fluent allows for a specified surface to release heat in the domain, needing only to set the heat release rate (HRR) per unit area. Despite seeming a straight and easy solution, a heat source defined as such is not suitable to simulate a pool or otherwise area defined fire; this is likely because the gradients are too high to be properly resolved with the available computational resources. The temperatures developed in the simulation soon increase at an unnatural rate, causing the energy equation and temperature solver either to force itself to limit the impossibly high temperatures reached in the mesh cells or to outright cause a catastrophic numerical divergence.

4.1.2 Volumetric heat source

This solution is inspired by the commonly used fire plume models that have been extensively used in fire dynamics calculations; in this case, a volumetric heat source was modelled, using a volume made of the same air as the rest of the domain associated with an energy source with a power output equivalent to the HRR of the fire. The dimensions of the volume are based on the Heskestad plume model equations, that correlate the area and HRR of a pool fire with the height of the plume (Karlsson & Quintiere, 1999). But much like the simple heat source, this model fails to deliver realistic temperatures and diverges quickly. One explanation to this behavior could be that such volumetric heat modelling was developed by ANSYS only for small scale applications such as simulations of electronic components' heating.

It can also be inferred that using "pure" heat sources lead to unrealistically high temperatures as it misrepresents the effects of air entrainment in the flame.

4.1.3 Usage of a basic definition of fire

Thus, a more rigorous approach was chosen; by using the basic equations governing the thermodynamics of a fire, its basic characteristics can be calculated, giving a simplified but suitable model for the bunker fire.

A supporting tool was used to carry out such calculations, namely the fire risk evaluation software ARGOS, developed by the Danish Institute for Fire and Security Technology (DBI).

This sets aside some features of an actual fire plume modelling as the one used in the FDS software:

- The radiation fraction of heat transfer from the plume is completely disregarded
- The small-scale entrainment occurring on the edges of the flame is not developed
- There is no actual modelling of the smoke layer and its effects

The decision to set aside these features in this project comes from the consideration that the physical scale of the fire is very small compared to the rest of the domain, and that only some of its characteristic need to be properly modeled, that is, the velocity and buoyancy effects on the general fluid flow, which in turn determine the dispersion of the tungsten particles.

4.2 A BENCHMARK CASE: THE STECKLER ROOM

To see how this modelling is accurate, a comparison was made with a famous benchmark case in fire dynamics' studies; the "Steckler room", which has been run as a series of field experiments on pool-fires by NIST, the very same agency that developed the FDS software for fire dynamics' centered CFD. FDS itself was extensively validated by comparing the data from the original Steckler cases with the corresponding simulations (Steckler, Quintiere, & Rinkinen, 1982).

Taking one of the cases from the Steckler series, the Steckler 16 case, the mass flow rate produced by the pool-fire is calculated using ARGOS to compare velocities between a validated FDS simulation and a Fluent simulation using the mass flow rate value of 0.6 kg/s yielded by ARGOS.

The geometry consists in a room measuring 2.8 x 2.8 x 2.2 m, where a pool-fire, having a heat release rate of 62.9 kW is placed in the center of the floor. A 1 x 1.8 m door opening is placed on one of the walls.

4.2.1 Limitations in the benchmarking

The benchmark comparison for the fire model validation only took velocity into account since, as already stated, smoke and temperature effects were assumed as not relevant for the particle dispersion, since effects such as thermophoresis are negligible on tungsten particles such as those modeled for this case, while smoke and radiation that occur in a fire are likewise not considered relevant for its effect on inert solid particles. The purpose of the validation is to check how close a modeled mass flow of air is to a validated modeled pool-fire combustion in terms of influence on the air flow in the building.

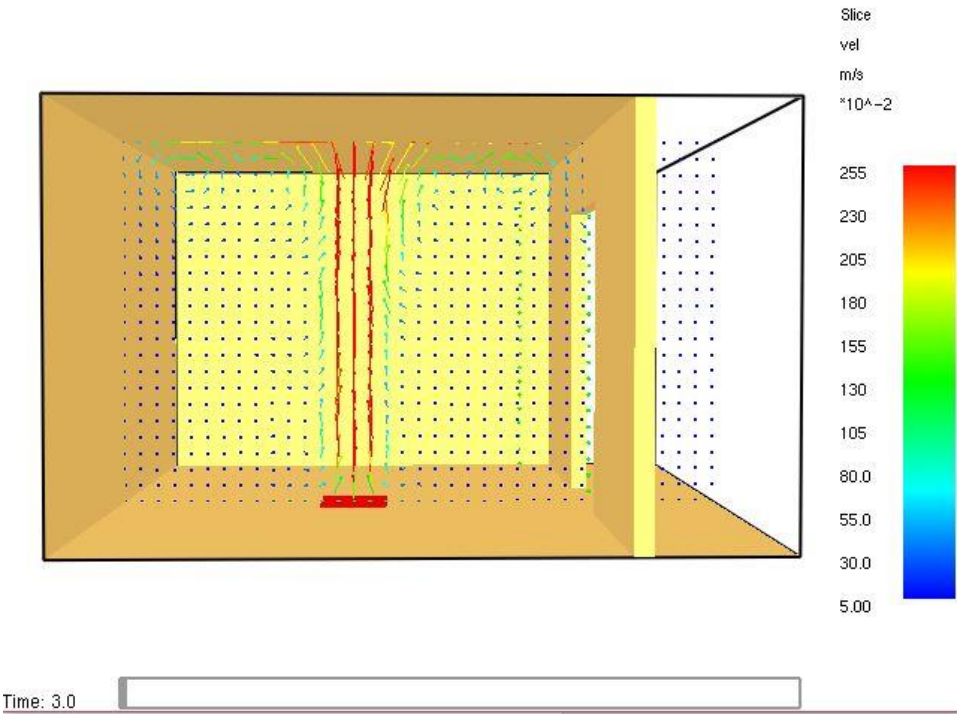

Figure 12 The Steckler 16 room on SmokeView, the viewer associated with FDS, after 3 seconds

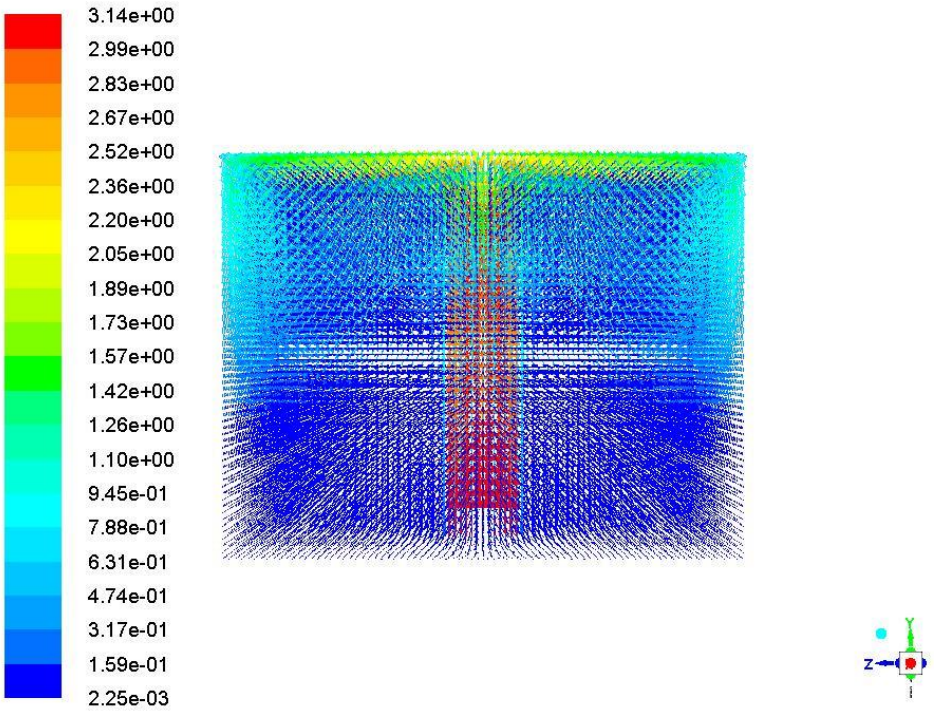

Figure 13 The Steckler 16 room on ANSYS Fluent, after 3 seconds

Figures 12 and 13 offer a direct visual confrontation between the results of the Steckler case 16 with FDS and the above described simplified fire model for the same case in Fluent. Both cases show the velocity magnitudes in the room after 3 seconds of simulation.

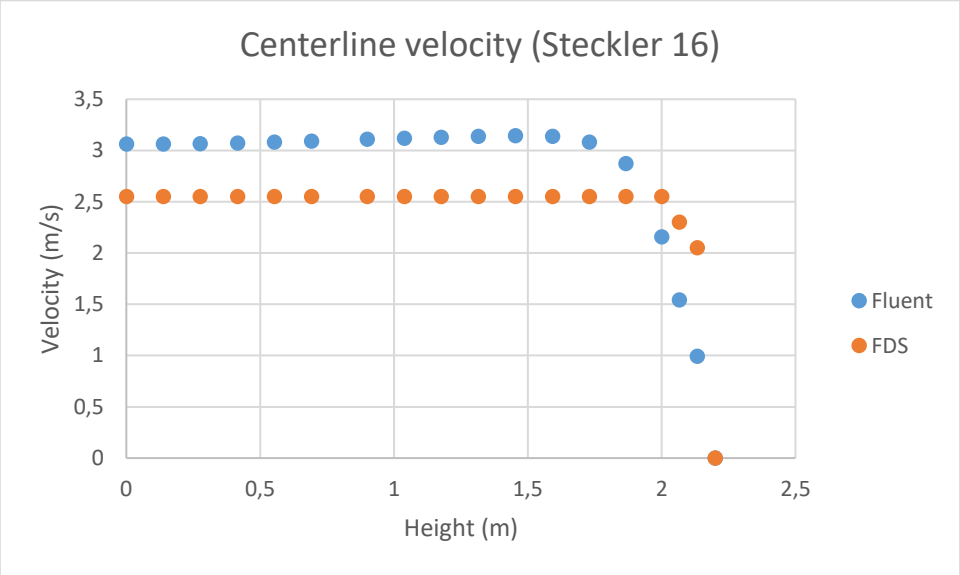

Figure 14 Comparison of centerline velocities

The values of velocity magnitude are indeed quite similar, especially when close to the ceiling, meaning that in this sense the simplified fire model is good enough in the evaluation of the effect of the fire on the general fluid flow. The higher values shown in the Fluent case at lower heights are most likely caused by the lack of entrainment effects in the "plume".

Given the HRR of the fire, the basic laws of thermodynamics allow to correlate it directly to the mass flow rate produced by the fire:

$$\dot{Q} = \dot{m} \cdot c_p \cdot \Delta T$$

Where $\dot{Q}$ is the HRR (W) and $\dot{m}$ is the mass flow rate (kg/s); knowing the pressure coefficient and the initial temperature (usually set at 300 K), the heat release rate can be correlated to the flame temperature and the mass flow rate of the fire.

The software ARGOS yields these values using known models for pool fires' plumes, which are based on databases obtained from field experiments (Deibjerg, Husted, Bygbjerg, & Westerman, 2003).

Therefore, a simplified fire can be set up in Fluent by setting the "poolfire" area's boundary conditions as those of a mass flow inlet whose initial values of mass flow rate (kg/s) and temperature (K) are those yielded by the ARGOS fire model.

5 CASE SCENARIO DESCRIPTION

5.1 GEOMETRIC MODELLING AND RESTRICTION OF THE SCENARIO

This report focuses on the dispersion of the tungsten trioxide particles; therefore, some simplifications and restrictions are made necessary.

The simulation doesn't include the monolith target area and the combustion of the moderators' liquid hydrogen, or the direct effect of the explosions, due to the remarkable complexity in both geometry and physics of these processes, especially regarding deflagrations and detonations, which are notably difficult to simulate with CFD software.

Of the instrument halls, only the smallest one has been chosen to be considered, to simplify the computational cost of calculations.

The geometry of the simulation is then restricted to the bunker and the instrument hall, keeping it as simple as possible.

The bunker

Given the actual geometric complexity of the bunker area and its relative small relevance in the particle dispersion behavior, a major geometrical simplification has been made to it.

The bunker is thus modelled as a 10x10x3 m parallelepipedal concrete chamber placed underneath the instrument hall. It comprises a velocity inlet from which particles and air flow are injected and a pool fire that summarizes the fire ongoing inside it. To approximate the damage caused by the hydrogen explosion, the roof of the bunker is not present, as to leave it exposed to the instrument hall.

This modelling choice is made to simplify the geometric modelling and focus on the upward movement of the particles pushed by the bunker fire, despite the fact that the bunker is actually on the same level of the instrument hall. No other elements are present inside the bunker, both for lack of knowledge on what an actual configuration of objects could be and to simplify the setup.

The instrument hall

The instrument hall follows the fairly simple geometry it will have in real life; it is then a parallelepipedal concrete chamber measuring 130x29x19 m, directly exposed to the bunker placed beneath it.

A pressure outlet is placed on the roof and a pressure inlet door is present on one of the side walls. Not knowing the exact final configuration of windows, these openings are placed as a reasonable approximation for an environment that is not certainly expected to be air tight.

The internal configuration of the instrument hall, including laboratory spaces and hardware, vehicles, hot cells and any other object, is not currently known with precision. To enhance the focus on the particle behavior the hall is thus considered as a completely empty volume, as the interaction of the flow or the particles with possible obstacles is not the focus of this model, neither is considered relevant to their overall behavior.

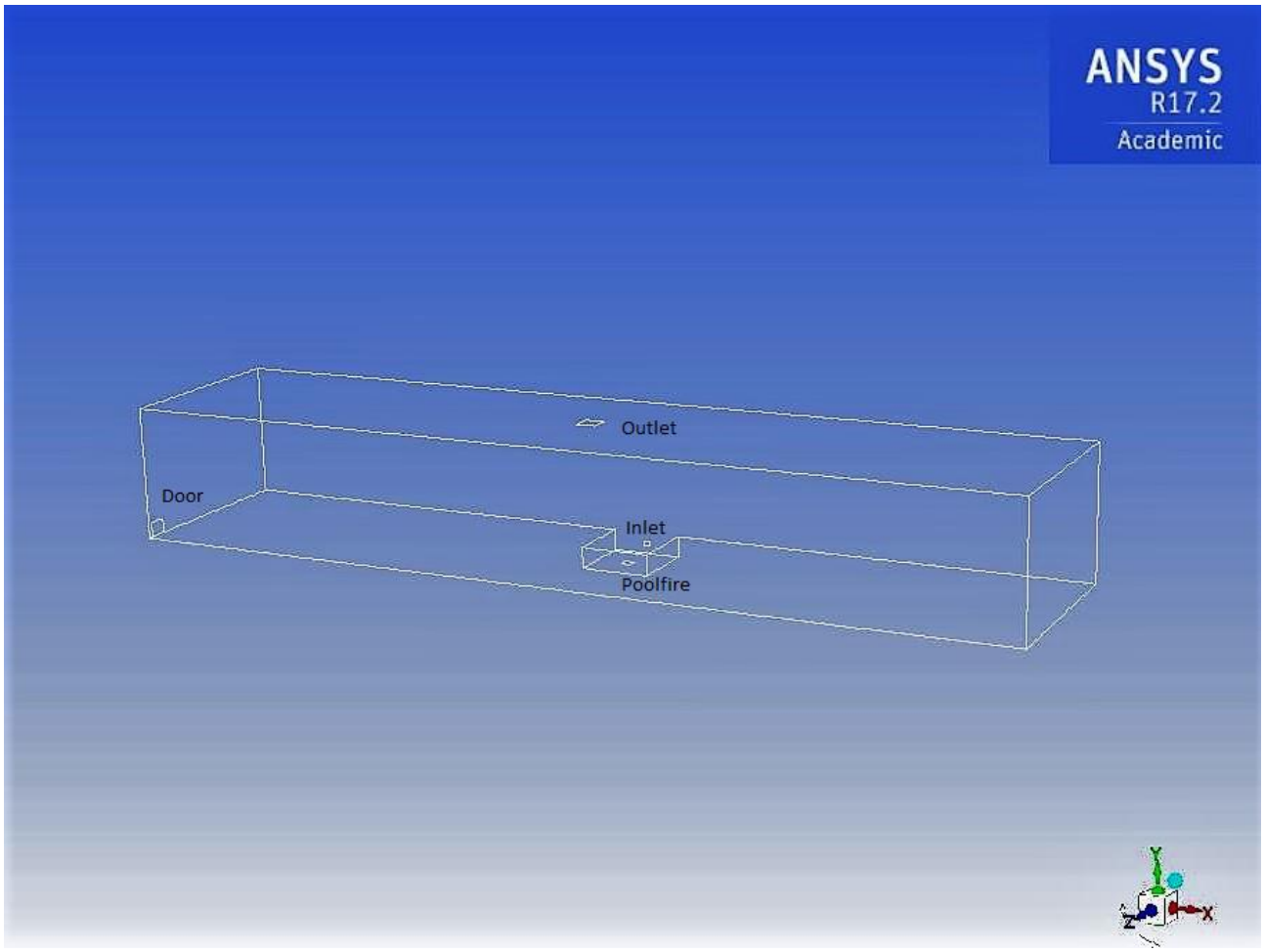

Figure 15 The geometry of the domain as it appears on the ANSYS graphic interface. The bunker is visible at the center, right underneath the instrument hall, comprising the pool-fire surface on the floor and the velocity inlet on the back wall. On the leftmost corner the pressure inlet door can be found, while the pressure outlet is the surface placed at the center of the roof of the hall.

5.2 MESHING OF THE COMPUTATIONAL DOMAIN

As previously said, the mesh grid making up the computational domain follows a hexahedral pattern. Using the meshing tool included in Fluent, a grid made of 453876 hexahedral cells was generated. The quasi-totality of the cells is composed by cubic volumes whose edges' length measure 0.55 m. For this geometry, this is the highest possible number of cells available with the ANSYS 17.2 software license (which allows a maximum of 512000 cell elements).

The mesh quality parameters were detected in the meshing tool as such:

Maximum skewness: 0.28162 (worth of notice, since almost all cells are cubic, skewness is nearly zero in most of the grid)

Aspect ratio: 1.0048 – 1.8763

Minimum orthogonal quality: 0.934 (almost 1 in most the grid)

As expected from a very regular grid, the quality parameters are indeed very good; this ensures that the mesh employed in the case is the best possible with the available tools.

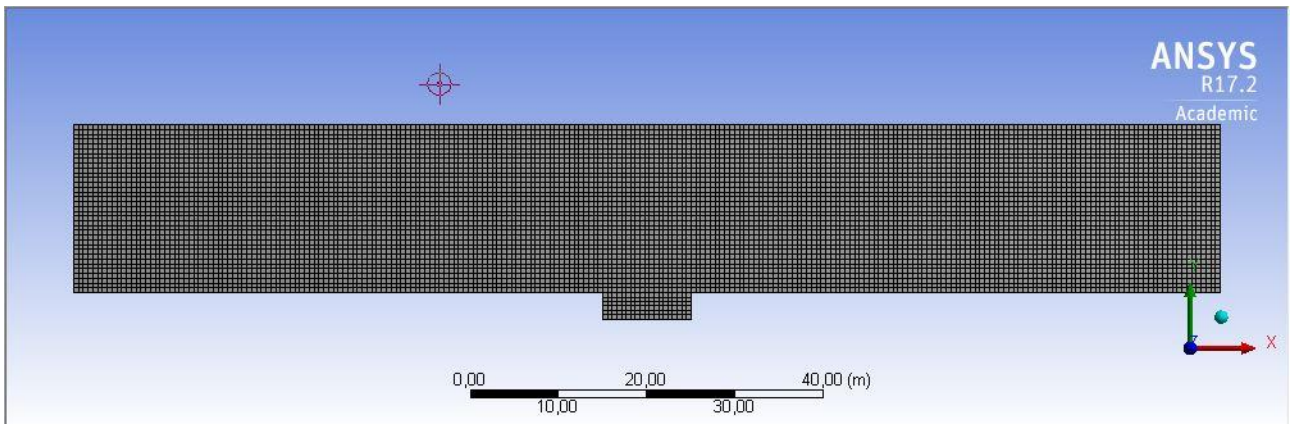

Figure 16 Front view of the mesh grid

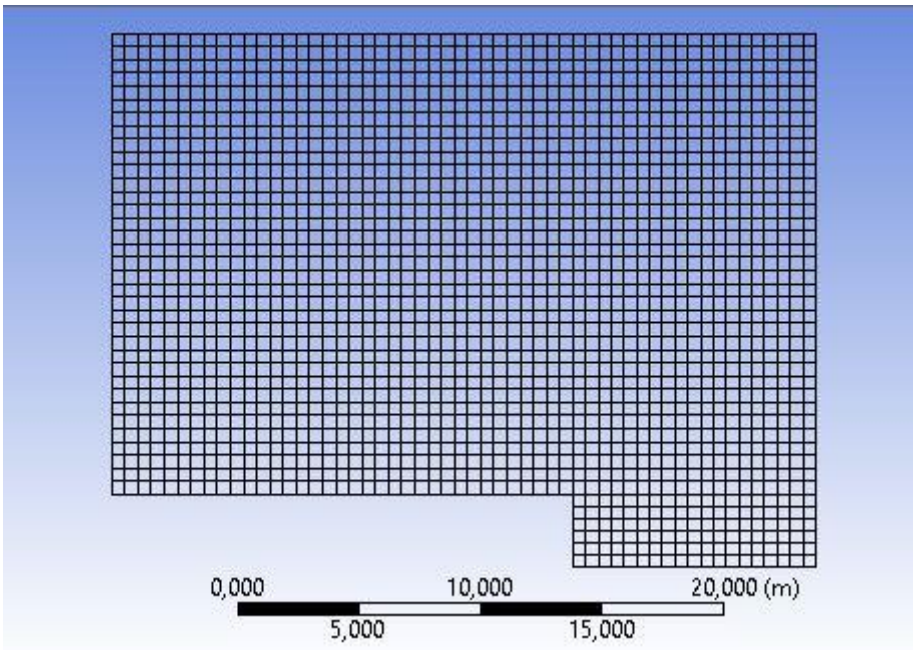

Figure 17 Side view of the mesh grid

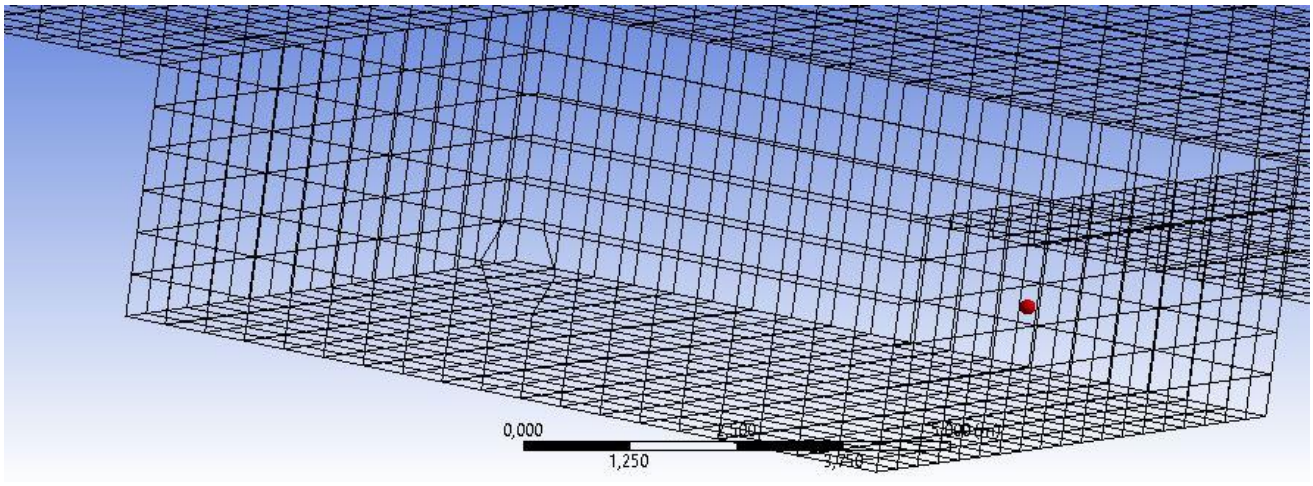

Figure 18 Detailed view of the meshing in the bunker

The length of the cells' edges is 0,55 m, which is around one order of magnitude larger than the previously estimated dissipative scales. This means that the LES can explicitly solve many intermediate turbulent scales, leaving only a relatively small number of inertial eddies to the SGS model.

5.3 GENERAL CONFIGURATION OF THE SCENARIO

As previously mentioned, the liquid hydrogen rapid combustion reaction is expected to make it deplete extremely quickly. Moreover, almost all the reactions involving it happen in the monolith. Therefore, it is reasonably safe to assume that no hydrogen is present in the air inflow from the bunker inlet to the instrument hall, and that room temperature atmospheric air makes up the whole content of the volumes considered.

The inflow of air and particles is thus assumed to be happening in the aftermath of the hydrogen explosion event.

Only tungsten trioxide (WO_3) particles are considered, despite in such a scenario many other materials would be present, given the varied composition of the monolith structure. But since these heavy and possibly highly radioactive particles are those with the highest impact on both human and environmental safety, their behavior assumes higher priority over others, and they are therefore the prime focus of this project.

The walls are all assumed to be made of standard concrete, which is considered close enough to the future actual configuration of the environment; since their physical characteristic are not considered of great relevance to the particle behavior, there will not be a detailed concern over them.

The setup of this scenario in the CFD simulation will now be described, together with a quantitative description of its initial and boundary conditions.

5.4 PARTICLE BOUNDARY CONDITIONS (PARTICLE/WALL INTERACTION).

Since the simulation only involves inert solid particles, the boundary conditions that are implemented are of the type “reflect” and “escape”. They are now briefly described.

5.4.1 Reflect

This is the boundary condition set for the solid surfaces included in the simulation. Setting to reflect, the particles hitting the walls will be rebounded back into the flow.

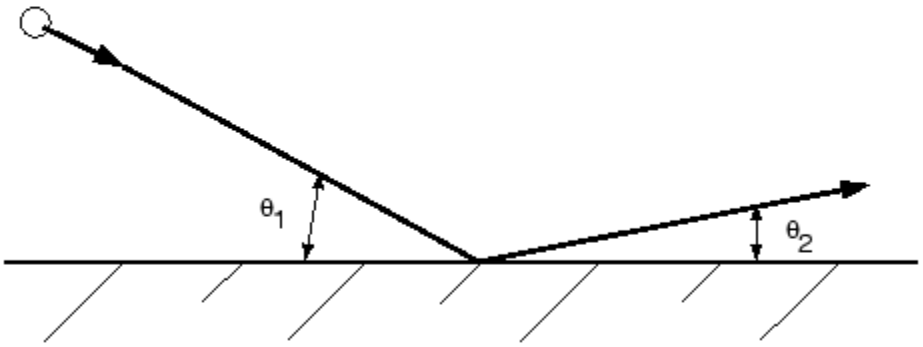

Figure 19 A graphical depiction of a reflected particle trajectory (Ansys, 2016)

Considering θ_1 as the incident angle and θ_2 as the outbound angle the restitution coefficient can be defined as the ratio between the normal components of relative velocities after and before the collision:

$$e_n = \frac{v_{2,n}}{v_{1,n}}$$

Therefore, a restitution coefficient value of 1 indicates a completely elastic collision, where the particle maintains all its kinetic energy and momentum. This is the setup chosen in the simulation.

5.4.2 Escape

This boundary condition is set for the openings of the simulation, such as the roof and the door outlets but also the inlet. With this condition, when a particle hits the surface it will disappear and be disregarded by the computational domain, and its trajectory will stop being calculated.

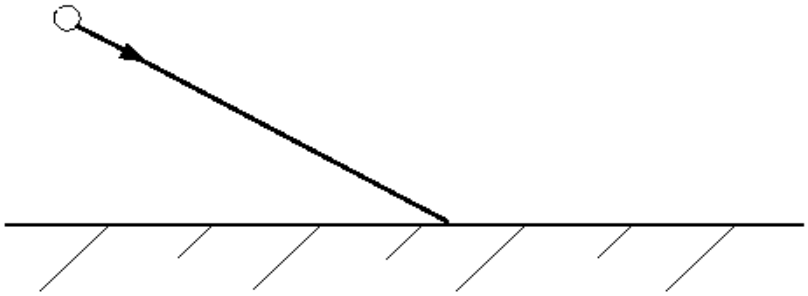

Figure 20 A graphical depiction of an escaped particle trajectory (Ansys, 2016)

5.4.3 Other possible particle fates

Particle trajectory could also result in other ways:

"Incomplete" trajectories occur when the maximum number of time steps is exceeded, therefore terminating the calculation of the trajectory.

"Aborted" trajectories occur because of round-off or other numerical errors that cause them to fail to be completed. The relative number of aborted trajectories is also indicative of the quality of the simulation; a too high number of aborted particles may require a change in the boundary conditions, in the meshing or in the time steps. A well converged simulation will most likely show no aborted trajectories.

5.4.4 Injection

The type of injection of particles in the environment doesn't have a great effect on the overall simulation – that because the domain is rather large, especially when compared to the particles' range of sizes.

A conic nozzle injection was chosen, since, in the ANSYS software, it is both very customizable, for instance in the number of streams and the time span of the injection and the most stable, since it doesn't directly depend on the surface mesh configuration.

Particles are not injected at the beginning of the simulation; the initial conditions of the simulation include null velocity for the fluid domain all over the instrument hall and the bunker, which is not a type of condition which would occur in real life, especially for a large room which cannot realistically be completely air tight. It is then necessary to let the air flow given by the opening establish itself to see a more realistic particle dispersion, since as the discrete phase is uncoupled, it is bound to follow the air flow streams.

Since the particles are injected from the velocity inlet, the stack effect that takes place in the building makes the first air streams travel directly from the inlet to the ceiling outlet. Injecting the particles at the beginning of the simulation would make them follow such streams, making them escape immediately from the domain in a too unrealistic way.

5.5 INITIAL AND BOUNDARY CONDITIONS

Firstly, the effect of gravity on the domain is set with a standard downward acceleration of 9.81 m/s^2. The initial speed in the whole domain is set to zero, the same as the dynamic pressure (defined as any additional pressure summing up to the standard atmospheric pressure). The temperature is set at the default value of 300 K.

The boundary conditions of the surface zones defined in the domain are as follows:

Inlet (velocity-inlet)

Velocity magnitude	**5 m/s**
Gauge pressure	0 pa
Discrete phase boundary condition	Escape
Temperature	300 K
Dimensions	1x1 m

Where the gauge pressure is the user defined value of dynamic pressure applied to the surface zone (not including the pressure gradients caused by the flow velocity)

Door (pressure-inlet)

Gauge pressure	**0 Pa**
Discrete phase boundary condition	Escape
Temperature	300 K
Dimensions	3x2 m

Outlet (pressure-outlet)

Gauge pressure	**0 Pa**
Discrete phase boundary condition	Escape
Temperature	300 K
Dimensions	4x4 m

Wall (interior wall – Domain boundary)

Discrete phase boundary condition	**Reflect**
temperature	300 K

As there is no pressure difference in the initial boundary conditions of the openings, air will start flowing from the inlet to the door and the ceiling outlet.

5.5.1 Particle injection

The injection of the tungsten particles is carried out from the velocity-inlet, although it is separately defined.

Total flow rate	**0.001 kg/s**
Temperature	300 K
Velocity magnitude	5 m/s

The parameters of the Rosin-Rammler diameter distribution are:

Min diameter	**10^{-7} m**
Max diameter	$2{,}3 \cdot 10^{-6}$ m
Mean diameter (size constant **d**)	10^{-6} m
Spread (size distribution **n**)	3,5

Note the maximum diameter value, down to $2{,}3 \cdot 10^{-6}$ m from the expected value of 10^{-5}, due to the software implementation of the Rosin-Rammler distribution, that discarded diameters whose numbers would not be statistically significant.

5.5.2 Sensitivity analysis: fire size

To provide some sensitivity analysis, the simulation was set with two different values for the magnitude of the fire; following the definition given in a previous study for the bunker fire, the HRR is expected to be between a minimum of 330 kW and a maximum of 1 MW (Jörud, 2013).

The heat release rate of the bunker fire was chosen as the only parameter in the simulation undergoing a sensitivity analysis. Other parameters such as the initial velocity of the flow form the velocity inlet or the initial velocity of the injected particles were not considered for such sensitivity analysis; the main reason for this is the current lack of knowledge and of studies about, which is not the case for the bunker fire size, which was evaluated in previous studies. It is indeed necessary for future developments, especially if new data on the initial conditions will be available, to expand the sensitivity analysis on these and on other parameters (such as the configuration of the openings in the building).

Therefore, using the data yielded by ARGOS for such heat release rates, the initial conditions for the pool-fire is:

Poolfire (mass flow-inlet)

Mass flow rate	**0.68 kg/s (330 kW)/2.07 kg/s (1MW)**
Temperature	780 K
Discrete phase boundary condition	Reflect
Dimensions	Ø 2 m

5.5.3 Initialization and calculation of the scenario

The actual calculation of the simulation is set with a time step of 0.1 seconds, in which up to 25 iterations are run. These parameters were empirically determined while testing the software, to see in which setup conditions it would achieve convergence.

The under-relaxation factors for pressure and momentum are left at their default of 0.3 and 0.7, as it is common practice on manuals to make sure the sum of these URF is always 1 when using a pressure-based solver. The URFs for forces and density are left at 1, while the one for energy was modified; since its default value of 1 is known to easily cause divergences, it was decided to keep the URF for energy at a safer 0.95 value (Ansys, 2016).

6 SIMULATION AND COMPARISON OF MODEL SETUPS WITH A SCALED DOWN GEOMETRY

The full geometry of the instrument hall is a remarkably large one, which makes the calculation process very long and laborious. For this reason, a good way to check the quality of the simulation model in a way that allows to run several simulations and to select which ones are worth investigating, is to use the setup in a smaller geometry. Having a smaller computational domain is the most direct way to reduce calculation expense and time while keeping the same setup, boundary and initial conditions.

6.1 THE SCALED DOWN GEOMETRY

Since one of the primary objectives of this project is to assess the possible escape of particles from the outlet, it is reasonable to preserve the central part of the geometry, including the bunker and the outlet, to highlight the upward motion of the particles. For this reason, the scaled down geometry consists in a 20 m longitudinal section of the instrument hall. The mesh is unmodified; therefore, it still consists of a grid of hexahedral cells with 0,55 m long edges.

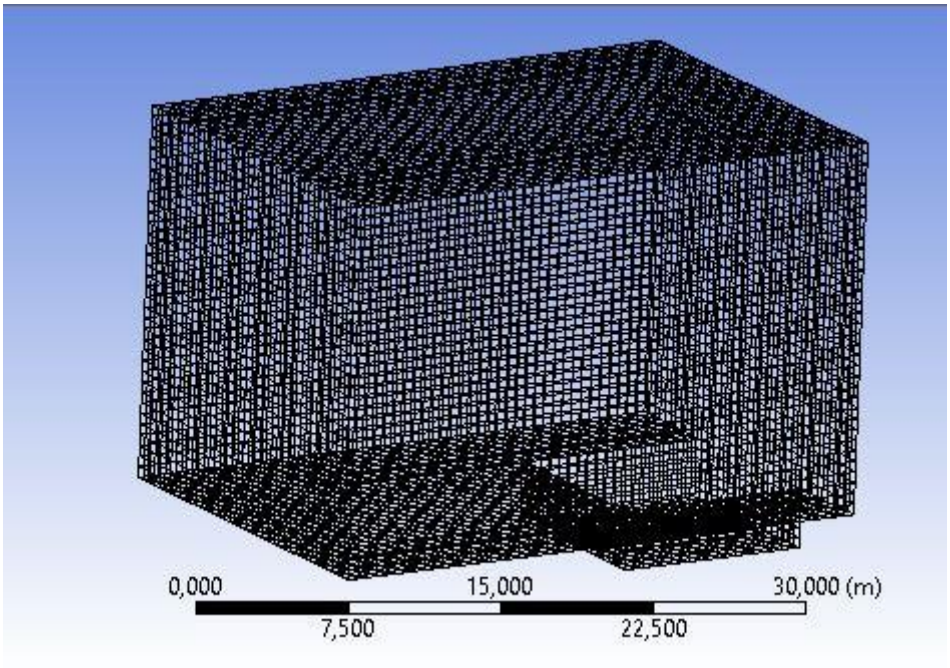

Figure 21 The mesh and geometry of the scaled down instrument hall

6.2 THE SETUP

The boundary conditions for the openings remain as previously described, that is, the simulation is ran for a 330 kW and a 1 MW pool-fire. The injection of particles is decided to occur in a 1-second time lapse with the same injection setup. The total simulation time is set at 200 seconds, where the injection takes place between 20 and 21 seconds from the start.

Table 3 Scaled-down setup

Total time	200 s
Time step	0,1 s (Max 25 iterations per time step)
Injection time lapse	20 to 21 s into the simulation
Total injected particle mass	0,001 kg
Maximum particle diameter	$2{,}3 \cdot 10^{-6}$
Minimum particle diameter	10^{-7}

As mentioned before, the reason why the injection takes place some seconds after the flow simulation starts is that as the overall velocity in the domain is zero, it is as if the air in the building was not moving at all at the beginning of the simulation. Letting the flow run for some time before the particle injection allows the flow to establish itself close to how it would be in real life.

6.3 SENSITIVITY ANALYSIS: STOCHASTIC TRACKING

An additional element of sensitivity analysis is added to the simulation scenario; one instance of the case is calculated with the addition of a stochastic tracking method for the tungsten particles. This model, known as the Random Walk Model, is employed to consider casual instantaneous turbulent fluctuations of the flow and their effect on the particle dispersion.

Stochastic tracking consists in dividing the velocity *u* of the particles in two components:

$$u = \bar{u} + u'$$

Where the first term is the mean velocity of the fluid flow while the second term u' is the fluctuating component of instantaneous velocity, calculated through a stochastic model called random walk model. This model is expected to randomize the trajectory of the particles, simulating the random behavior of eddies in a turbulent flow.

The stochastic tracking method will be employed for the 1 MW pool-fire, since having an overall higher mass flow rate, the turbulent effects have a higher magnitude, meaning that fluctuations due to turbulence are more easily appreciable.

6.4 HIGHLIGHTS OF THE RESULTS

In all three simulations, the total quantity of particles injected into the domain is 1 g; all three cases last until three minutes have passed after the injection.

The amount of tungsten particles that have escaped outside the instrument hall is highlighted, indicating how much escaped from each one of the possible openings (outlet, door or inlet). Another important result that is highlighted is the time it takes, for each case, for the first particles to leave the instrument hall; the time lapse and the quantity of escaped particles are useful data for the assessment of human safety and environmental risk. The average rate of particle egress is also shown.

The particle diameter distribution after three minutes in the three cases is also shown, showing the mass-weighted percentages of the ranges of diameters.

Table 4 Scaled down results comparison

	330 kW bunker fire	**1 MW bunker fire**	**1 MW with stochastic tracking**
Escaped particle mass	0,029 g (2,9%)	0,0786 g (7,86%)	0,0692 g (6,92%)
Escape location percentages	100 % from outlet	96,5% from outlet, 3,5% from door	89,3% from outlet, 1,4% from inlet, 9,3% from door
Time lapse of escape from outlet	82,8 to 180 s after injection	60,1 to 180 s after injection	113,2 to 180 s after injection
Time lapse of escape from door		146,5 to 178 s after injection	163,2 to 175 s after injection
Time lapse of escape from inlet			0,4 to 0,89 s after injection
Average mass flow escape rate from outlet	0,00029 g/s	0,00065 g/s	0,001 g/s

Particle diameter distribution

This table shows how the overwhelming majority of the particles' diameters lies in the order of magnitude of 1e-07 m; there is indeed little difference between the three scenarios, meaning that in general most particles are to be expected in this diameter range. Comparing the percentage with that of the initial distribution, it can also be inferred that most particles escaping the hall are also in the 1e-07 m diameter range.

Table 5 Particle diameter distribution for the scaled down cases

	Distribution at injection	**330 kW**	**1 MW**	**1 MW with stochastic tracking**
1e-07 - 2,3e-07 m	99,96%	95,77%	95,95%	95,7%
2,3e-07 - 4,6e-07 m	≈0%	0%	0,00045%	0%
4,6e-07 - 6,9e-07 m	0,016%	2,12%	1,98%	2,1%
6,9e-07 - 9,2e-07 m	≈0%	0%	0,003%	0%
9,2e-07 - 1,15e-06 m	0,011%	0,06%	1,84%	0,044%
1,15e-06 - 1,61e-06 m	0,009%	1,93%	0,11%	2,03%
1,61e-06 - 2.07e-06 m	0,0013%	0,06%	0,06%	0,072%
2,07e-06 - 2,3e-06 m	0,0004%	0,05%	0,042%	0,046%

Particle diameter over height

The following graphs show the particle sizes correlated to their vertical position; that is, they show which particle sizes are found at any given height inside the domain, three minutes after their injection.

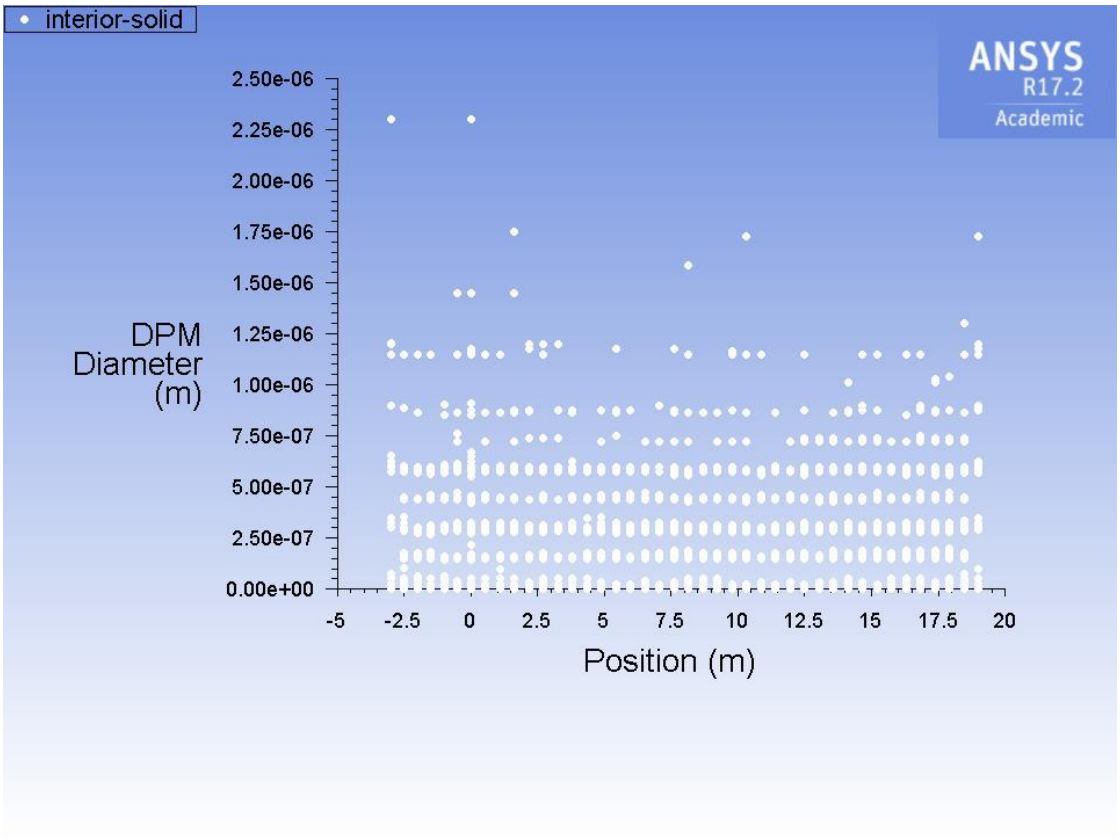

Figure 22 Particle diameter versus height for the 330 kW case

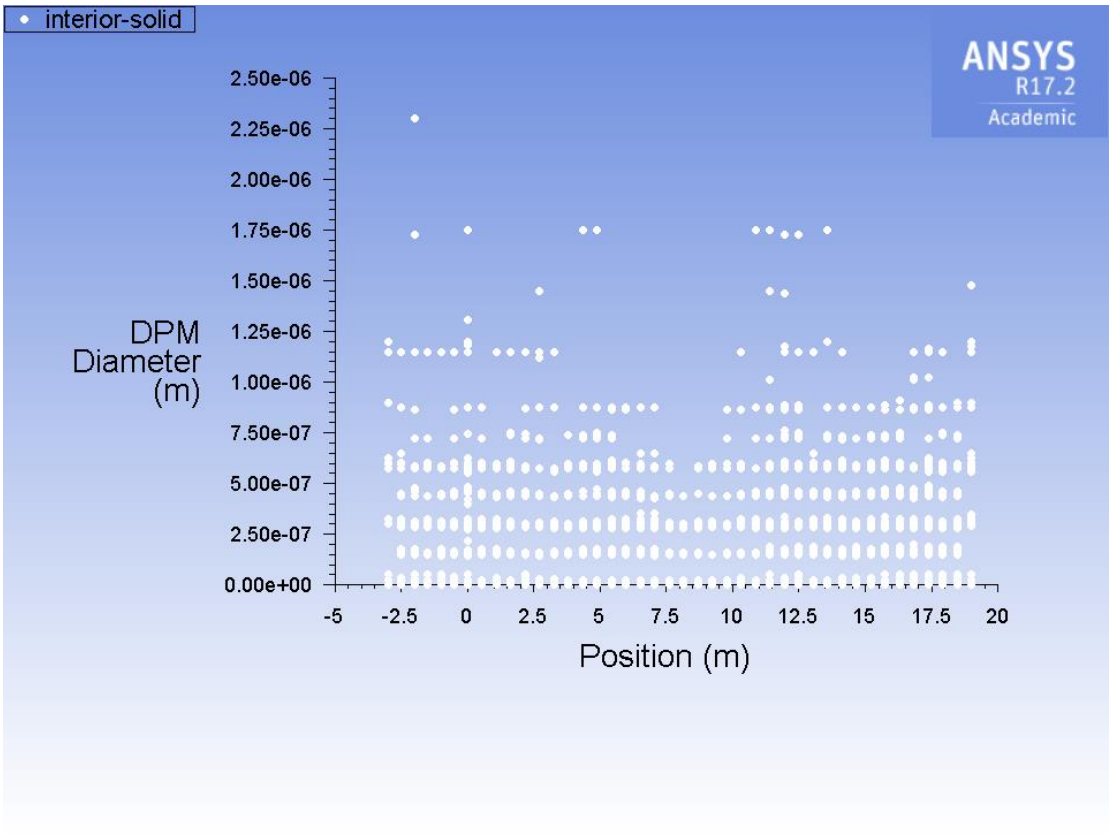

Figure 23 Particle diameter versus height for the 1 MW case

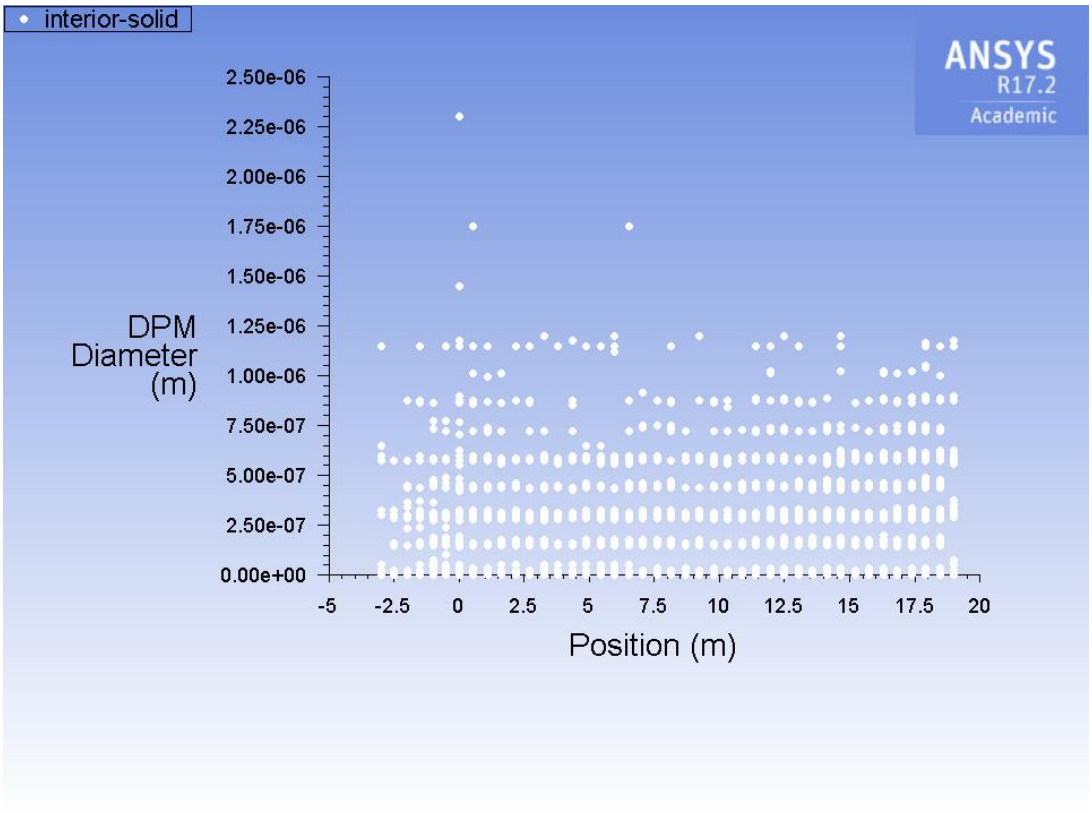

Figure 24 Particle diameter versus height for the 1 MW case with stochastic tracking

Figures 22 to 24 show how particles of sizes inferior to 1,25e-06 m of diameter are evenly spread all over the room from the floor to the roof, while those with diameters equal or superior to 1,5e-06 are mostly found near the ground level. As for higher levels, the 330 kW and the 1 MW case show an appreciable spread of particles sizes: it can be seen how the presence of larger particle sizes decreases with height. The 1 MW case shows more particles larger than 1e-06 m at higher levels, implying that the higher magnitude of the fire has a stronger push on heavier particles. On the other hand, in the case employing the stochastic tracking, almost all particles larger than 1,25e-06 are instead on ground level.

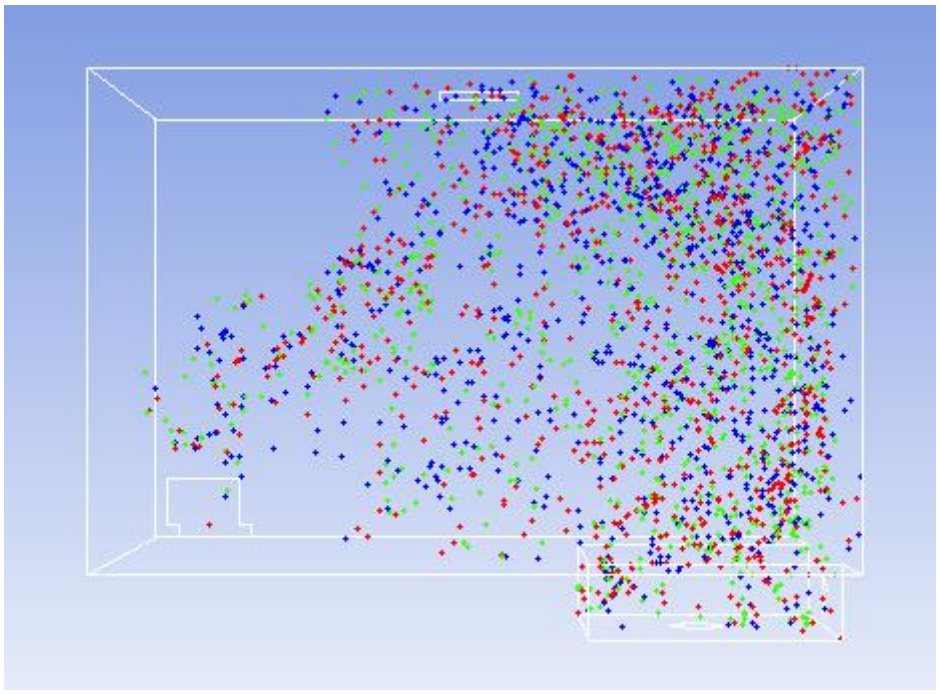

Figure 25 Side view for the 330 kW case

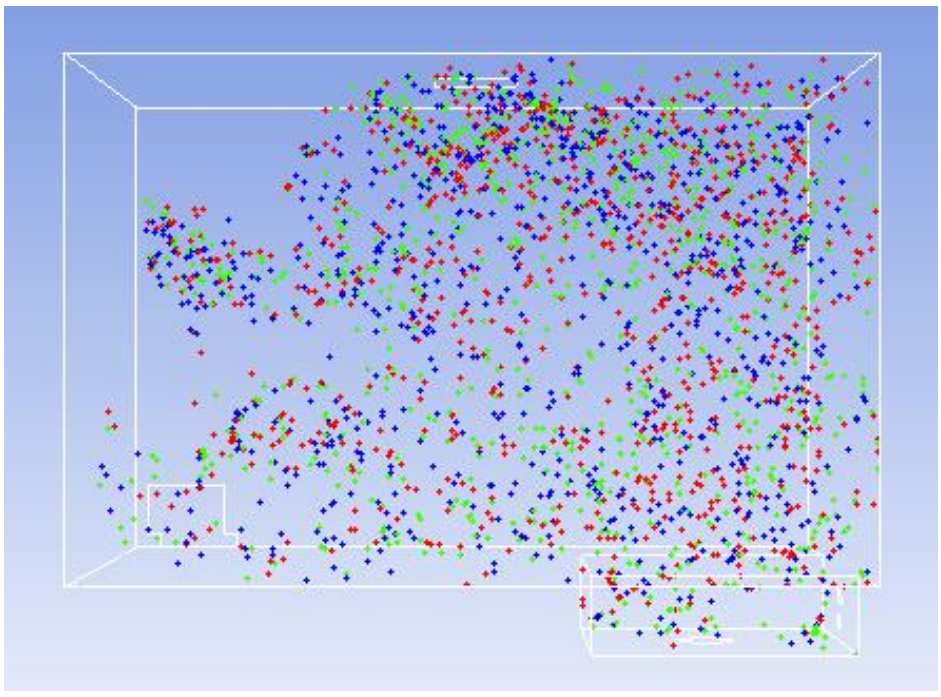

Figure 26 Side view for the 1 MW case

6.5 CONSIDERATIONS AND CONCLUSIONS

As seen from the results, running the same case, with an otherwise identical setup, employing a stochastic random walk model, makes a remarkable difference; without this tracking model, particles start escaping from the domain almost one minute in advance. This implies that, including the fluctuations due to the random walk model, the upward trajectories of the tungsten particles are more irregular and take longer paths to travel the same distances. The rates at which the particles leave do not remarkably differ, meaning that the forces acting on the particles and the coupling with the flow are not substantially affected. Nevertheless, it is not possible to tell if this tracking method yields more reliable results.

The diameter distribution of the particles is not significantly different in the three setups; the common conclusion that can be inferred is that smaller particles, of diameters of the order of magnitude of 1e-07 m, since they also constitute the majority of the particles, are those leaving the instrument hall and dispersing in the external environment. Regarding the spatial distribution of particle sizes, it is shown that a higher magnitude for the bunker fire pushes heavier particles significantly higher, if the stochastic tracking is not involved.

After three minutes from the injection of particles, the relative quantity of particles leaving the domain is much higher for the 1 MW cases, being almost 7% for the case employing stochastic tracking and almost 8% for the other; the 330 kW bunker fire case sees a percentage of escaping particles of less than 3%.

The almost totality of the particles escapes through the ceiling outlet; the number of particles leaving through the ground level door is negligible if not zero in the 330 kW fire case.

Of the three cases, the one that could pose a higher risk for environmental dispersion of potentially radioactive particles is the 1 MW case (without stochastic tracking), since it is the one with the lowest trajectory time lapse and the higher quantity of released particles. This implies that bunker fires with higher release rates cause dispersed particles to escape more quickly. For this, the scenario with a 1 MW bunker fire should receive additional attention.

7 SIMULATION OF THE FULL-GEOMETRY CASE SCENARIO

As previously mentioned, the scenario comprising a 1 MW bunker fire is the one deserving additional attention; therefore, the simulation is run with this heat release rate for the full-scale geometry described in chapter 5.

Table 6 Setup of the full-scale scenario

Total time	1200 s
Time step	0,1 s (Max 25 iterations per time step)
Injection time lapse	40 to 41 s into the simulation
Total injected particle mass	0,001 kg
Maximum particle diameter	$2{,}3 \cdot 10^{-6}$
Minimum particle diameter	10^{-7}

The setup is the same used in the previous scaled-down scenarios; one difference is the time for the particle injection, which occurs 40 seconds after the start of the simulation. The choice of a later time to inject the particles is taken considering how in the full-scale geometry it takes more time for the fluid flow to establish itself. The other setup change is that the simulation is run for a longer time, for a total of 20 minutes.

7.1 PARTICLE ESCAPE

Because of the larger scale of the complete instrument hall, upward movement of the particles is less prevalent and escape from the outlet occurs more than two minutes after injection, and in smaller quantities. No particle escapes from other openings. Implications to these results are that entrance and exit from ground level doors may occur without increasing the dispersion of particles into the environment, while the time up to beginning of escape, despite being more than twice that of the scaled down scenario, is still rather short for any kind of emergency response.

Table 7 Particle escape times

	1 MW (full geometry)
Escaped particle mass	
Time lapse of escape from outlet	146 s to 1200 s after injection
Time lapse of escape from door	/
Time lapse of escape from inlet	/

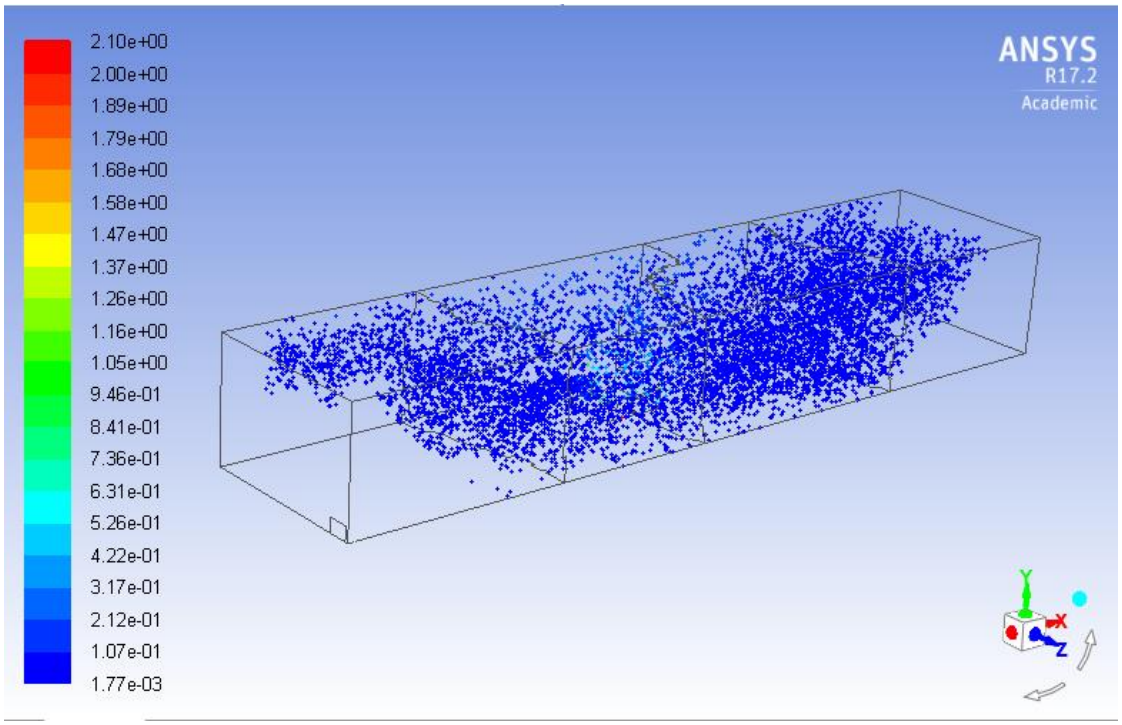

Figure 27 Isometric view of the particles in the hall after 20 minutes

7.2 PARTICLE DIAMETER DISTRIBUTION

Similarly to the previous cases, due to the mass fractions determined by the Rosin-Rammler distribution, the majority of the particles is within the 0,1 - 0,2 µm diameter range, albeit it can be noted how the larger diameters have overall higher and more balanced numbers. This implies that higher numbers of larger particles remain in the building, especially for diameters larger than 1,6 µm.

*Table 8 Particle diameter distribution for full-scale scenario**

	Distribution at injection	**1 MW (full geometry)**
1e-07 - 2,3e-07 m	99,96%	98,3%
2,3e-07 - 4,6e-07 m	≈0%	0,193%
4,6e-07 - 6,9e-07 m	0,016%	0,191%
6,9e-07 - 9,2e-07 m	≈0%	0,194%
9,2e-07 - 1,15e-06 m	0,011%	0,188%
1,15e-06 - 1,38e-06 m	0,009%	0,186%
1,38e-06 - 1,61e-06 m	≈0%	0,185%
1,61e-06 - 1,84e-06 m	0,0013%	0,187%
1,84e-06 - 2,07e-06 m	≈0%	0,187%
2,07e-06 - 2,3e-06 m	0,0004%	0,18%

*due to approximation, the total could not be 100%

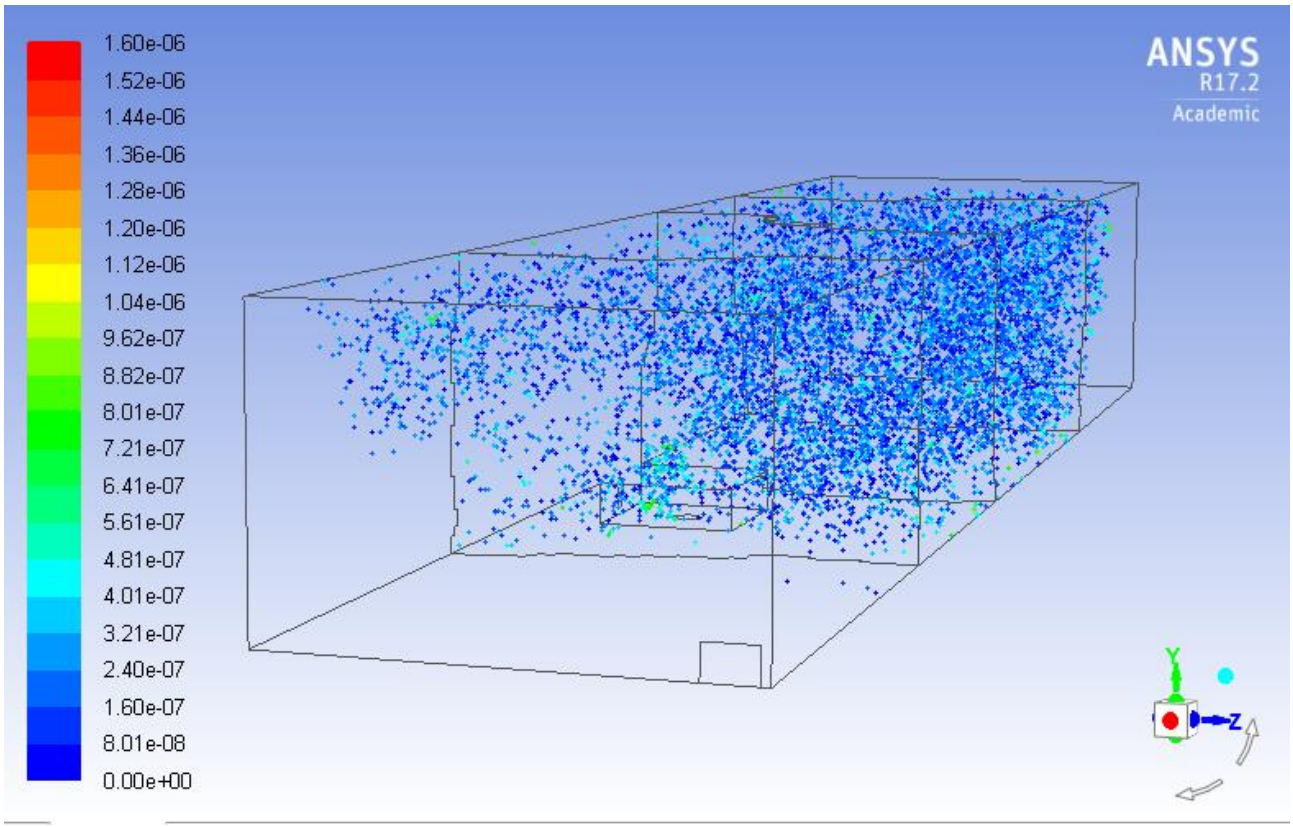

Figure 28 Highlight for particles under 1,6 µm. Diameters are rather evenly distributed in space, although larger particles (lighter in color) are slightly more easily found at lower heights.

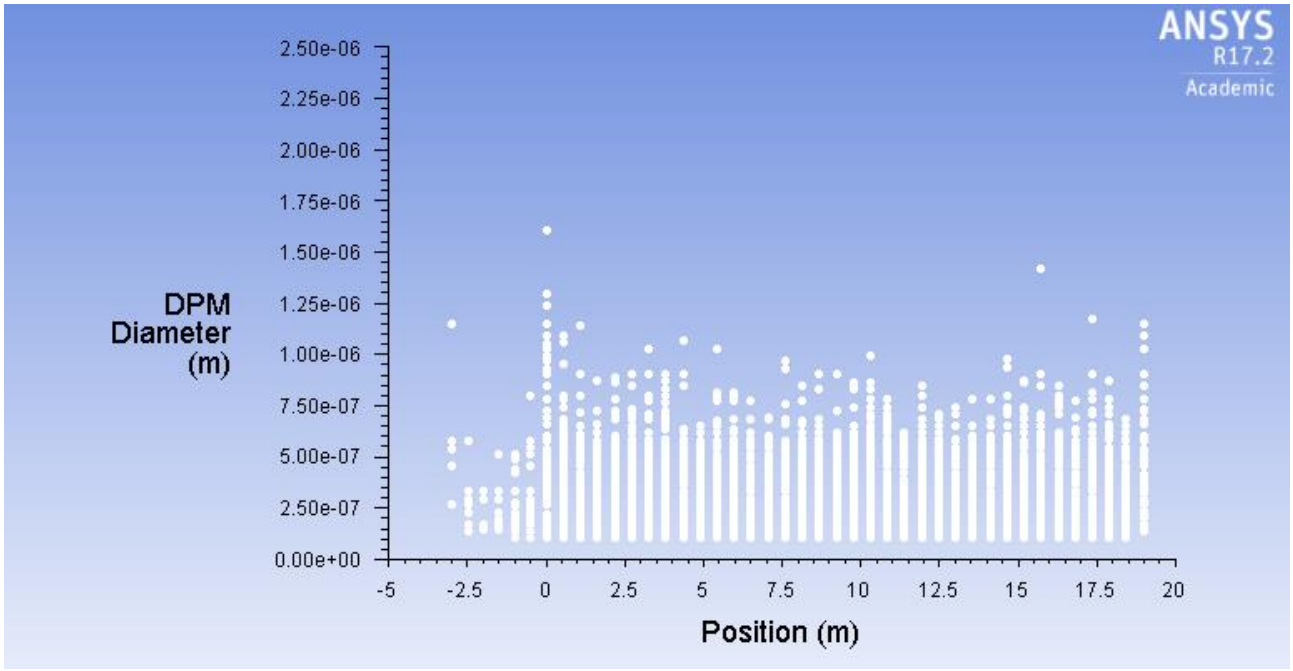

Figure 29 The above graph shows how, analogously to the previous scaled-down simulations, smaller particles are evenly spread on all heights, while larger ones (> 1,6 µm) have a slight tendency to stay on lower heights.

7.3 PARTICLE VELOCITIES

The simulation shows, for the dispersed particles after 20 minutes, very low velocities. As seen in the images below, most particles' velocities have values in the order of magnitude of 10^{-3} m/s, down from speeds in a range between 1 and 2 m/s in the proximity of the bunker fire.

Table 9 Particle velocity range

Minimum particle velocity	$1{,}77 \cdot 10^{-3}$ m/s
Maximum particle velocity	2,11 m/s

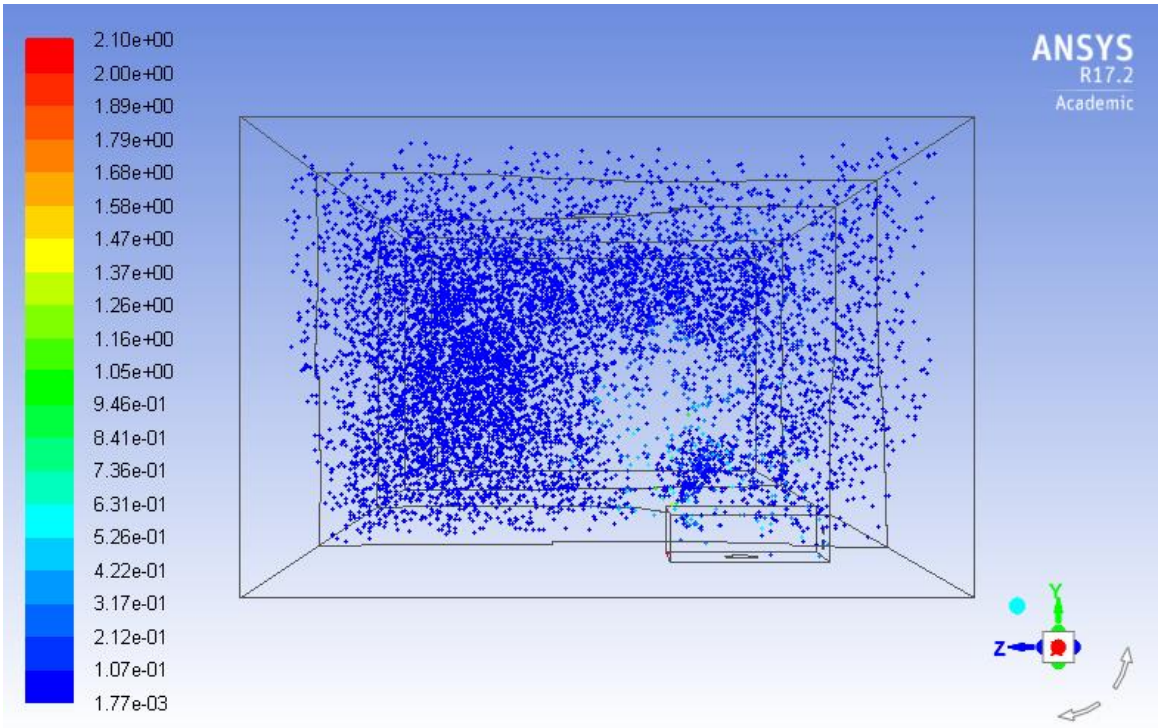

Figure 30 Side view of the particle spread in the hall

Figure 30 shows how the overwhelming majority of the particles moves at the lowest detected velocities. Figure 31 below shows the velocity vectors of the particles near the bunker fire, showing the upward push caused by the fire and the subsequent slowing down in farther areas. This furtherly confirms the influence of the fire on the particle dispersion.

7.3.1 Terminal velocities

Knowing the velocity magnitude of the particles in the building, it can be useful to check how close they are to the particle terminal velocities.

The terminal velocity of a body in a fluid is defined as the highest velocity it can attain while falling through such fluid domain, i.e. the velocity at which the drag force equals the gravity force (and other additional forces if present) so that it ceases to accelerate and it starts free falling.

Using the following formula, from the Stokes' law (Vesilind, Peirce, & Weiner, 1994):

$$V_t = \frac{g d^2 (\rho_p - \rho_{air})}{18\mu}$$

For three sample diameters of the tungsten particles we obtain:

Particle diameter	Terminal velocity (m/s)
0,1 µm	$3{,}57 \cdot 10^{-6}$ m/s
1 µm	$3{,}57 \cdot 10^{-4}$ m/s
2,3 µm	$1{,}89 \cdot 10^{-3}$ m/s

The minimum velocity encountered in the simulation after 20 minutes is $1{,}77 \cdot 10^{-3}$ m/s, which corresponds, solving again the Stokes' law equation, to the terminal velocity for a tungsten trioxide particle with a 2,24 µm diameter. This implies that the almost totality of the particles is, after 20 minutes, still above their terminal velocity, therefore in suspension inside the building as shown in the simulation. Since most particles are in the order of magnitude of 0,1 µm, they are expected to stay suspended in the instrument hall for a long time, provided no action is taken.

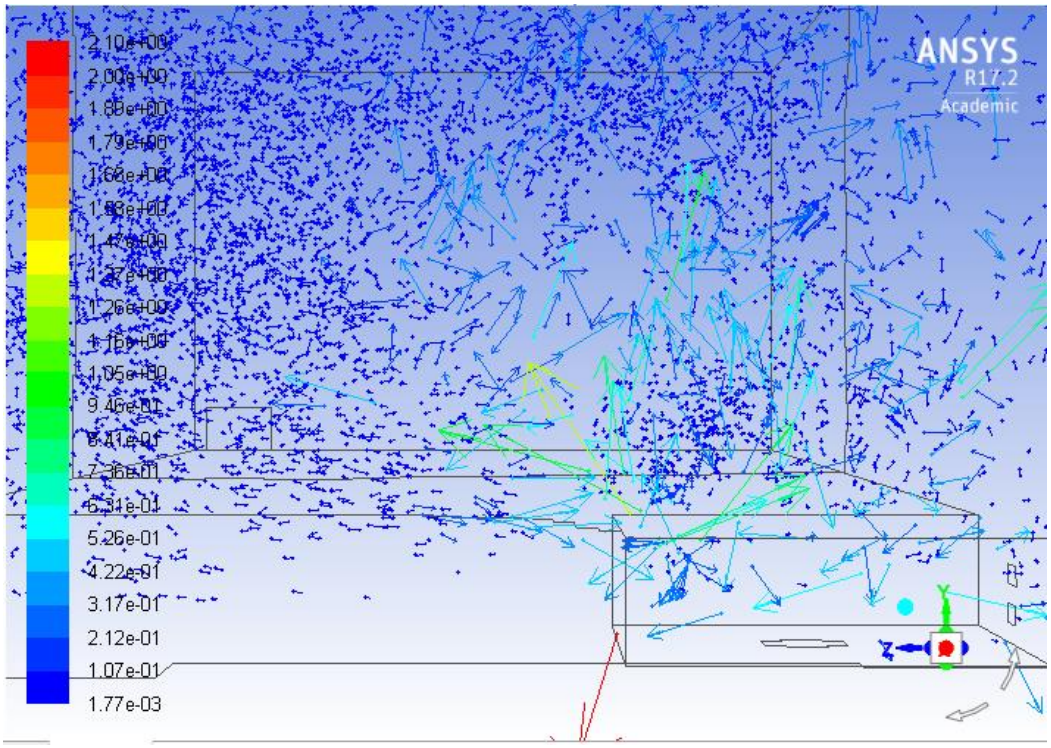

Figure 31 Zoomed side view of particle velocity vectors

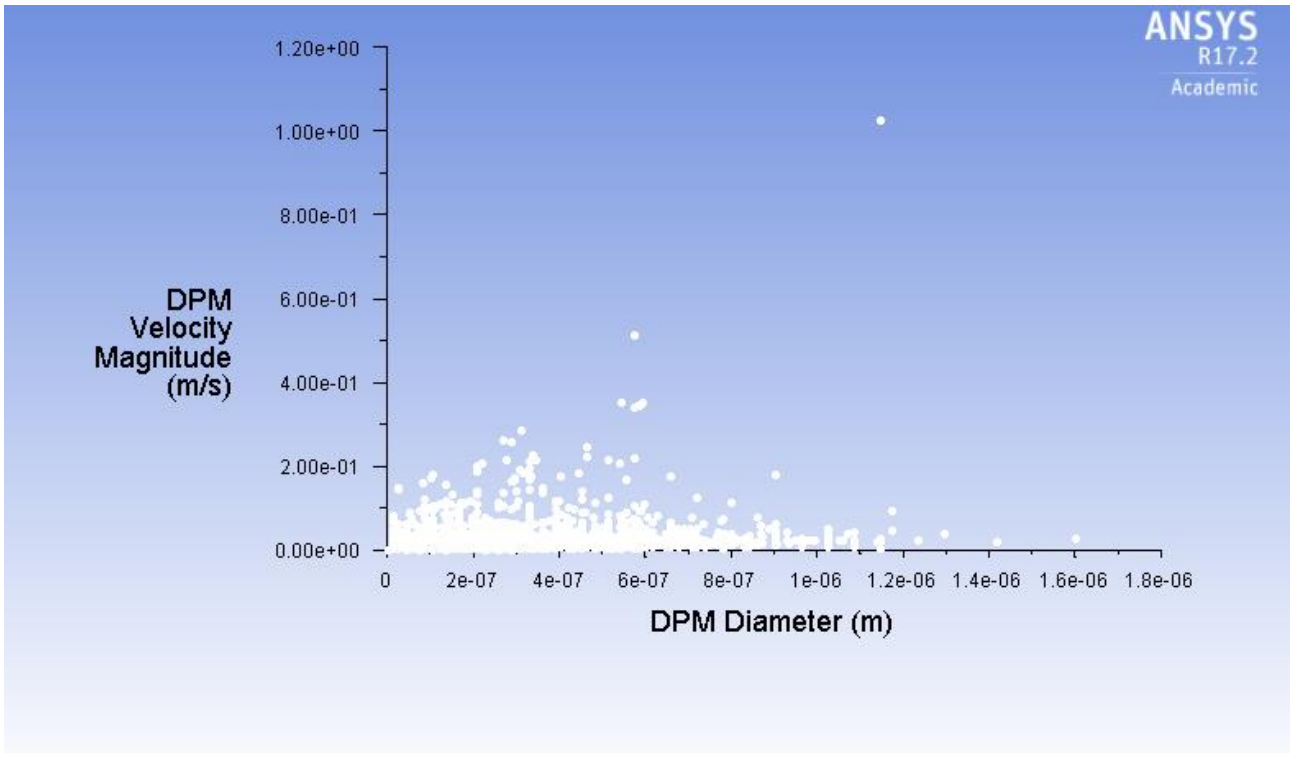

Figure 32 Particle velocity/diameter diagram

Figure 32 shows that particle velocity magnitude does not seem to heavily depend on their diameter, as there is no evident correlation between velocity and diameter, as already hinted in the previous images.

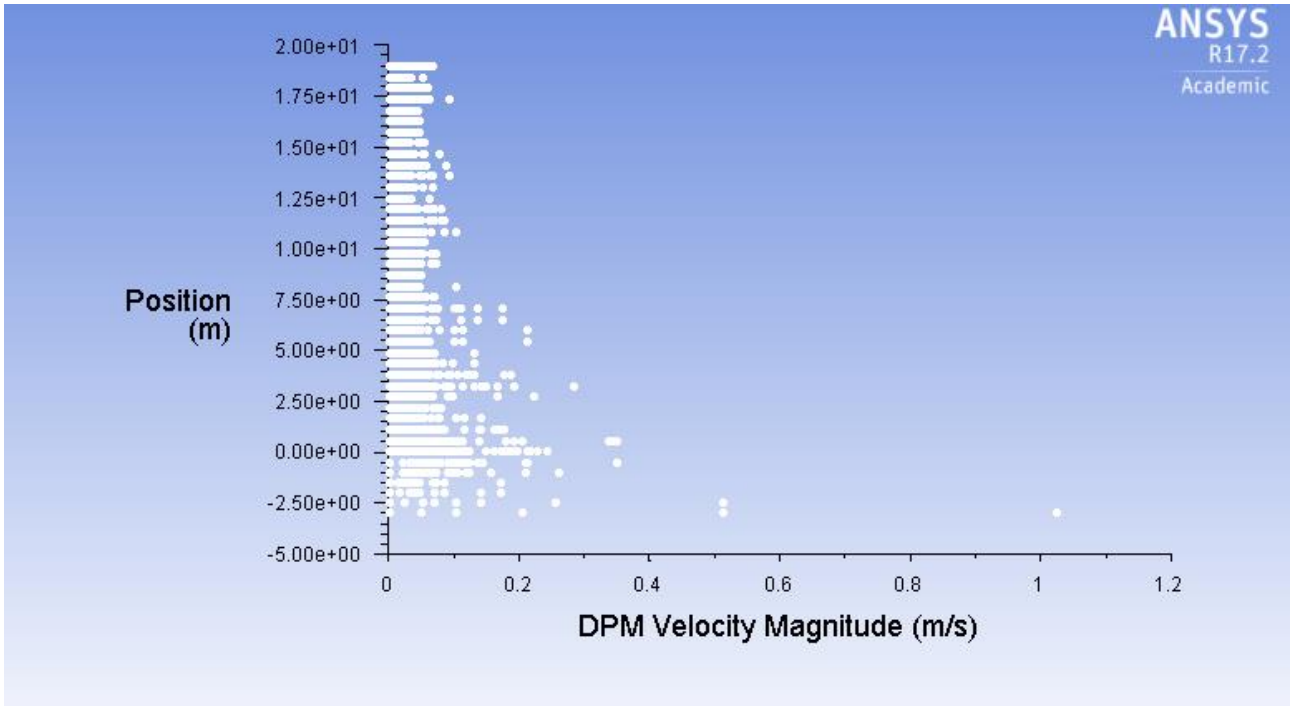

Figure 33 Particle velocity/height diagram

On the other hand, particle velocity tends to steadily decrease with height, as seen in this other graph in Figure 33, even though most particles at all heights stand at the lowest registered velocities.

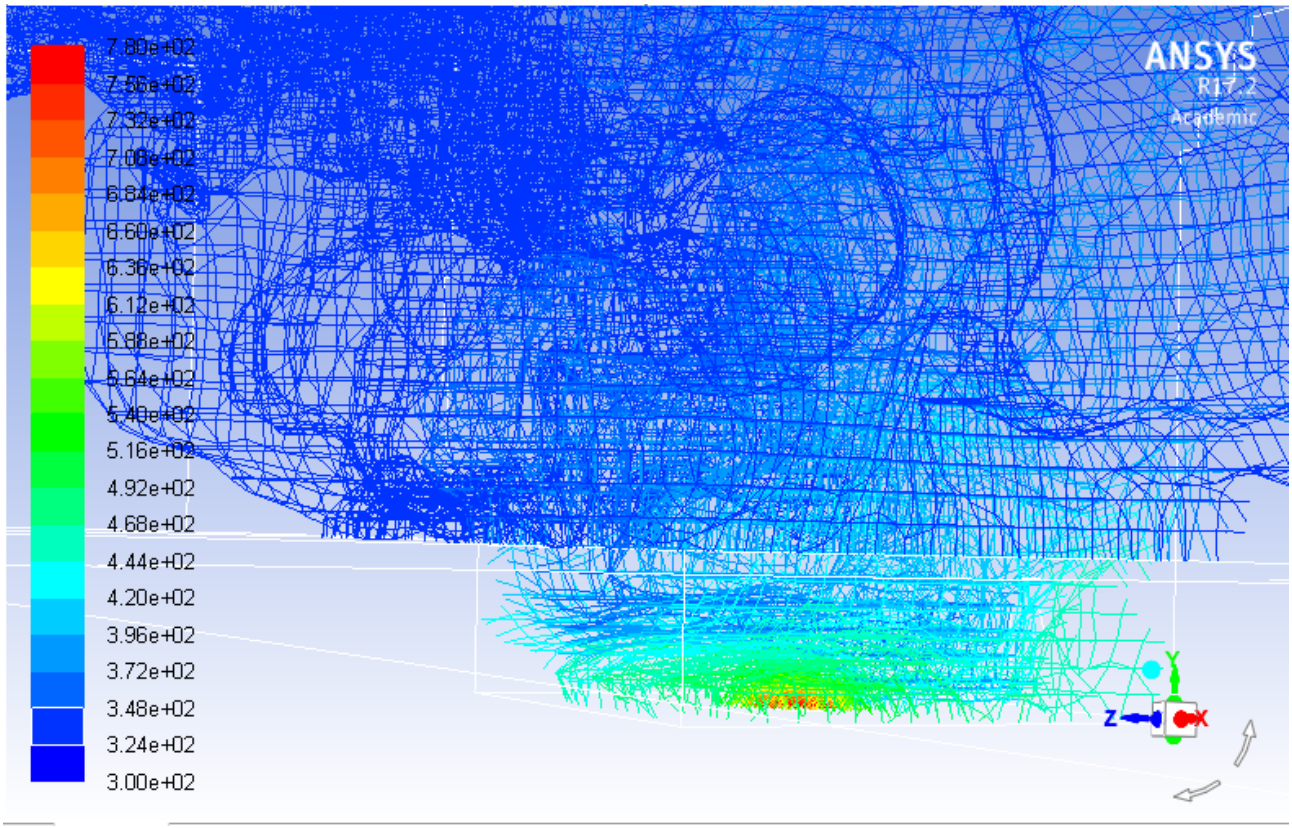

Figure 34 Representation of the air flow temperature profile inside the bunker and the surrounding hall; temperatures are in K. It can be appreciated how temperatures degrade quickly to room temperature levels right outside the bunker itself

7.4 SUMMARY FOR THE FULL-SCALE SIMULATION

The full-scale simulation confirms much of what already seen in the previous scaled-down scenarios; particles escape the building exclusively from the ceiling outlet, starting after little more than two minutes from injection and continuing steadily but slowly until the end of the calculation. Little less than 11% of the particle mass has escaped after 20 minutes; the particle diameter distribution shows how escaped particles are those with the smallest diameters, of the order of 0,1 µm. Particle sizes are quite evenly spread in height, although particles larger than 1 µm have a slight tendency to stay on lower heights. Particle velocities do not seem to have strong correlation with their diameters. The push exerted by the bunker fire moves particles upward at velocities of 1-2 m/s in its proximity, while degrading to velocities close to 10^{-3} m/s when further away, confirming the importance of the fire in the particle dispersion. Overall, the velocity of particles degrades with height.

7.5 REMARKS ON CONVERGENCE

All the above described simulations demonstrated to be well-behaved regarding the convergence of the calculations. As shown in Figure 35 below, residuals kept lower than the previously mentioned values suggested by the user manuals of Ansys Fluent (Ansys, 2006).

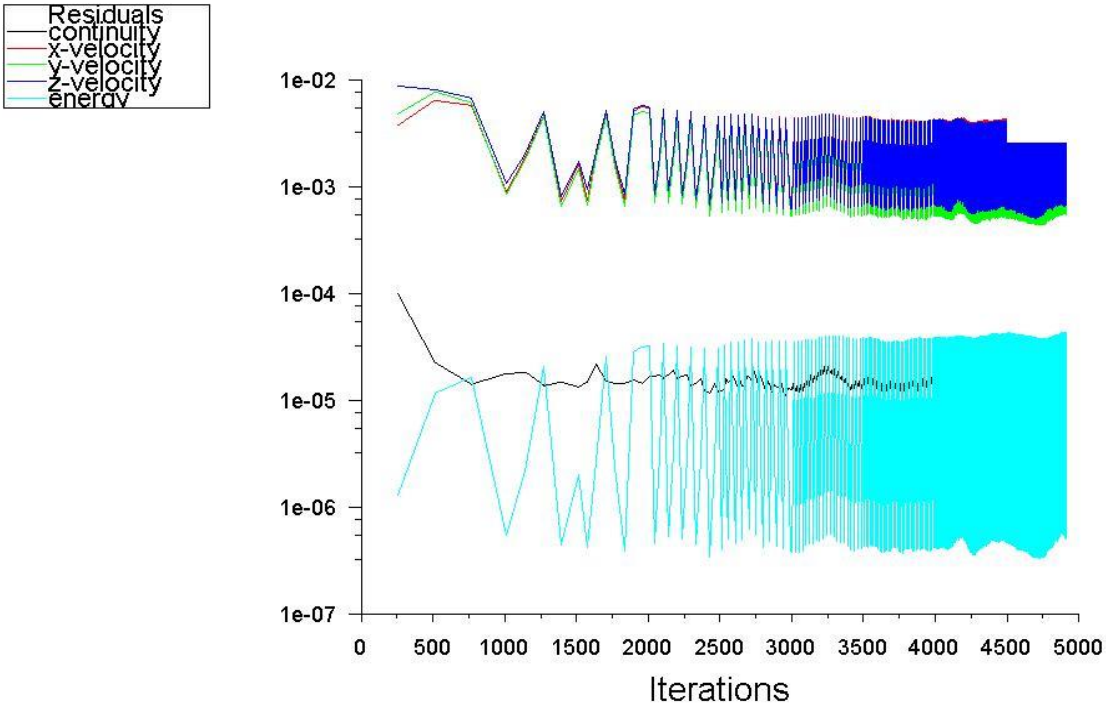

Figure 35 Convergence history of the full-scale simulation

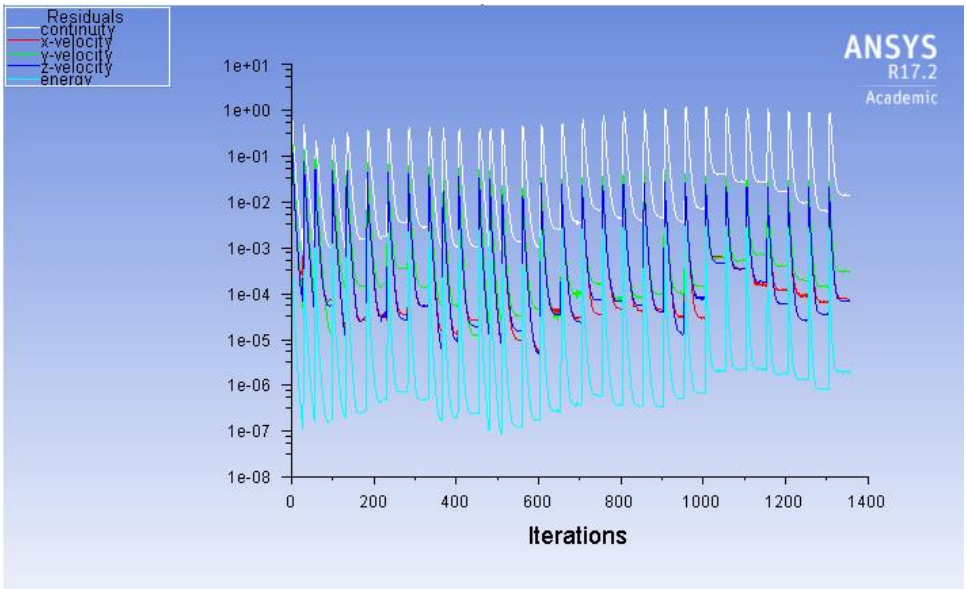

Figure 36 Convergence history of the Steckler room simulation

The simulations start converging pretty quickly, after only a few iterations.

For both scaled down and full scale scenarios the velocity residuals keep consistently, after few iterations, under 10^{-3}. The continuity equation residuals are particularly low, reaching almost 10^{-5}, two orders of magnitude lower than suggested by the guidelines. The energy equation residuals at around 10^{-6} are lower than advised by one order of magnitude.

The drop in the residuals' values is, for all of them, by only one order of magnitude. This suggests, since the iterations converge easily, that the initial conditions constitute a good enough guess. All in all, residuals' and convergence history demonstrate the quality of the simulation itself.

8 RISK ASSESSMENT

An exhaustive and comprehensive risk assessment for this incident scenario is still not possible, since at this point many aspects are not fully known or assessed. As stated in the problem delimitation, probabilities and other statistic elements cannot be defined in quantitative terms. Similarly, there is no data for toxicity in this case, given the difficulty in defining and calculating exposure doses or toxic effects. This means that risk itself, as in its typical definition of product between likelihood and consequences of an event, cannot be quantified. However, despite these limitations, the scenario model can still allow a simplified, qualitative yet incomplete risk assessment, allowing to yield some guidelines for future developments. The risk picture has already been defined with the description of the case scenario. The results from the CFD simulation of such scenario allow to proceed with the identification and treatment of risk.

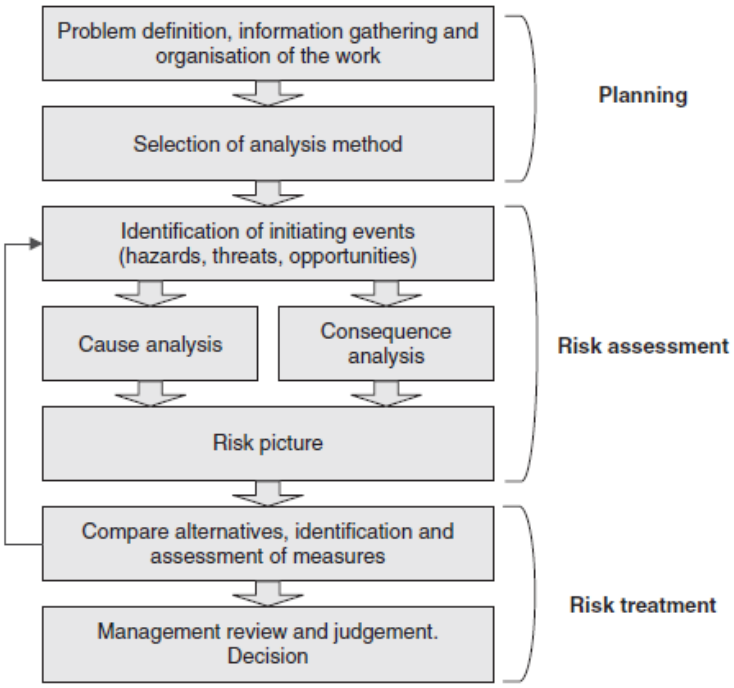

Figure 37 General configuration for risk assessment (Aven, 2008)

8.1 RISK ANALYSIS AND IDENTIFICATION

The main elements found in the dispersion model can be quickly summed up as such:

- The heat release rate of the fire in the bunker has a decisive effect on the particle dispersion: higher heat release rates cause tungsten particles to spread faster, escaping the building in shorter times and in larger quantities.

- After 20 minutes, particles spread evenly and are suspended at all heights in the instrument building, their velocity magnitudes being for the most part higher than their terminal velocities.

- Tungsten particles start escaping the instrument hall approximately two minutes after their release in the building

- After 20 minutes, approximately 11% of the released particle mass has escaped the instrument hall to be dispersed in the outside environment

- No particle escape occurs from ground level openings

The main risk elements arising from the case scenario are therefore:

- The effect of tungsten contamination on the personnel inside the instrument hall

- The effect of tungsten contamination on the outside environment

The size of the bunker fire has also been established as a major influence, especially regarding the environmental risk. Since most particles remain dispersed inside the instrument hall, it is safe to say that the personnel inside the building is exposed to a higher risk than the outside environment.

Despite the increasing presence of tungsten in several fields and industries, its toxic properties have not yet been properly understood. Tungsten is not currently thought to have carcinogenic properties on humans. (Lemus & Venezia, 2015) What is known about the effect of tungsten on human health is the increased prevalence of stroke in case of chronic exposure, prolonged for several years (Tyrrell et al., 2013). The exposure due to this particle dispersion scenario would be rather acute, but on the other hand the inhalation of particles could cause them to deposit in the workers' lungs for long periods, creating a situation akin to a chronic exposure. The simulation showed how particles are spread also at lower heights where they can be inhaled; those with larger diameters tend to stay at lower heights, leading to possible higher toxicity levels at eye level; toxic exposure to tungsten could indeed be a serious threat for the health of those inside the instrument hall.

The effects of tungsten on the environment are not being fully understood either, but recent reports pointed out their relevance; metabolic dysfunctions in small animals have been reported after acute exposure to heavy metals, including tungsten alloys.

8.2 RISK TREATMENT

Through a risk treatment process, risk can be mitigated, avoided or transferred.

The measures to be taken by ESS in this case scenario, based on the above risk analysis and identification, can be directed towards three main directions:

Bunker fire: as it has already repeatedly stated, the fire has the main role in the dispersion of tungsten particles. Therefore, limiting or eliminating its influence has an overall paramount importance.

- Risk mitigation: It is not yet known what the internal configuration of the bunker will be, but limiting the amount of possible fuel for the bunker fire would affect its heat release rate, therefore its effect on the dispersion.

- Risk avoidance/mitigation: Fire extinguishing would be highly effective in preventing or limiting the spread of particles from the bunker to the instrument hall. A sprinkler system could work well in that sense, since it would give an immediate and automatic response, even though its ability to withstand the initial deflagration and its effect on the particles need to be verified. Otherwise, human intervention from a firefighting or rescue team to suppress the fire could also be employed, although it would be more time consuming and costly.

- Risk transfer: The local fire department could send a firefighting team to suppress the fire, although it would be the most time-consuming option.

Personnel safety: The majority of the tungsten particles disperses in the instrument building at all heights; therefore, their effect on the personnel inside the hall must be taken into account.

- Risk mitigation: the main procedure would be a complete evacuation of the personnel from the instrument building. In this regard, organizing an evacuation plan would benefit from the dispersion model results, that show how no particles tend to escape from ground level openings. Therefore, evacuation can be carried out without furthering the release of particles in the outside environment.

- Risk transfer/mitigation: a need could arise for evacuating injured or incapacitated people from the instrument building. A rescue team, which may be organized by ESS itself or from local firefighters, could ingress the hall for such necessity, also benefitting from not influencing the particle release by using ground level entrances.

Environmental safety: The simulation results yield that 11% of the particle mass is dispersed in the environment outside the hall 20 minutes after release. This implies both that tungsten particles are indeed able to escape the building and that the risk of environmental damage is to be taken into account, despite being decidedly smaller in magnitude than the risk to human safety inside the building.

- Risk avoidance: a filtering system or a tight sealing for all openings from which particles are expected to escape could, if activated before the short escape time of the particles, prevent them from leaving the building or at least reduce their escape. A filtering or sealing system should be expected to be effective for particles of diameters in the 0,1 μm order of magnitude.

- Risk mitigation/transfer: The particles released in the environment could also affect any personnel or civilians in the ESS and its surroundings. It is then necessary to have an alert and communication procedure inside ESS itself (for instance, to order personnel to stay indoors) and to nearby facilities and institutions, such as the MAX IV synchrotron radiation facility, placed 1 km away from ESS, or the future Science Village Scandinavia.

8.3 ORGANIZATION AND EQUIPMENT

It is then clear that the main actions to be undertaken are:

- the evacuation of the personnel on site (and possibly of surrounding structures)
- the suppression of the bunker fire

These topics are still in a planning and developmental stage at ESS, and as such were discussed at meetings such as the *Workshop on fire protection for physics research* facilities that took place on site in November 2016 and June 2017. (Svensson, 2017) (Marklund, 2017)

8.3.1 Evacuation

The ESS Evacuation Plan is being developed and will most likely have to be fully defined when the facility will be completed and operational.

The scope of evacuation is to:

- Egress of all personnel from the building in the fastest and most efficient way

- Check and verify whether everyone has been safely evacuated

- If needed, support evacuation for injured/incapacitated personnel

An evacuation routine must be established and carried out in the quickest possible way, so that the fire extinguishing can start.

An Evacuation Leader must be appointed to direct and supervise this process; furthermore, they must also effectively coordinate and communicate with the operational management in the ESS and with external

entities such as the local fire brigade. Is also of capital importance checking the status of anyone involved in the accident scenario.

Technical elements that will be needed for the evacuation are:

- *Evacuation alarm*: an alarm akin to a standard fire alarm for the instrument hall building, that can in case be activated by the Evacuation Leader at their discretion.

- *Outdoor alarm*: since the dispersion model showed that particles will be released outdoor, an external alarm for the rest of the facility is necessary to alert any personnel outside the instrument hall

- *Communication devices*: radio and cellphone communication between the Evacuation Leader and other agents must be ensured, together with possible other means such as indoor screens and intercoms.

- *Outdoor assembly and sheltering points*: the evacuated personnel must be assembled and gathered in specified shelters where they cannot be exposed to the tungsten particles released outdoor. The outdoor alarms must be activated primarily for this purpose.

8.3.2 Bunker fire suppression

The fire taking place in the bunker, as it has been simulated in the case scenario, does not have a high heat release rate, and, in itself, it is not expected to pose a great hazard to personnel or to the environment.

Nevertheless, since it is the main driving force for the particle dispersion, and seeing from the simulation that the outdoor release starts little more than two minutes after the particles are dispersed in the building, the main issue for the suppression of the bunker fire is the short timing. Furthermore, there is yet no knowledge over the possibility of having a dedicated sprinkler system for the bunker.

It is expected for the local fire brigade to reach the ESS facility and intervene around 25 minutes after being alerted, which compared to the timing seen in the simulation, is a rather long time, if the particle dispersion is to be halted or mitigated.

This means that in our case scenario the First Responder, i.e. a figure appointed from inside ESS to react to emergencies, must take immediate action to suppress the bunker fire.

The First Responder must then be properly equipped to evaluate and extinguish the fire without external support. Their mission is to investigate the fire and identify it, then take action to extinguish it or at least limit it before the fire department can take over. Given the small scale of the fire, it is reasonable to expect the First Responder to be able to suppress the fire by themselves, provided they have the right equipment, which would be composed of:

- Standard grade firefighting gear, including a filtered breathing apparatus to prevent particle inhalation

- Infra-Red and thermal camera to control heat and temperature of the fire, and make a direct evaluation of the bunker fire size

- High pressure extinguishing system, to directly extinguish the fire, having also the capability to be used from outside the bunker (if the walls are thin enough)

- Extinguishing grenade, adapted to the bunker environment

Figure 38 Demonstration of a high-pressure extinguishing system in Borås, Sweden

8.4 CONCLUSIONS ON RISK TREATMENT AND UNCERTAINTIES

Summing up from the elements obtained from the dispersion model and the considerations made regarding risk assessment:

- Human safety risk inside the instrument hall is to be treated with a complete evacuation of the building, which would not worsen the outdoor release of particles. Evacuation should be planned in advance and directed by an appointed Evacuation Leader. To ensure the safety of both evacuated and outside personnel from particles released in the environment, sheltered assembly points must be set up.

- Given the short time from the occurrence of the accident scenario and the outdoor release of particles caused by the bunker fire, suppression of such fire is to be taken by a local appointed First Responder equipped with proper firefighting gear.

For future developments in the assessment of this dispersion scenario, some elements which are still uncertain may be addressed, if more knowledge on the definitive layout and configuration of the instrument hall building will be available in the future:

- Sprinkler fire extinguishing system inside the bunker

- Internal configuration inside the bunker

- Air filtering in the instrument hall

- Openings configuration in the instrument hall

Figure 39 Map of ESS and MAX IV in the future Science Village Scandinavia

9 CONCLUSIONS AND FINAL OBSERVATIONS

This project sought to assess a hypothetical accident scenario with a CFD simulation, to answer some questions and set the course for possible future developments.

There is yet no way to quantify how the model is an accurate representation of reality; nonetheless, the turbulence modelling, mesh quality and convergence behavior, together with the partial validation of the fire model, make the model setup reliable enough to be used as a base for future and more detailed developments. The chosen software tool, Ansys Fluent 17.2, demonstrated to be suitable for this task.

The model showed that in this scenario the dispersed particles escape the instrument hall, taking them approximately two minutes to start egressing. Nevertheless, the overall mass fraction of particles leaving the building is rather low, being less than 11% after 20 minutes for the last full scale simulation. Out of them, only particles of diameters around 0,1 µm, out of a size range between 0,1 and 2,3 µm, tend to escape.

An important aspect of particle escape is that it occurs exclusively from the ceiling level outlet; no particles escape from ground level openings, implying major implications for future evacuation and rescue planning.

The size of the bunker fire decidedly influences the particle dispersion; the CFD simulations showed how a fire with higher heat release rate causes particles to escape the hall in less time and pushes larger particles higher up. In addition to this, the particles appear to be more evenly spread for a larger fire.

Overall, the model allows to infer the main safety issues that arise from the accident scenario it simulates; most tungsten particles are evenly spread inside the instrument hall, posing a potentially serious risk of exposure from the toxic effects from inhalation for the workers and researchers. The potential damage for the outside environment is lower in magnitude, given the relatively small mass fraction of particles escaping the building, although it remains relevant and worth of further analysis.

The simulation calculated through the model described in this project provided significant data for a future risk assessment of accident scenarios involving particle dispersion into the instrument halls of ESS.

9.1 GENERAL OBSERVATIONS FOR FUTURE DEVELOPMENTS

This project, as already explained in the problem limitation paragraph, could not address the full extent of the accident scenario, neither in the description or simulation nor in the full assessment of its consequences, even though it laid a base to further developments, that are briefly listed below:

- ***Geometry of the scenario****:* the geometry of the bunker and the instrument hall can be made to be closer to the definitive layout of the finished structure, when more information will be made available, especially regarding size and position of openings or equipment.

- ***Turbulence scales and LES filtering****:* the assumptions made on the sizes of turbulence scales in the instrument hall have been used as justification for the use of the LES turbulence model and for the size of the mesh elements, which was accepted as suitable for the simulation to give an accurate enough solution.

The project has been primarily focused on building a functioning and well-behaved model to simulate the given scenario; therefore, these assumptions were not deeply researched, also because of the difficulty in assessing turbulence scales for a given case, geometry and initial conditions. Having a better knowledge of the sizes of the different turbulent scales could allow to see how much the LES model “leaves behind” to the sub-grid scale modelling algorithm and which would be the best grid refinement.

Another feature that could help in this regard, and that was not pursued given the time and the resources, is a grid independence test, i.e. checking the same simulation with progressively finer meshes, comparing the convergence history to see at which level of refinement the solution stops depending on the grid.

- ***Fire model***: the bunker fire has been implemented into the simulation via a simplified model that was subsequently compared to a validated model in the FDS software. This functioned as a partial validation that justified the use of this simplified fire model in the full scenario simulation. With a better knowledge of the fuel and the layout inside the bunker, the fire model can be evolved and improved, perhaps with a dedicated combustion model, if more computational resources are available. With a better knowledge of the case, also the physics' description can be improved.

- ***Visual interface****:* the visual output from the simulations is rather limited in this project, because of the sheer size of the domain compared to the limited computational resources. Showing results such as particle tracks or animations of the scenario would have greatly improved the understanding of the project and its results, but only more capable hardware could allow to do that.

- ***Sensitivity analysis****:* A wider sensitivity analysis on the simulation would have allowed to obtain a better insight on the scenario. Nonetheless, the limited time and resources did not allow to implement it. With better resources, that would allow for shorter simulation times, the simulation could have been rerun using, for example, different geometry configurations, initial conditions, or particle distribution patterns.

10 APPENDIXES

10.1 APPENDIX A: NUCLEAR SPALLATION

The term *spallation* indicates an interaction between energetic subatomic particles and atomic nuclei; such kind of interaction is obtainable by means of a particle accelerator and a target made of heavy elements (Conrad, 2012).

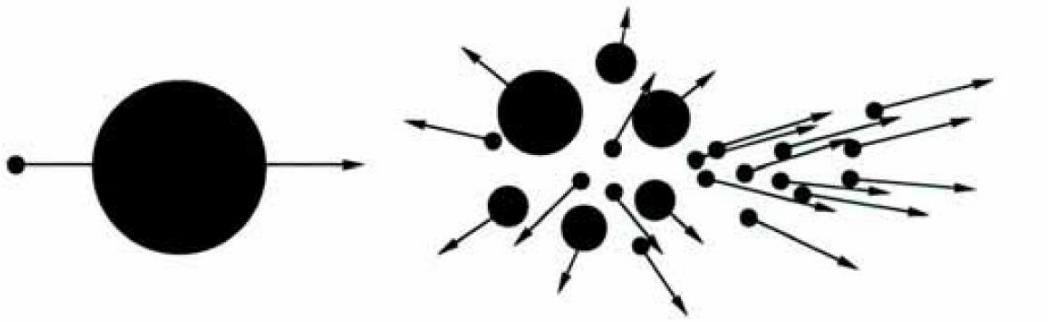

In the ESS, spallation is achieved by accelerating protons (obtained by hydrogen gas, where protons and electrons are separated) to impact the tungsten nuclei of the target. The spallation process can then be described in two consecutive phases:

- A first phase, called *intranuclear cascade,* in which the impacting proton directly interacts with the nucleons (neutrons and protons inside the nucleus), causing an internal energetic cascade that makes some of these particles escape the nucleus at high energies while leaving the remaining ones in an excited state.

- A second phase called *nuclear de-excitation*, where the nucleus balances its energetic state by evaporating nucleons and releasing radiation; what makes spallation particularly interesting for research and engineering applications is the fact that most of these releases are indeed neutrons at relatively low energies, which can be moderated and channeled. During the de-excitation of the nuclei, other reactions may take place, such as fissions and fragmentations of the nuclei.

In general, it can be summarized that the first phase yields high-energy neutrons while the second one emits mostly low-energy neutrons, in higher numbers than the first phase.

Before spallation was fully discovered and developed, nuclear fission, such as that normally taking place in most nuclear reactors, was the process of choice for neutron sources; however, spallation of heavy metal nuclei is more efficient than nuclear fission to produce neutrons, needing a far lower amount of power output. Another advantage of spallation over fission is the much higher degree of control on the reaction, since it needs an external output (the accelerated protons) to be triggered and cannot sustain itself for long without it, unlike the chain reactions occurring in a nuclear fission (Conrad, 2012).

Spallation produces less heat and less gamma-ray radiation than fission, while at the same time yielding more neutrons per nucleus. Nevertheless, the emitted neutrons have higher energies than those produced from fission.

On a safety and containment perspective, this implies that a spallation source such as ESS needs, in comparison to fission reactors, less shielding from heat (even though heat dispersed from the proton acceleration remains a major issue) and from gamma rays, while at the same time needing an increased focus on neutrons. High-energy neutrons need to be properly confined in the target, since they are highly

penetrating, potentially very dangerous for living organisms and may disrupt experiments; at the same time, low-energy neutrons are to be facilitated in leaving the target area, to let them be channeled to the instrument halls (Russell, 1990).

Therefore, the main safety issue of the spallation process is protection of personnel and environment from all emitted neutrons, especially those too energetic to be employed in research.

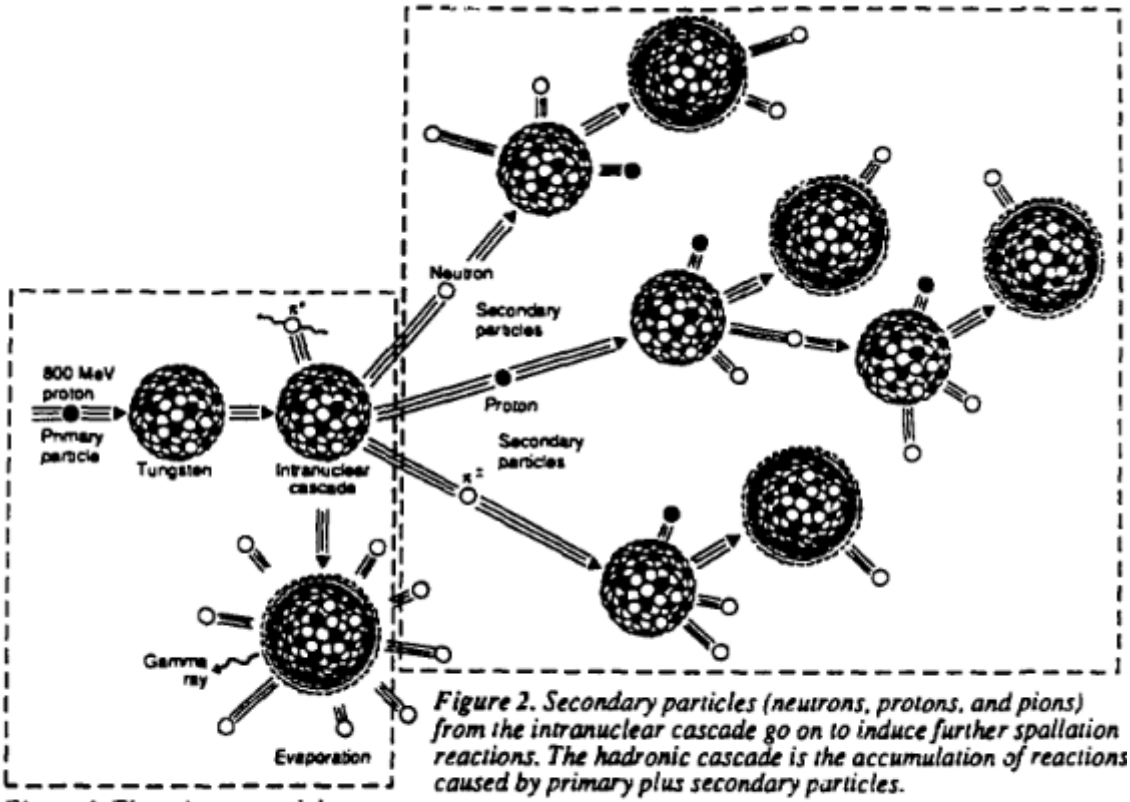

Figure 1. The primary particle (800- MeV proton) hits the tungsten nucleus, inducing spallation (the intranuclear cascade and evaporation).

Figure 2. Secondary particles (neutrons, protons, and pions) from the intranuclear cascade go on to induce further spallation reactions. The hadronic cascade is the accumulation of reactions caused by primary plus secondary particles.

Figure 40 A description of the spallation process in tungsten nuclei (Russell, 1990)

10.2 TUNGSTEN

Tungsten (chemical symbol W) is considered the best material of choice for spallation targets in most neutron sources, including the ESS. In fact, tungsten is the element that yields the highest number of low energy neutrons while not being fissile, i.e. posing risks of spontaneous fission reaction. It is a very heavy element with a high melting point, a much-needed characteristic given the high temperatures that may arise in a spallation reaction (NCBI, 2005).

10.2.1 Hazard from tungsten inhalation or exposure

Despite the increasing presence of tungsten in several fields and industries, its toxic properties have not yet been properly understood. Tungsten is not currently thought to have carcinogenic properties on humans. (Lemus & Venezia, 2015) Recent studies have pointed out a correlation between prolonged exposure to tungsten and occurrence of cardiovascular or neurological diseases, suggesting that chronic exposure leads to an increased chance of stroke (Tyrrell et al., 2013). Experiments taken on rats detected metabolic dysfunctions after acute exposure to heavy metals, including tungsten alloys. Nevertheless, there are no reported health effects from acute exposure on humans. Information gathered from most recent studies points that tungsten and its alloys do not affect organisms through dermal contact (Lemus & Venezia, 2015).

Despite there have been attempts at establishing a minimum reference dose of exposure to tungsten, there is still no consensus on this.

10.3 APPENDIX B: WORKING ENVIRONMENT

To carry out the simulations, an ASUS F550C laptop, with 8 GB of RAM, i7 2.0 Ghz CPU was used. A more capable desktop computer was provided by the LTH supervisor for the final calculations.

The software for the CFD simulation, ANSYS Fluent 17.2, ran on the ANSYS Workbench 17.2 working environment:

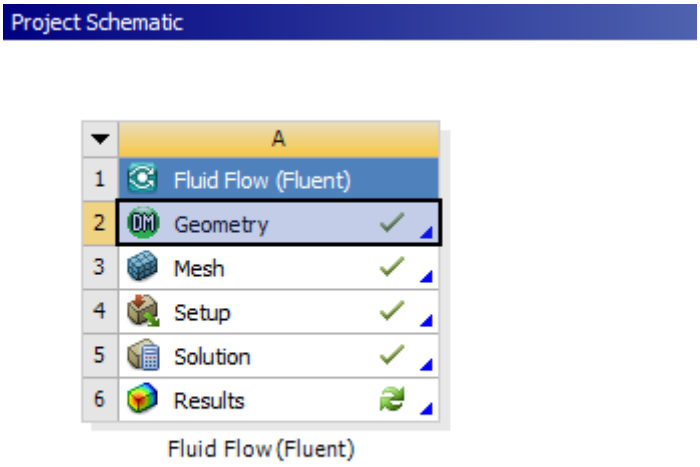

Figure 41 ANSYS Workbench project schematic

This environment allows to follow the pre-processing steps, building the geometry, the mesh and the simulation setup, sequentially and gathered in a single file.

10.3.1 - Geometry

Firstly, the Design Modeler tool, acting as a standalone 3D mechanical design tool, is used to draw the main geometry, the instrument hall and the bunker, as well as the surfaces delimiting the openings and the pool-fire, which are highlighted as “Named Selections”

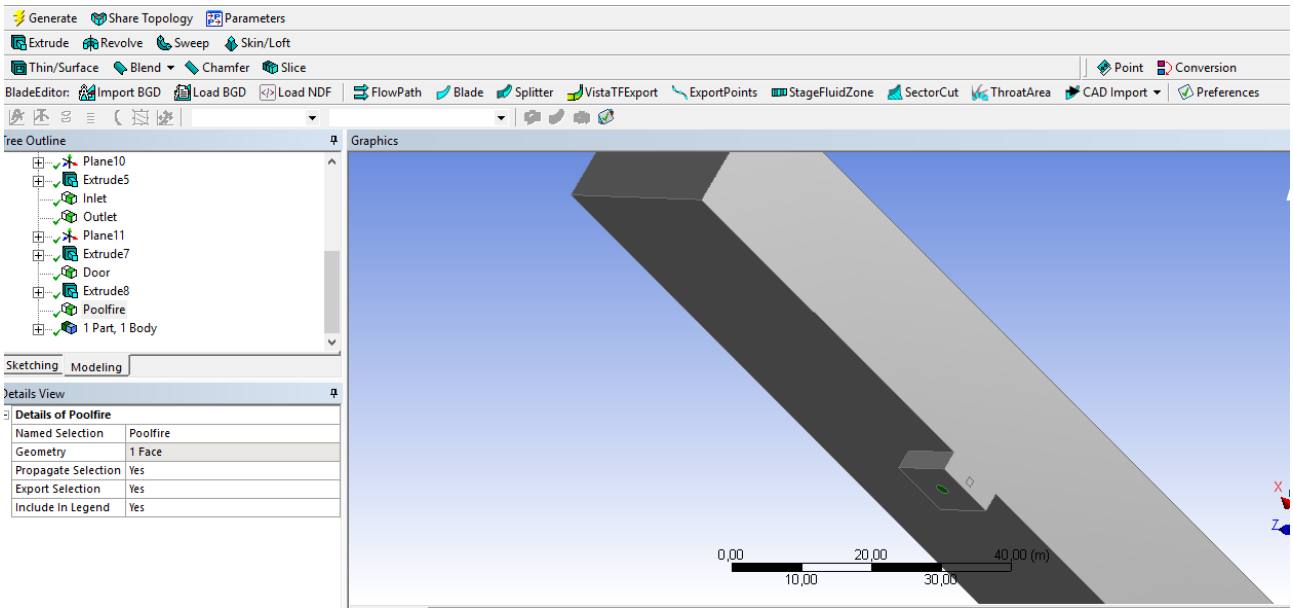

Figure 42 Detail of the built geometry, highlighting the “Poolfire” named selection

10.3.2 - Meshing

Afterwards, the built geometry is loaded into the Meshing tool, to assign it a mesh grid.

As already mentioned in chapters 3.4 and 5.2, the default mesh configuration employs tetrahedral cells, and it has been changed to a cubic cells configuration.

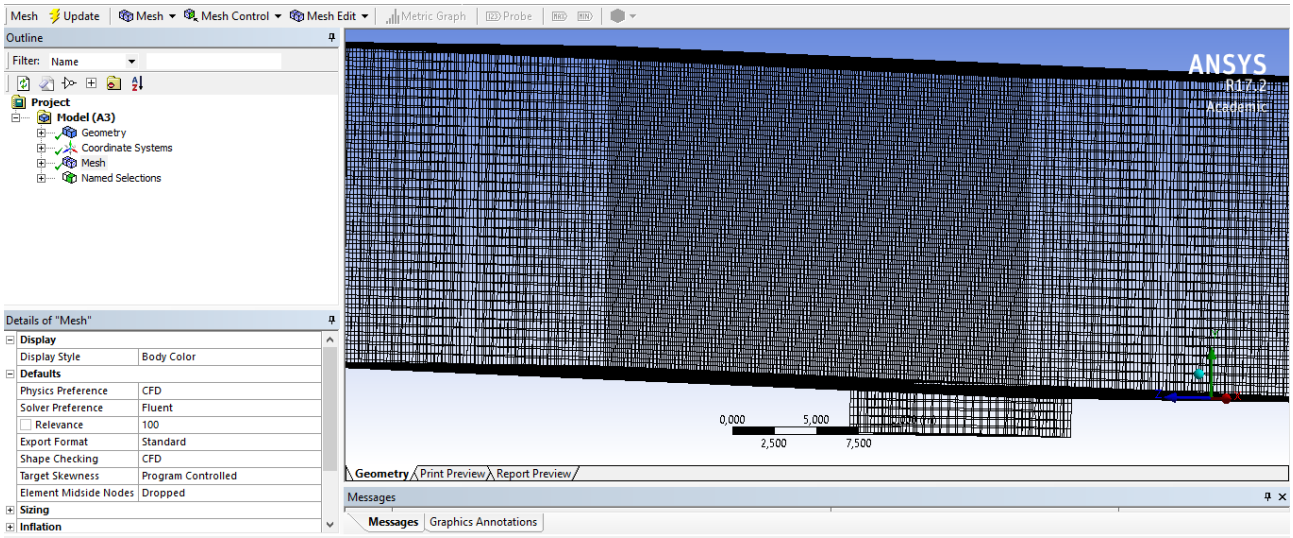

Figure 43 Detail of the meshing tool

10.3.3 - Setup

With the geometry and meshing completed, ANSYS Fluent proper is opened to setup the simulation, with the turbulence modelling, solver settings, boundary conditions, initial conditions and particles injection.

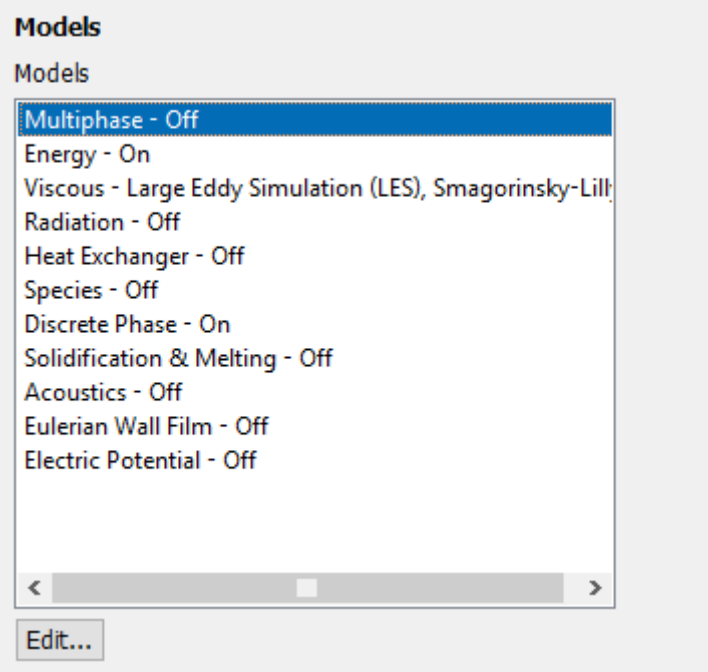

Figure 44 General settings for the simulation, including the turbulence model

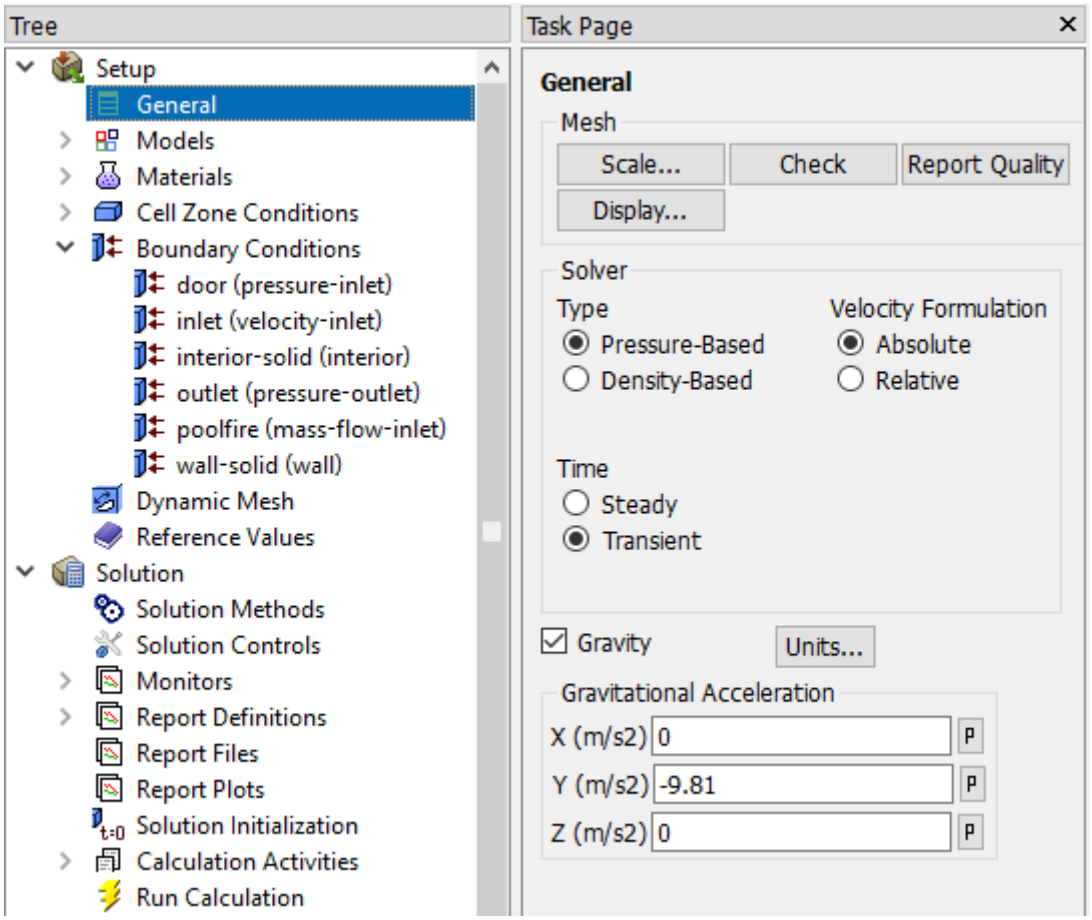

Figure 45 Main screen for the setup, listing the boundary conditions for the openings and fire on the left and some solver settings on the right

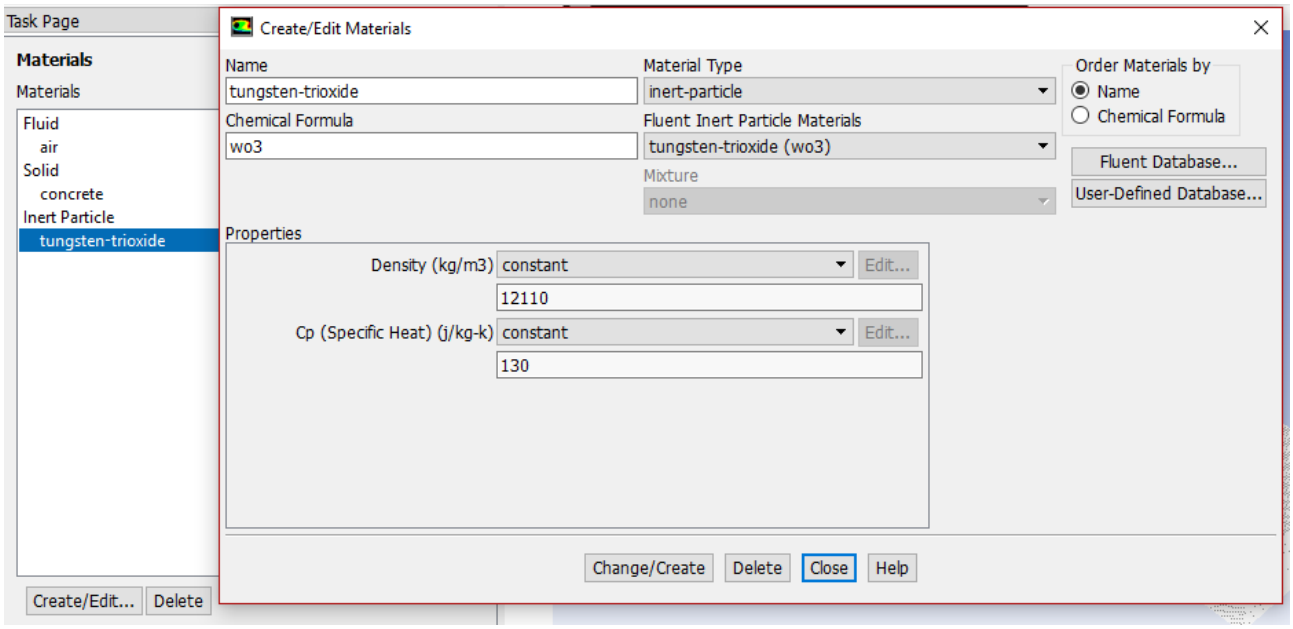

Figure 46 Setup window for the materials used in the simulation

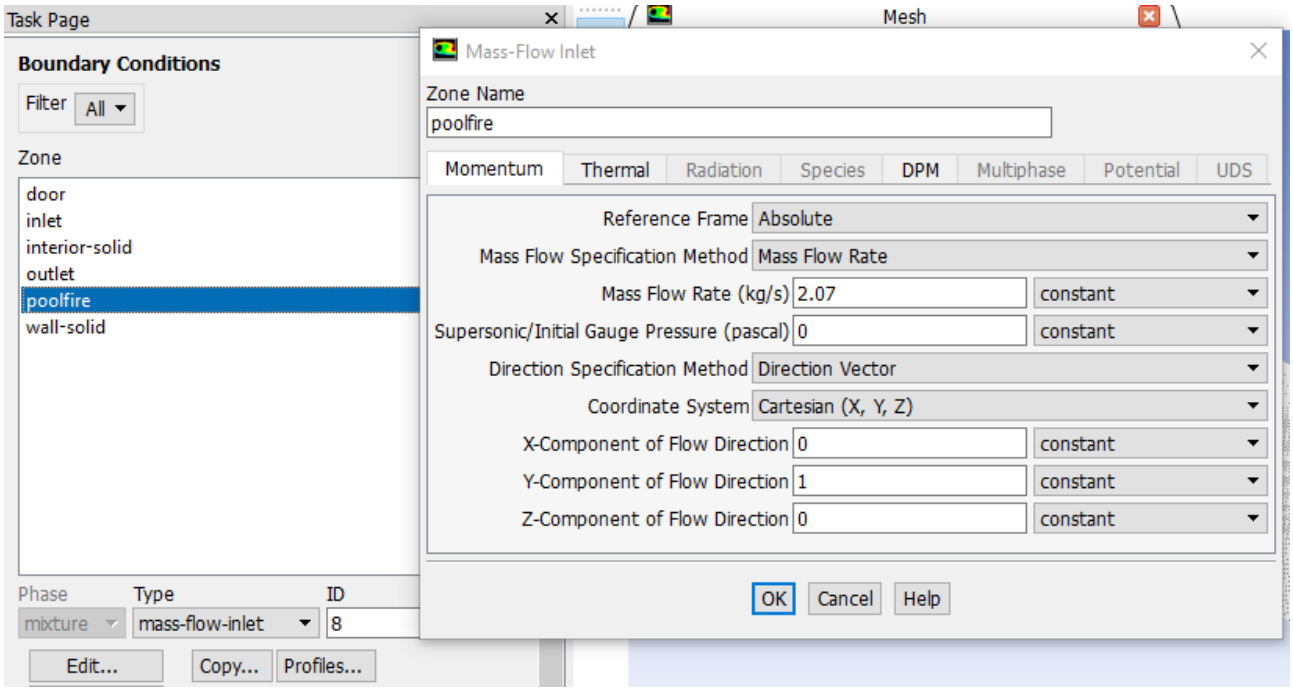

Figure 47 Setup window for the boundary conditions of the pool-fire

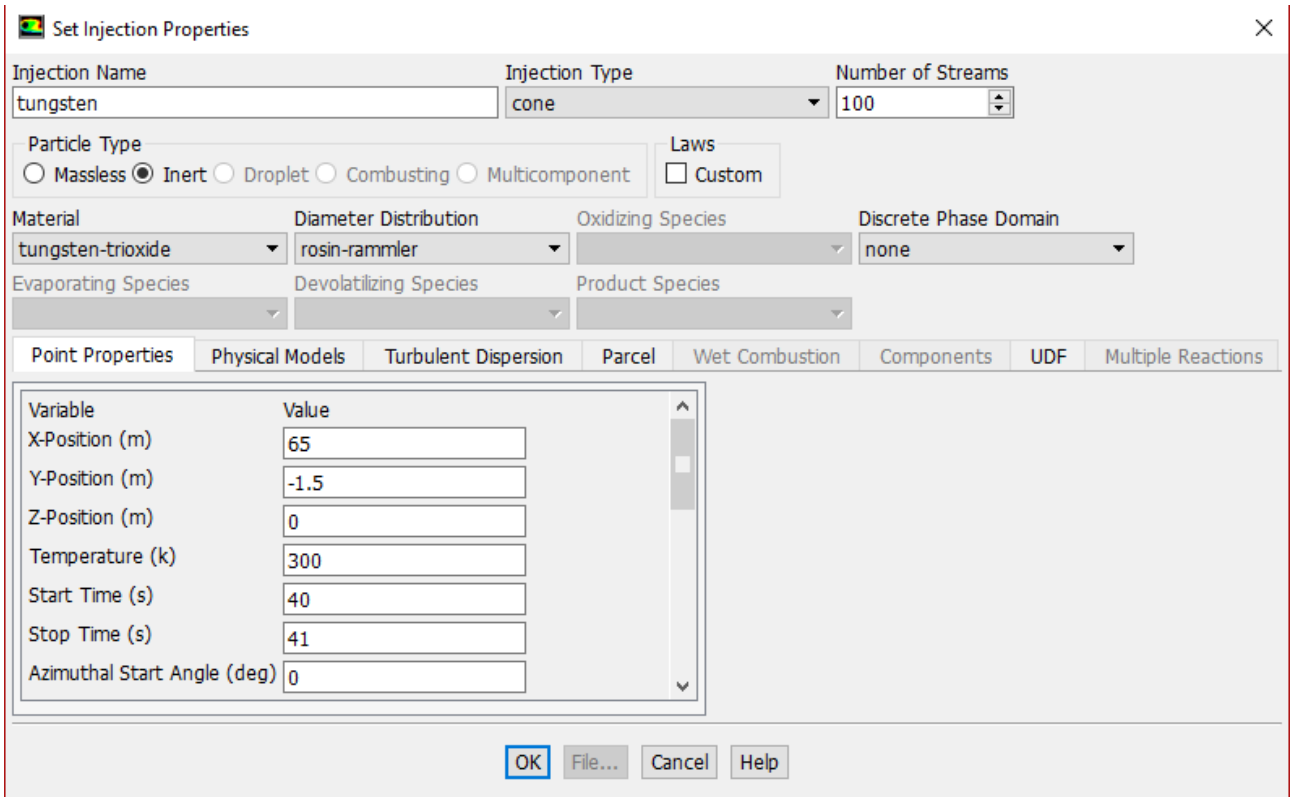

Figure 48 Setup window for the tungsten particles, including the initial and boundary conditions of their injection

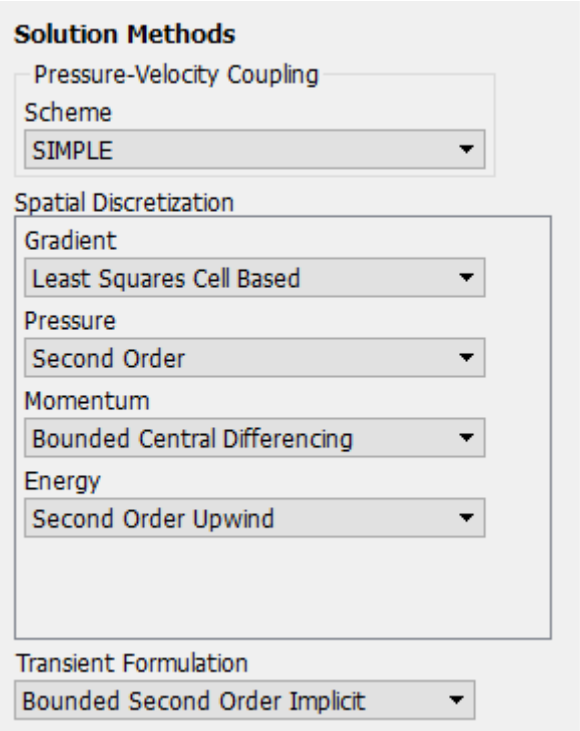

Figure 49 Setup window for the solver algorithm settings and for discretization methods

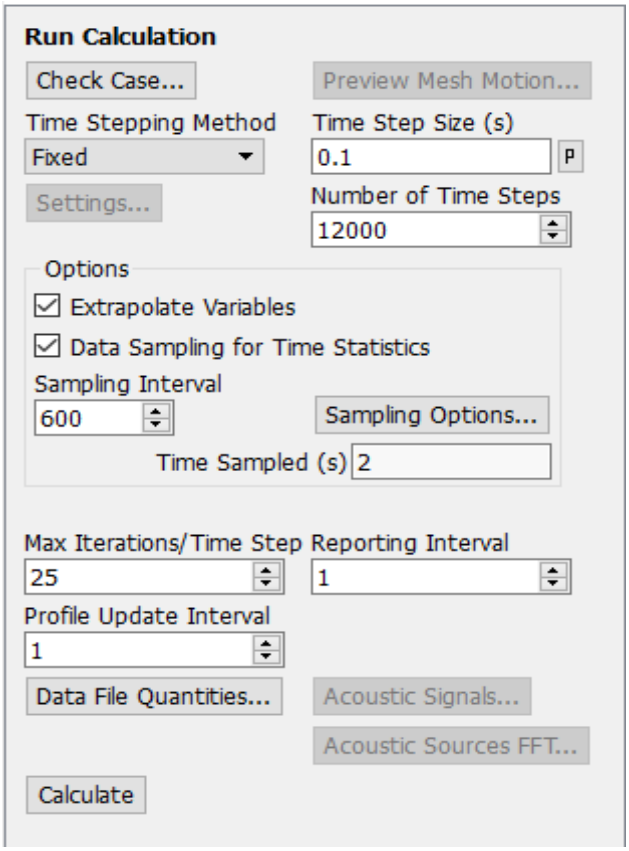

Figure 50 The final setup window, from which the calculation is started, after setting up time steps, iterations and simulation time (by number of time steps)

11 REFERENCES

Ansys. (2006). Solver Settings - Introductory FLUENT Training. Retrieved from http://www.engr.uconn.edu/~barbertj/CFD%20Training/Fluent/4%20Solver%20Settings.pdf

Ansys. (2014). *Ansys Convergence*. Paper presented at the Monterrey Ansys Conference, Monterrey, Mexico.

Ansys. (2016). Fluent 17.2 Theory Guide.

Aven, T. (2008). *Risk analysis: assessing uncertainties beyond expected values and probabilities*: Wiley.

Bakker, A. (2006a). Lecture 10 - Turbulence Models. Retrieved from http://www.bakker.org/dartmouth06/engs150/10-rans.pdf

Bakker, A. (2006b). Lecture 15 - Discrete Phase Modeling. Retrieved from http://www.bakker.org/dartmouth06/engs150/15-dpm.pdf

Conrad, H. (2012). Spallation – Neutrons Beyond Nuclear Fission. In C. Grupen & I. Buvat (Eds.), *Handbook of Particle Detection and Imaging* (pp. 719-757). Berlin, Heidelberg: Springer Berlin Heidelberg.

Davidson, L. (2016). Fluid mechanics, turbulent flow and turbulence modeling. *Chalmers University of Technology*, 24-27; 66-68; 163-171.

Deibjerg, T., Husted, B., Bygbjerg, H., & Westerman, D. (2003). Argos User's Guide

Jadidi, M., Moghtadernejad, S., & Dolatabadi, A. (2015). A comprehensive review on fluid dynamics and transport of suspension/liquid droplets and particles in High-Velocity Oxygen-Fuel (HVOF) thermal spray. *Coatings, 5*(4), 576-645.

Jasak, H. (2009). OpenFOAM: Open source CFD in research and industry. *International Journal of Naval Architecture and Ocean Engineering, 1*(2), 89-94. doi:http://dx.doi.org/10.2478/IJNAOE-2013-0011

Jörud, F. (2013). *ESS-0001126 Definition of Fire*. Retrieved from

Karlsson, B., & Quintiere, J. (1999). *Enclosure Fire Dynamics*: CRC Press.

Lemus, R., & Venezia, C. F. (2015). An update to the toxicological profile for water-soluble and sparingly soluble tungsten substances. *Crit Rev Toxicol, 45*(5), 388-411. doi:10.3109/10408444.2014.1003422

Marklund, M. (2017). *Support for the Operational Action Plan*. Paper presented at the Workshop on fire protection for physics research facilities - FCC study collaboration, Lund, Sweden. https://indico.esss.lu.se/event/768/contributions?&filter=yes&sessionShowNoValue=1&selSessions=10&selSessions=0&selSessions=1&selSessions=7&selSessions=4&selSessions=11&selSessions=9&selSessions=5&selSessions=6&selSessions=3&selSessions=8

McGrattan, K., Hostikka, S., McDermott, R., Floyd, J., Weinschenk, C., & Overholt, K. (2014). *Fire Dynamics Simulator - User's Guide*

McMurtry, P. (2000). Length and time scales in turbulent flows. *ME 7960: Turbulence.*

Moore, G. E. (2006). Cramming more components onto integrated circuits, Reprinted from Electronics, volume 38, number 8, April 19, 1965, pp.114 ff. *IEEE Solid-State Circuits Society Newsletter, 11*(5), 33-35. doi:10.1109/N-SSC.2006.4785860

NCBI. (2005). TUNGSTEN TRIOXIDE. from PubChem https://pubchem.ncbi.nlm.nih.gov/compound/14811

Oberkampf, W. L., & Trucano, T. G. (2002). Verification and validation in computational fluid dynamics. *Progress in Aerospace Sciences, 38*(3), 209-272. doi:http://dx.doi.org/10.1016/S0376-0421(02)00005-2

OpenFOAM. (2016). OpenFOAM.

Russell, G. J. (1990). Spallation Physics - An Overview. *ICANS-XI International Collaboration on Advanced Neutron Sources*.

Samokhin, A. V., Alekseev, N. V., Vodop'yanov, A. V., Mansfeld, D. A., Sinaiskii, M. A., Tsvetkov, Y. V., . . . Plotnikov, I. V. (2015). Production of WO3 tungsten oxide nanopowders by evaporation-condensation process using focused 24-GHz microwave radiation. *High Energy Chemistry, 49*(4), 267-272. doi:10.1134/s0018143915040141

Steckler, K. D., Quintiere, J. G., & Rinkinen, W. J. (1982). *Flow induced by fire in a compartment*. Retrieved from

Svensson, J. (2017). *ESS Evacuation Plan*. Paper presented at the Workshop on fire protection for physics research facilities - FCC study collaboration, Lund, Sweden. https://indico.esss.lu.se/event/768/contributions?&filter=yes&sessionShowNoValue=1&selSessions=10&selSessions=0&selSessions=1&selSessions=7&selSessions=4&selSessions=11&selSessions=9&selSessions=5&selSessions=6&selSessions=3&selSessions=8

Tyrrell, J., Galloway, T. S., Abo-Zaid, G., Melzer, D., Depledge, M. H., & Osborne, N. J. (2013). High Urinary Tungsten Concentration Is Associated with Stroke in the National Health and Nutrition Examination Survey 1999–2010. *PLoS ONE, 8*(11). doi:10.1371/journal.pone.0077546

U.S.N.R.C. (2007). *Verification and Validation of Selected Fire Models for Nuclear Power Plant Applications* Retrieved from Rockville, MD:

Versteeg, H. K., & Malalasekera, W. (2007). *An Introduction to Computational Fluid Dynamics: The Finite Volume Method*: Pearson Education Limited.

Vesilind, P. A., Peirce, J. J., & Weiner, R. F. (1994). *Environmental Engineering*: Butterworth-Heinemann.

Wikipedia.org. (2017). Tungsten trioxide. Retrieved from https://en.wikipedia.org/wiki/Tungsten_trioxide

Wols, B. (2011). *Computational Fluid Dynamics in Drinking Water Treatment*: IWA Publishing.

Zhiyin, Y. (2015). Large-eddy simulation: Past, present and the future. *Chinese Journal of Aeronautics, 28*(1), 11-24. doi:http://dx.doi.org/10.1016/j.cja.2014.12.007